UNIVERSITÀ DEGLI STUDI DI MODENA E REGGIO EMILIA
Dipartimento di Ingegneria “Enzo Ferrari”

Ph.D. School in "Industrial and environmental engineering"
Enzo Ferrari – XXXII cycle

THE DEVELOPMENT OF A BUILDING-RESOLVED AIR QUALITY FORECAST SYSTEM BY A MULTI-SCALE MODEL APPROACH AND ITS APPLICATION TO MODENA URBAN AREA

Candidate: Giorgio Veratti

Tutor: Prof. Grazia Ghermandi

Co-tutor: Prof. Alessandro Bigi

Ph.D. School Director: Prof. Alberto Muscio

ABSTRACT - English

In Europe, emissions of many air pollutants have decreased substantially over the past decades, resulting in improved air quality across the region. However, air pollutant concentrations are still too high, and air quality problems persist. The Po Valley, located in the northern part of Italy, is one of the most critical areas of the country in terms of pollution level. The reason to this problem is not only related to the high population density with its activities, but it is also due to the orographic conformation of the territory which appears surrounded by mountains on three sides: the Alps to the west and to the north and the Apennines to the south. These geographical characteristics lead to meteorological conditions unfavorable to the atmospheric dispersion: average annual wind speed less than 2 m s^{-1}, recurrent thermal inversions at low altitude, low mixing layer heights and persistent foggy and hazy events during winter time.

One of the main critical air pollutants in terms of health effects is nitrogen dioxide (NO_2), whose levels in the last years exceeded national and WHO (World Health Organization) standards in many urban areas across the Po Valley, exposing urban population to the risk of pollution-related diseases and health conditions.

The main goal of this study was to develop a multi-scale modelling system able to provide hourly NO_x ($NO + NO_2$) concentration fields at a building-resolving scale in the urban area of Modena, a city in the middle of the Po Valley, in order to support environmental policies, epidemiological studies and urban mobility planning.

The modelling system relied on two different models: the Weather Research and Forecasting model coupled with Chemistry (WRF-Chem), which is able to compute concentration fields over regional domain by considering specific emission scenarios, and the Parallel Micro SWIFT and SPRAY (PMSS) modelling suite accounting for dispersion phenomena within the urban area. The PMSS modelling suite was used to simulate at building-scale resolution the NO_x dispersion produced by urban traffic flows in the city of Modena. Conversely, the WRF-Chem model was selected to estimate the NO_x background concentrations on multiple domains with a nesting technique, in order to take into account emissions both at regional and local scale by excluding traffic emissions sources over the city of Modena.

In the first part of the work the modelling system was performed for the period between 28 October and 8 November 2016, the same period whereby a direct vehicle flow measurement campaign was carried out continuously with 4 Doppler radar counters in a four-lane road in Modena, in order to reproduce the hourly modulation rates of the emissions.

In second section of the study the modelling system was set-up with the aim of produce hourly forecast of NO_2 and NO concentrations, up to one day ahead, for the city of Modena for the entire month of February 2019.

Simulated and observed hourly concentrations exhibited a large agreement in particular for urban traffic site where detailed traffic emission estimations proved to be very successful in reproducing the observed trend. At urban background stations, despite a general underestimation of the observed concentrations, the combination of WRF-Chem with PMSS provided daily pattern in line with observations. Finally, the statistical analysis showed that PMSS combined with WRF-Chem at both traffic and background sites fulfilled standard acceptance criteria for urban dispersion model evaluation, confirming that the proposed multi-modelling system can be employed as a tool to support human exposures and health impact assessments as well as the effects of local traffic policies on urban air quality.

ABSTRACT - Italiano

La Pianura Padana, situata nella parte settentrionale dell'Italia, è una delle aree più critiche del paese per livelli d'inquinamento. La ragione di questo problema non è solo legata all'elevata densità di popolazione con relative attività antropiche, ma è anche dovuta alla conformazione orografica del territorio, delimitato dalla catena alpina ad ovest e a nord e dagli Appennini a sud. Queste caratteristiche geografiche determinano condizioni meteorologiche sfavorevoli alla dispersione atmosferica, quali: velocità medie annue del vento inferiori a 2 m s^{-1}, inversioni termiche ricorrenti nei primi strati di atmosfera a contatto con il suolo, ridotte altezze dello strato rimescolato e persistenti nebbie durante il periodo invernale.

Uno degli inquinanti atmosferici più rilevanti per effetti critici sulla salute umana è il biossido di azoto (NO_2), i cui livelli negli ultimi anni hanno superato i limiti nazionali e dell'OMS in molte aree urbane della Pianura Padana, esponendo la popolazione al rischio di patologie legate all'inquinamento.

L'obiettivo principale di questo studio è stato lo sviluppo di un sistema di modellazione multi-scala in grado di fornire campi di concentrazione oraria di NO_x ($NO + NO_2$) sulla città di Modena ad una scala spaziale in grado di risolvere gli effetti dovuti alla presenza degli edifici, al fine di supportare politiche ambientali, studi epidemiologici e di aiutare la pianificazione della mobilità urbana.

Il sistema di modellazione si basa su due diversi tool: il modello euleriano di chimica e di trasporto WRF-Chem, in grado di calcolare campi di concentrazione su un dominio regionale considerando specifici scenari di emissione, e Parallel Micro SWIFT e SPRAY (PMSS) suite modellistica sviluppata per risolvere i fenomeni di dispersione all'interno di ambienti urbani.

PMSS è stato utilizzato per simulare la dispersione di NO_x prodotta dai flussi di traffico urbano nella città di Modena, mentre il modello WRF-Chem è stato applicato per stimare le concentrazioni di NO_x di fondo su più domini innestati fra loro, utilizzando emissioni a scala regionale ed escludendo allo stesso tempo le fonti di emissioni da traffico entro la città di Modena.

Nella prima parte del lavoro il sistema di modellazione è stato impiegato per riprodurre le concentrazioni comprese nell'arco temporale tra il 28 ottobre e l'8 novembre 2016, corrispondente al periodo in cui è stata condotta una campagna di rilevazione dei flussi di

traffico, attraverso radar Doppler su una strada di Modena a quattro corsie, al fine di riprodurre una modulazione temporale delle emissioni il più possibile realistica.

Nella seconda parte dello studio lo stesso sistema di modellazione è stato utilizzato per produrre previsioni orarie delle concentrazioni di NO_2 e NO, fino ad un giorno in avanti, per tutto il mese di febbraio 2019 sulla città di Modena.

Le concentrazioni orarie simulate e osservate mostrano un andamento molto concorde fra loro, specialmente per il sito di traffico urbano, dove le stime dettagliate sulle emissioni del traffico si sono dimostrate molto efficaci nel riprodurre la tendenza osservata. Nella stazione urbana di fondo, nonostante una generale sottostima delle concentrazioni osservate, la combinazione di WRF-Chem con PMSS ha fornito comunque un andamento medio giornaliero in linea con le osservazioni. Infine, l'analisi statistica ha mostrato che il sistema di modellazione, in entrambi i siti urbani (di traffico e di fondo), soddisfa i criteri di accettazione standard per la valutazione dei modelli di dispersione urbana, confermando che tale sistema può essere impiegato come strumento per verificare gli effetti delle politiche locali riguardanti il traffico e a supporto di valutazioni di impatto sulla salute umana.

Table of Contents

ABSTRACT - English i

ABSTRACT - Italiano iii

Table of Contents ..... vi, viii

List of Figures ix

List of Tables xiii

1. Introduction 1

2. Models background 8

2.1 Models introduction 8

2.1.1 Eulerian models 12

2.1.2 Lagrangian models 14

2.2 Modelling chain description 20

2.3 WRF-Chem model description 24

2.4 PMSS modelling system description 30

3. Traffic emissions 35

3.1 Exhaust Emissions Overview 37

3.2 Exhaust Emissions Computation 40

3.3 VERT (Vehicular Emission from Road Traffic) model 44

4. Case study area 49

5. Testing the hybrid modelling system in analysis mode 54

5.1 WRF-Chem set-up 57

5.2 PMSS Set-up 60

5.3 Anthropogenic emissions 62

5.4 Model evaluation 69

5.5 Results and discussion 71

5.5.1 Meteorology 71

5.5.2 WRF-Chem nitrogen oxides 78

5.5.3 WRF-Chem combined with PMSS 80

5.5.3.1 Micro-scale wind field 80

5.5.3.2 Micro-scale NO_x concentrations 84

6. Testing the hybrid modelling system in forecast mode 93

6.1 WRF-Chem set-up 96

6.2 PMSS Set-up and urban traffic emissions estimation 99

6.3 Results and discussion 106

6.3.1 Meteorology 106

6.3.2 WRF-Chem nitrogen dioxides and nitrogen oxides 112

6.3.3 WRF-Chem combined with PMSS 114

6.3.3.1 Micro-scale wind field 114

6.3.3.2 Micro-scale concentrations 118

Conclusion..... 125

References 131

Acknowledgments..... 149

List of Figures

Figure 2.1: Outline of the multi-model approach implemented to generate hourly NO_x concentrations fields.....23
Figure 2.2: Mass vertical coordinates in presence of a mountainous relief. 25
Figure 3.1: Example of Modena traffic flow simulation for all vehicle categories which can be used as input for VERT emission model.....45
Figure 3.2: VERT flow chart. Orange boxes represent the functions implemented into VERT and Circles are the input/output data in spatial format (filled by light blue) or scalar/vector format (empty circles).....46
Figure 3.3: Example of VERT output. Modena NO_x emissions from traffic sources related to the morning rush hour. 48
Figure 4.1: Overview of the location of the city of Modena in the middle of the Po Valley. The Alps are situated to the North and to the West. Apennines chain is to the South of the city. Adriatic Sea is about 100 km to the East and the Ligurian Sea is also about 100 km to the South-West.....49
Figure 4.2: Wind-rose computed between January 2015 and December 2018 at the station placed on top to the tower of the Geophysical Observatory of the University of Modena and Reggio Emilia (42 m height above the ground) and located in the historical part of the city of Modena. 50
Figure 4.3: Observed monthly average of daily wind speed and temperature between January 2105 and December 2019 at the Geophysical Observatory tower in Modena.....52
Figure 4.4: Monthly average Mixing height in Modena estimated by the COSMO meteorological model (Arpae Emilia-Romagna) during the whole 2016.....53
Figure 5.1: Wind-rose of the observed wind between 28 October and 8 November 2016 at the station placed on top to the Geophysical Observatory tower.....55
Figure 5.2: Overview of the WRF-Chem model domains on the left (Geographic coordinate system-WGS84) and PMSS investigation domain with the considered Modena street network represented as red lines on the right (UTM32-WGS84).....57
Figure 5.3: Total NO_x traffic emissions (SNAP sector 71-75) in the province of Modena. On the left the original TNO-MACC III inventory emissions (resolution ca. 14 km x 7 km). At the centre the TNO-MACC III inventory emissions downscaled to a resolution of 1 km x 1 km and distributed according to the street traffic flow estimated by PTV VISUM. On the right the TNO-MACC III inventory emissions downscaled to a resolution of 1 km x 1 km without the emissions by road traffic in the urban area of Modena.....64
Figure 5.4: PMSS computational domain (left side) and view of the radar traffic counters position (right side). Radars are represented by yellow dots, air quality urban background station by orange triangle and urban traffic station by blue triangle. Urban meteorological stations are also depicted by green dots along with their label names...65

Figure 5.5: Comparison between weighted NO_x hot EFs used in this study, computed following the EMEP/EEA guidelines (green rectangles) and the corresponding average NOx hot EFs computed between Germany, Austria, Switzerland, France, Norway and Sweden following the handbook of emission factors (HBEFA) version 4.1 (red rectangles). With horizontal black segment are also indicated the minimum and maximum HBEFA EF for the same six European countries. Please note the difference in the scale on the y-axis in each panel. 67
Figure 5.6: Map of the stations inside the WRF-Chem d03 domain. Site of the meteorological stations are reported by the green dots and site of air quality station are reported by the blue triangles. 73
Figure 5.7: Pearson correlation coefficient (r) reported as function of the Mean Bias (MB) between modelled hourly 2 m temperature (T2) and observation at 33 measurements sites for the three WRF-Chem resolutions: 15 km (d01), 3 km (d02) and 1 km (d03)... 75
Figure 5.8: Root Mean Square Error (RMSE) reported as function of the Mean Bias (MB) between modelled hourly 10 m wind speed (ws10) and observation at 27 measurements sites for the three WRF-Chem resolutions: 15 km (d01), 3 km (d02) and 1 km (d03)... 76
Figure 5.9: Mean Absolute Error (MAE) reported as function of the Root Mean Square Error (RMSE) between modelled hourly 10 m wind direction (wd10) and observation at 27 measurements sites for the three WRF-Chem resolutions: 15 km (d01), 3 km (d02) and 1 km (d03). 77
Figure 5.10: Factor of two (FAC2) reported in function of the Normalized Mean Bias (MB) between modelled hourly NOx concentrations and observation at 10 rural background sites for the three WRF-Chem resolutions: 15 km (d01), 3 km (d02) and 1 km (d03)... 79
Figure 5.11: Hourly observed wind speed at MOD (on top), at OSS (in the middle) and at POL (on bottom) meteorological site along with hourly simulated wind speed by Micro-SWIFT, from October 28 to November 8, 2016. 81
Figure 5.12: Hourly observed wind direction at MOD (on top), at OSS (in the middle) and at POL (on bottom) meteorological sites along with hourly simulated wind direction by Micro-SWIFT, from October 28 to November 8, 2016. 83
Figure 5.13: Scatter plots of predicted NO_x concentrations at urban traffic ("via Giardini") and urban background ("parco Ferrari") stations for different models configurations: PMSS combined with WRF-Chem at 3 km resolution (labelled as "d02+PMSS") and PMSS combined with WRF-Chem at 1 km resolution (labelled as "d03+PMSS")..... 85
Figure 5.14: Hourly observed concentrations of NOx at urban traffic (on top) and urban background (on bottom) measurements stations along with hourly simulated concentrations by WRF-Chem at 3 km resolution and PMSS combined with WRF-Chem at the same resolution, from October 28 to November 8, 2016. Please note the difference in the scale on the y-axis in each panel. 88
Figure 5.15: Overview of the diurnal cycle of the traffic emission intensity for WRF-Chem (light blue) and the average diurnal cycle for PMSS (red) for working and non-working days. 89

Figure 5.16: Mean daily cycle of observed NO_x concentrations (black), modelled by the combination of WRF-Chem and PMSS model (red) and the only contribution of WRF-Chem (light blue), by station type (traffic or background) and by WRF-Chem resolution (3 km or 1 km). Green lines show the mean daily cycle of planetary boundary layer height modelled by WRF-Chem and used in the micro-scale dispersion. Solid lines represent the daily mean cycle, meanwhile shaded area show the variability between 25th and 75th percentiles. 92
Figure 6.1: Observed mean daily temperature and mean daily wind speed at Geophysical Observatory tower between February 1 and February 28, 2019. 94
Figure 6.2: Wind rose of hourly wind on February 11 (on the left), 12 (in the centre) and 23 (on the right), observed at the Geophysical Observatory tower. 95
Figure 6.3: February 2019 wind-rose observed at the Geophysical Observatory tower 95
Figure 6.4: Overview of the WRF-Chem model domains on the left (Geographic coordinate system-WGS84) and PMSS investigation domain with the considered Modena street network represented as red lines on the right (UTM32-WGS84). 96
Figure 6.5: Location of the inductive loop spires (dots) and road streets network (segment). The colours represent the respective modulation computed from the cluster analysis and assigned to each spires and then to each roads according to the proximity between the road took as a reference and the nearest inductive loop sensor. 102
Figure 6.6: Cluster Dendogram related to the traffic modulation recorded by 230 inductive loop spires. At the bottom there are single clusters (leafs) and on top all the clusters are merged together in only one modulation (root). 103
Figure 6.7: Hourly modulation according to the day of the week of the two Clusters computed from the 230 inductive loop spires data (Cluster Classes 1 and 2) and from the traffic modulation campaign (Cluster Class 3). 105
Figure 6.8: Pearson correlation coefficient (r) reported as function of the Mean Bias (MB) between modelled hourly 2 m temperature (T2) and observation at 20 measurements sites for the two WRF-Chem resolutions: 15 km (d01) and 3 km (d02). 109
Figure 6.9: Root Mean Square Error (RMSE) reported as function of the Mean Bias (MB) between modelled hourly 10 m wind speed (ws10) and observation at 19 measurements sites for the two WRF-Chem resolutions: 15 km (d01) and 3 km (d02). 110
Figure 6.10: Mean Absolute Error (MAE) reported as function of the Root Mean Square Error (RMSE) between modelled hourly 10 m wind direction (wd10) and observation at 19 measurements sites for the two WRF-Chem resolutions: 15 km (d01) and 3 km (d02). 111
Figure 6.11: Factor of two (FAC2) reported in function of the Normalized Mean Bias (MB) between modelled hourly NO_x and NO_2 concentrations and observation at 10 rural background sites for the two WRF-Chem resolutions: 15 km (d01) and 3 km (d02). 113
Figure 6.12: Hourly observed wind speed at MOD (on top), at OSS (in the middle) and at POL (on bottom) meteorological site along with hourly simulated wind speed by Micro-SWIFT, from February 1 to February 28, 2019. 115

Figure 6.13: Hourly observed wind direction at MOD (on top), at OSS (in the middle) and at POL (on bottom) meteorological sites along with hourly simulated wind direction by Micro-SWIFT, from February 1 to February 28, 2019. 117
Figure 6.14: Scatter plots of predicted NO, NO_2 and NO_x concentrations by PMSS combined with WRF-Chem at 3 km resolution, at urban traffic ("via Giardini") and urban background ("parco Ferrari") stations. 119
Figure 6.15: Mean daily cycle of observed NO, NO_2 and NO_x concentrations (black), modelled by the combination of WRF-Chem and PMSS model (red) and the only contribution of WRF-Chem (light blue), by station type (traffic or background). Green lines show the mean daily cycle of planetary boundary layer height modelled by SURFPRO and used in the micro-scale dispersion. Solid lines represent the daily mean cycle, meanwhile shaded area show the variability between 25th and 75th percentiles. 124

List of Tables

Table 5-1: WRF-Chem model set-up and parameterisation. 58
Table 5-2: Micro-SWIFT and Micro-SPRAY set-up 61
Table 5-3: Observation sites. Locations are provided in Geographic coordinates (WGS84). Available parameters are: "T2" for temperature at 2 m height above the ground, "ws10" for wind speed and "wd10" for wind direction at 10 m above the ground and "NO_x" for NO_x concentrations. 71
Table 5-4: Statistics of hourly wind speed computed for the period between October 28 and November 8 at three urban meteorological stations. MB and RMSE are expressed in m s^{-1}. 81
Table 5-5: Statistics of hourly NO_x concentrations computed for the period between October 28 and November 8, considering two different model configurations. 86
Table 6-1: WRF-Chem model set-up and parameterisation. 97
Table 6-2: Micro-SWIFT and Micro-SPRAY set-up for the forecast case study 100
Table 6-3: Mass fraction of NO_2 in NO_x emissions (f-NO_2) expressed for different Emission Standard and Category 100
Table 6-4: Number of clusters suggested by sixteen different indices computed considering four different distance methods. 104
Table 6-5: Observation sites. Locations are provided in Geographic coordinates (WGS84). Available parameters are: "T2" for temperature at 2 m height above the ground, "ws10" for wind speed and "wd10" for wind direction at 10 m above the ground, "NO", "NO_2" and "NO_x" respectively for NO, NO_2 and NO_x concentrations. 106
Table 6-6: Statistics of hourly wind speed computed for the period between February 1 and February 28 at the three urban meteorological stations. MB and RMSE are expressed in m s^{-1}. 116
Table 6-7: Statistics of hourly NO, NO_2 and NO_x concentrations computed for the period between February 1 and February 28. 120

1. Introduction

Air pollution is the biggest environmental risk to health and according to the World health Organization report ("WHO | Ambient air pollution", 2016), is responsible for about one in every nine deaths annually worldwide. Outdoor air pollution alone accounts for an estimated 4.2 million deaths each year and only one person in ten lives in a city that complies with the WHO air quality guidelines. At the same time almost three billion people worldwide continue to live in an economy based on biomass fuels, kerosene and coal for their energy needs, increasing the environmental pressure at an alarming rate which dramatically affects people's quality life.

The main source of ambient air pollution can be addressed to the burning of fossil fuels (electricity production, industry or transport), the solvent use in industrial processes, the waste management (incinerators, landfills, composting plants) and the emissions produced by all agricultural practices such as crops and farms. It is worth saying that human activities are not the only responsible for pollution level, but volcanic eruptions, windblown dust, sea-salt spray and emissions of volatile organic compounds from plants are examples of natural emission sources that can also contribute to local air quality. Other forms of air pollution are based on mechanical and chemical processes that involved precursors: primary pollutants in the atmosphere react producing secondary pollutants. The most popular example of secondary pollutant is the tropospheric ozone, which is not emitted by any natural or anthropogenic sources but is formed when hydrocarbons (HC) and nitrogen oxides (NO_x) combine in the presence of sunlight.

Concurrently with these phenomena, household air pollution led to more than 4 million premature deaths each year among children and adults mostly in low and middle income countries by the combustion of dung, wood and coal in inefficient stoves or open hearths. The main pollutants generated with these processes are particulate matter, methane, carbon monoxide, polyaromatic hydrocarbons and volatile organic compounds, which indoor exposure can lead to a wide range of adverse health outcomes, from respiratory illnesses to cancer, to eye problems and may also cause a higher risk of burns, poisonings,

musculoskeletal injuries, increased blood pressure for pregnant women and accidents (Quinn et al., 2016, 2017; White and Sandler, 2017).

Air pollution in Europe, as reported in the last European Environmental Agency report ("Air quality in Europe 2019", 2019), continues to have significant impacts on the health of the population, particularly in urban areas with a higher population density where a complex mixture of pollutants is produced by inefficient combustion of fuels in internal combustion engines, power generation and other human activities like domestic heating and cooking. The three most serious pollutants in terms of harm to human health are fine particulate matter ($PM_{2.5}$), nitrogen dioxide (NO_2) and ground-level ozone (O_3). Relative health impacts attributable to exposure to air pollution indicate that $PM_{2.5}$ concentrations in 2016 were responsible for about 412 000 premature deaths originating from long-term exposure in Europe (Colette et al., 2016). By contrast the estimated impacts of exposure to NO_2 and O_3 concentrations in 2016 were around 71 000 and 15 100 premature deaths per year.

Air pollution also has several important environmental impacts which can affect vegetation, the quality of the water and the soil as well as the climate and the global warming. For example, nitrogen oxides (NO_x, the sum of nitrogen monoxide NO, and NO_2), and ammonia (NH_3) emissions can damage the ecosystems by introducing an excessive amount of nitrogen nutrients increasing the eutrophication phenomena and leading changes in species diversity. NO_x together with SO_2 may also lead to the acidification processes of lakes, rivers and soil causing loss of biodiversity. Moreover, O_3 can damages crops and plants by several types of symptoms including chlorosis and necrosis which direct effects are the reduction of their grown rate and the loose of biodiversity and ecosystem services. Finally, several air pollutants are also climate forcers: tropospheric ozone, methane (CH_4) and black carbon (BC) are example of species that are short-lived climate forcers and can contribute directly to global warming.

Vehicular traffic related air pollution is ranked as a major emission source that can affect air quality in the cities. Even though this is especially problematic in many low- and middle-income countries where the number of motor vehicles is rapidly increasing and existing environmental regulations are weak or not well enforced, it continues to be a serious problem also in most developed countries, posing different challenges in terms of mitigation and stewardship.

In addition to the well-documented air pollution adverse respiratory and cardiovascular health effects, in the last years toxicological and epidemiologic studies pointed out that pollutants generated by traffic and other urban air sources are toxic to the central nervous system of children and adults (Annavarapu and Kathi, 2016; Costa, Chang, et al., 2017). In particular, fine particulate matter ($PM_{2.5}$) may lead to central nervous system damage (Fonken et al., 2011; Win-Shwe et al., 2008, 2012) and ultrafine particulate matter (UFP) also has the capacity to pass through the blood-brain barrier and appears to be capable of creating perturbations in central nervous system functioning (Block and Calderón-Garcidueñas, 2009; Costa, Cole, et al., 2017; Peters et al., 2006).

Recent papers have also highlighted new health problems, not deeply studied in past, related to the exposure of pollution due to traffic emissions. Two of these documented effects are the increased child-reported depression and anxiety from diesel vehicular exhaust products (Yolton et al., 2019) and also the impact on memory, verbal, and general cognition in children (Lertxundi et al., 2019). A second aspect that has been shown to affect the health issues is the proximity to the source. Bowatte et al., (2018) found that living closer to major roads at a distance less than 200 meters, increase the incidence and persistence of asthma in the population. Meanwhile, Khan et al., (2019) discovered that children that live at a distance less than 100 meters of heavy traffic pathways demonstrated to be affected of neurobehavioral impairment like deficits in memory, attention, and coordination.

Effective actions to reduce the impact of air pollution effects on human health have proved to be very successful in a number of documented studies. The main effects they brought were the decrease in mortality risk, especially cardiovascular and respiratory (Laden et al., 2006), increased lung function in children with and without asthma (Gauderman et al., 2015) and the decreasing in asthma incidence (Abrams et al., 2019; Garcia et al., 2019).

Based on the positive effects that a reduction in pollution level can give, the European Union developed an extensive legislation which established standards and objectives for a number of pollutants in air (2008/50/EC Directive on Ambient Air Quality and Cleaner Air for Europe and 2004/107/EC Directive on heavy metals and polycyclic aromatic hydrocarbons in ambient air). These directives set pollutant concentrations thresholds that shall not be exceeded in a given period of time and in case of exceedances, authorities must develop and implement air

quality management plans aiming to bring concentrations of air pollutants to levels below the limit and target values.

One of the novelties presented in the 2008/50/EC Directive was the coupling of air quality measures with the use and application of models as either a tool to provide supplementary information or for assessment purposes when reporting exceedances of air quality standards.

Despite the air quality models produce outputs with higher level of uncertainty with respect monitoring stations, their use in combination with measures can be beneficial for a number of applications. The main advantages can be summarized in three key points: firstly, measures have a distribution limited in space, by contrast models can cover large areas providing concentrations on a regular grid also where monitoring is not carried out. Secondly, modelling can be used to produce air quality forecast over a specific portion of the earth by the means of prognostic equations that can simulate the meteorological and chemical process in order to predict atmospheric concentrations. Finally, model output results are directly linked with the emissions considered in the computation, for this reason they can be employed to estimate the sources, the causes and the processes that generate air pollution.

Models obviously do not provide all the answers related to the reduction and management of air pollutants, indeed they are affected by a series of limitations that prevent them to be the only integral solution for any environmental problem. Among the main limitations that characterize models there is the uncertainty in their predictions: non-linear processes that occur in real atmosphere are usually linearized into models code to keep the computing time limited and to not discretize the process in a too complex way; a second aspect is also that not all the variables are resolved to describe a process, but it is common to omit the less important of them to keep the problem simple. Moreover, air quality modelling system nowadays accounting for an increasing number of coupled physical processes described using hundreds of modules, introducing a portion of uncertainty in the final computation. Furthermore, air quality modelling systems typically depend on external sources for the inputs of meteorology and emissions data, as well as for boundary conditions. These fields are generally produced by other models and after a pre-processing procedure are used by air quality modelling systems with no guarantee of being unbiased and/or accurate. The last limitation, but not less important than the others, are the competences required for controlling and interpret the results provided by these complex tools, which need expert users with qualified skills.

The Po Valley, located in the northern part of Italy, is one of the areas with the most severe air pollution problems in the country and in Europe. The reason to this issue is not only related to the high population density with its related activities, but it is also due to the orographic conformation of the territory which appears surrounded by mountains on three sides: the Alps to the west and to the north and the Apennines to the south. These geographical characteristics lead to meteorological conditions unfavorable to the atmospheric dispersion: average annual wind speed less than 2 m s^{-1}, recurrent thermal inversions at low altitude, low mixing layer heights and persistent foggy and hazy events during winter time.

One of the main critical air pollutants in terms of health effects that affect this region is nitrogen dioxide (NO_2), whose concentrations levels in the last years exceeded national and WHO standards in many urban areas across the Po Valley, exposing urban population to the risk of pollution-related diseases and health conditions.

The present thesis has as its goal the estimation of the air quality in the urban area of Modena, a city in the central Po Valley, in terms of NO_x ($NO + NO_2$) atmospheric concentrations. More in detail, the aim of the project is to support environmental policies, epidemiological studies and urban planning and management.

Current approaches to produce spatial maps of urban air pollution include the use of interpolation methods and land-use regression (LUR) models (Hoek et al., 2008; Ryan and LeMasters, 2007; Sahsuvaroglu et al., 2006). However, all these techniques need a large number of in-situ observations at strategic locations to represent the full spatial and temporal pollutant variability and cannot be used to take into account turbulent atmospheric dispersion. To meet this need, a variety of micro (Moussafir et al., 2004; Oettl, 2015) and local (Tinarelli et al, 1992; Bellasio and Bianconi, 2012; Cimorelli et al., 2005) scale air dispersion models have been developed in the last few years, as they can provide a high-resolution information on air pollution level within urban city area by taking into account space-time emissions distribution and local meteorological characteristics (Ghermandi, Fabbi, et al., 2015; Ghermandi, Teggi, et al., 2015).

A key issue is the quantitative estimation of the different contribution to air pollution level from emissions sources located within the city urban environment and from countryside areas, also known as rural background. An approach that has been used for several years to account for both urban and rural contribution is generally called “Lenschow” approach (Lenschow et al., 2001), which envisages the influence of a city as the difference between the

concentrations in the urban environment and the concentrations at rural site. This methodology is generally applied in source apportionment studies in order to estimate the primary and secondary component of PM by means of receptors models (Bove et al., 2014; Pirovano et al., 2015), or in urban impact assessments through an approach combining measurements and modelling results. In this latter case, the model is used to evaluate the contribution (effects) of the sources located within the city, while measured background concentrations are added to the simulated concentrations to account for remote sources outside the simulation domain (Berchet et al., 2017; Ghermandi et al., 2019).

Despite the flexibility in enforcing measured-based activity and modelling results, a number of criticisms related to the applicability of this methodology were recently highlighted. Following Thunis, (2018) the city urban impact can be defined as the sum of three components: the Lenschow urban increment, which is the concentration difference between the city and background locations, the "city spread" meaning the impact of the city at the rural background location, and the "background deviation" that quantifies the concentration difference between city and background location when city emissions are set equal to zero. According to this definition, the "Lenschow" approach can be correctly employed only when the "city spread" and the "background deviation" are negligible or compensate each other, i.e. the urban impact in background area is close to zero and when background levels are spatially homogenous.

An alternative approach to quantify the different contributions to air pollution in the city is based on Chemical Transport Models (CTMs) which, unlike the Lenschow incremental approach, are able to generate different emission scenarios on multi spatial scale, from regional to local, which can be exploited to estimate background concentrations keeping city emissions set to zero.

Based on the advantages given by CTMs, the methodology employed in this study was a modelling activity relied on the NO_x dispersion by combining two different models: the Weather Research and Forecasting (WRF) model coupled with Chemistry (Grell et al., 2005), which is able to compute concentrations fields over regional domain by considering specific emission scenarios, and the Parallel Micro SWIFT and SPRAY (PMSS, Moussafir et al., 2013, Oldrini et al., 2017) modelling suite accounting for dispersion phenomena within the urban area.

In this project, the PMSS modelling suite was used to simulate at building-scale resolution the NO_x dispersion produced by urban traffic flows in the city of Modena. Conversely, the WRF-Chem model simulations were performed to estimate the NO_x background concentrations on multiple domains with a nesting technique, in order to take into account emissions both at regional and local scale by excluding traffic emissions sources over the city of Modena.

In the first part of the thesis (Chapter 2) the most relevant theoretical aspects of pollutant dispersion modelling are presented. Chapter 3 provides an overview regarding the exhaust traffic emissions formation, the different methodologies suggested by the European Environmental Agency to estimate them as well as the description of the tool used in this project to account for NO_x emissions for the city of Modena. Chapter 4 provides an overview of the case study. Chapter 5 is devoted to the estimation of the NO_x concentration in the urban area of Modena between 28 October and 8 November 2016, the same period whereby a traffic measurement campaign was carried out. In Chapter 6 the hybrid modelling system developed in this study is applied to provide hourly forecast of NO_2 and NO concentrations, up to one day ahead, for the entire month of February 2019. Finally in the last Chapter (7) the conclusions of the project are highlighted.

2. Models background

2.1 Models introduction

As introduced in the previous chapter, a model is a simplified representation of the reality. It doesn't contain all the features of the real system but contains only the characteristics of interest for the scientific problems we wish to solve by its use. Models are widely used in different science sectors to make predictions or to solve issues and are often used to identify the best solutions for the management of specific environmental problems.

Contaminants discharged into the air can be transported over long distances by large scale air flows and dispersed by small scale winds or turbulence, which mix contaminants with clean air. This dispersion is a very complex process due to the presence of different sized eddies in atmospheric flow. Even under ideal conditions in a laboratory, the dynamics of turbulence and turbulent diffusion are some of the most difficult processes to model in fluid mechanics. The governing equation of the air flow motion is provided by the conservation principles like the conservation of mass and momentum. The main difficulties in getting a general solution for the formulas describing the turbulent flows essentially arise from: the non-linearity of the equations, the three-dimensional character of the velocity field and the enormous number of scales involved in such motion. The first point means that it is not possible to find analytical solutions to the equations. Secondly, the high computational cost required to find a numerical solution for all the scales involved pushed the scientists in the past to find a statistical methods for studying a random velocity field.

Investigation of fate of pollutant emissions in the atmosphere is extremely complex, since they depend on the meteorological condition and also on physical and chemical transformations that can occur. Indeed, pollutants concentrations do not depend only on emissions and dispersion phenomena, but they are also affected by wet and/or dry deposition processes and by chemical reactions that can decrease their amount in a specific portion of the atmosphere.

Atmospheric phenomena at any specific scale are influenced by the ensemble of interacting processes occurring at various scales. The phenomena at local and urban scales have a horizontal extension that span from several meters to hundreds of km and have a characteristic time scale from several minutes to several days. The same spatial-temporal

characteristics can be found also for pollutants driven by the atmospheric motion. Despite the atmosphere presents these multi-scales features, from a practical point of view, not all the motions occurring in reality can be simulated at the same time by enforcing a single modelling system: the computational effort required to perform a simulation like this would not be feasible for any machine made up to now. In fact, the common modus operandi for atmospheric modelling that has been proven to be quite successful is to adopt a scale separation procedure by approximating and parametrising the scales of motion which are not suited for the particular interest. Specific scale models should be capable of simulating in detail phenomena occurring in that scale.

Local scale simulations are widely used to assess the contributions to air pollution from different anthropogenic sources mainly vehicular traffic, industrial areas and power-plants that are present on the simulation domain (from 10 km up to 100 km). This type of models should be applicable for simulations of orographic effects, urban heat island and land-sea breezes, while the smaller scale phenomena (small turbulence eddies) are parameterised.

As well as larger scale phenomena (e.g. climate analysis or trans-boundary pollution) need to be considered in larger spatial domains such as mesoscale (100 - 1 000 km) or synoptic scale (over 1 000 km) simulation: large scale winds have greater importance with respect to small vortex that can be generated for mechanical turbulence due to the friction between the air and obstacles. For these reasons, smaller scale winds have to be prescribed in an urban scale model and a nesting approach is the most useful technique used to investigate a sub-domain with increased spatial resolution.

On the other hand, in urban areas where the effects of obstacles on wind flow and pollutant behaviour are not completely negligible, we distinguish urban scale models which relative domain is the size of a town or a part of the city (up to 10km x 10km) and street canyon models, suited for describe processes that occur inside street canyons where the forcing on wind field induced by the presence of buildings need to explicitly resolved.

In local scale modelling the simulations usually span over the period of weeks or months in order to analyse different meteorological conditions according to seasonality. By contrast, since their scope is to study a particular event in a very complex environment, simulations executed in a very high resolution domain (spatial scale in the order or meters) have a time scale that span over a daily or hourly period.

As urban air quality has become more and more important part of environmental and health protection, innovative modelling techniques have recently focused on urban micro-scale simulation of pollutant dispersion within a complex environment. The role of this type of models is to estimate the pollutants concentrations in the lowest portion of the atmosphere affected by small scale vortex which relative wind circulation has greater impact with respect synoptic scale meteorology condition. The reason why the scientific community is interested in study this portion of the atmosphere is due to the fact that human population lives close to the ground, thus their health condition can be directly influenced by the pollutants concentrations that persist in this ambience.

In order to simulate the dispersion phenomena within urban canopy the geometry of buildings and the shape of other relevant obstacles like bridges, tunnels or galleries need to be reconstructed inside the computation domain. At the same time the micro-scale models need to be able to account for these complex structures when simulating the 3D wind field and the turbulence eddies generated in the narrow zone among building facades. Target of these models can be road traffic or domestic heating emissions and emergency response in case of industrial accident, malicious or terroristic attack.

Since the applications of this type of models are not designed for seasonal variability or for multi-year analysis, also the time scale which characterizes them is very different, as introduced before, generally it spans over hourly or daily time lapse. The second reason why these simulations have limited time extension is the CPU demand that they need, which explain also the limited diffusion of CFD (computational fluid dynamics) models in urban dispersion modelling.

From a technical perspective, an air quality modelling system consists by three main parts: a meteorological model, an emissions model, and an air quality model. The meteorological model calculates as a function of time the three-dimensional fields of wind, temperature, relative humidity, pressure, and in some cases, turbulent eddy diffusivity, clouds and precipitation. The emissions model estimates the amount and the chemical speciation of primary pollutants based on the source characteristics. Taking into consideration for example traffic emissions, their pollutant rate depends on the vehicle fluxes, which differ for working and not working days and for every month of the year, but not only, related emissions vary also in space, due to the different traffic load which each street is characterized. Finally, the outputs of the emission and meteorological models are input into the air quality model, which

calculates the concentrations and deposition rates of gases and aerosols as a function of space and time.

The mathematical models are the most used type of models nowadays, they are suited to describe a specific system by a set of mathematical relationships and equations which simulate the physics and the chemistry governing the transport, dispersion and transformation of pollutant in the atmosphere. Mathematical models are divided into two main classes: deterministic and stochastic models. In the field of atmospheric pollution deterministic models are based on cause-effect relationships, otherwise the latter one are based on statistical analysis of data, i.e. on previous measures at fixed points and only for those points it is possible to predict the future value of pollutants concentration. Stochastic models are used where it is possible to have a high number of measurements available and therefore they are generally used in urban or industrial contexts, where for example a real-time control and alarm levels are required. Deterministic models are the most used, the input variables that characterize them assume fixed values and the results obtained do not take into account possible factors of uncertainty (unlike stochastic models).
The deterministic models aim to quantitatively reconstruct the phenomena that regulate the space-time evolution of the pollutants concentration in the air. Based on the different perspective of observing and describing the properties of a specific fluid two main types of numerical models are distinguished: Eulerian and Lagrangian.

2.1.1 Eulerian models

The Eulerian models refer to a fixed coordinate system and the pollutant transport is estimated by integrating the differential diffusion Equation (2.1), obtained from the mass balance applied to an infinitesimal volume of air under certain hypotheses that allow obtaining a solution to the problem. The main simplification hypothesis considers that the molecular diffusion is negligible with respect to turbulence, the wind vertical component is negligible (not acceptable in case of land-sea breeze or in presence of complex orography), the horizontal turbulent diffusivity coefficient depends only on the vertical coordinate but it is independent from the two horizontal coordinates and the removal processes are negligible if the considered pollutant is inert or poorly reactive.

$$\frac{\partial C}{\partial t} = -\nabla(\boldsymbol{v}C) + \nabla\left(\overline{\overline{K}} \cdot \nabla C\right) + \nabla(D \cdot \nabla C) - R + S \tag{2.1}$$

Where C is the pollutant concentration, $\boldsymbol{v}$ is the vector velocity, D the molecular diffusion coefficient, $\overline{\overline{K}}$ the turbulent diffusivity tensor and R and S are respectively a removal and source factor. Depending on how the differential Equation (2.1) is solved, three types of models are available: analytical models (puff or Gaussian), box models and grid models.

Gaussian analytical models are able to describe the ground down-wind pollutant concentrations due to a continuous point source, and plume shows a Gaussian pollutant concentration profile along the perpendicular axis of the main wind direction. They are easy to use because they adopt a series of simplifications such as stationary and homogeneity of weather conditions, horizontal wind speed in the main wind direction not equal to zero and on average equal to zero on the orthogonal plane on it, flat terrain and absence of chemical transformations. The drawback is the coarse approach to the description of atmospheric turbulence, they lack of precision in simulating pollutant dispersion in low-wind and calm conditions and in presence of thermal inversion. Therefore, the Eulerian Gaussian models are only suitable to describe average seasonal conditions without critical events.

The puff models represent an extension of the Gaussian models and allow reconstructing the pollutant concentrations in non-homogeneous and non-stationary conditions. The

concentration value in a point is the sum of the contributions of various puffs within the domain, which distribution always follows a Gaussian law.

Eulerian box model enclose a region of the atmosphere into one or more cells to have a height, equal for example to the mixing layer height in which pollutants are considered perfectly mixed. This mixing height may be allowed to vary diurnally to simulate the evolution of the atmospheric mixing state. The model is based on the mass conservation of a species inside a fixed Eulerian box and this simplifications, knowing some fundamental parameters such as background concentrations, wind velocity and directions, allows rewriting the mass balance equation in an easy solvable way.

Grid models, as for the box approximation, divide the computation domain into three-dimensional cells within which the solution of the atmospheric differential diffusion equation is obtained by applying finite difference techniques, able to give a concentration value for each grid cell. Increasing the number of node the computational complexity increases as well, for this reason the resolution of this type models cannot be in the order of meters but generally the horizontal dimension of the cells is a few kilometers, while the vertical dimension is a function of the atmospheric layers that must be studied (from a few meters to hundreds of kilometers).

2.1.2 Lagrangian models

The second type of models is the so called Lagrangian particle dispersion models (LPDM), which provide an alternative method for simulating atmospheric diffusion. The main difference between the Eulerian and Lagrangian view is that the Eulerian reference system is fixed (with respect to the earth) while the Lagrangian reference system follows the instantaneous fluid velocity. In a Lagrangian particle model the moving fluid is divided in a multitude of small particles that move independently from one to each other following stochastic trajectories, hence the airborne pollutant dispersion is simulated by diving pollutant mass flow in a set of virtual particle, whose number is proportional to the mass flow that move in the atmosphere. The fictitious particles are considered small enough to follow the motion of smallest eddies and, at the same time, big enough to contain a large number of molecules so that interactions among molecules are not taken into account during the particle motion. The motion of these air masses (or particles) at each time step is characterized by a transport component, due to the mean wind, and by a diffusion term, related to the turbulent wind velocity fluctuations.

In the single particle models, the trajectory of each particle represents an individual statistical realisation in a turbulent flow characterised by certain initial conditions and physical constraints. Therefore the motion of any particle is independent of the other particles, and consequently the concentration field must be interpreted as an ensemble average. Following this approach the concentration C at time t and located in x will be given by this basic relationship:

$$C(t,x) = Q\ P(x,t \mid x_0,t_0) \tag{2.2}$$

Q is the emitted mass at time $t = 0$ and $P(x, t \mid x_0, t_0)$ is the probability that a particle that was at x_0 at time t_0 arrives at x at time t. To compute $P(x, t \mid x_0, t_0)$ it is necessary to release a large number of particles, to follow their trajectories and to calculate how many of them arrive in a small volume surrounding x at time t. It is worth noting that particles move in the computational domain without any grid, using as input the values of the first two or three moments of the probability density distribution of wind velocity at the location of the particle. This input information comes either from measurements or from parameterisations

appropriate to the actual stability conditions (unstable, neutral, stable), to the type of site (flat, complex terrain, coast side), and to the time and space scales considered.

The basis assumption behind this theory is that spatial and temporal evolution of turbulent field is affected by random fluctuations that cannot be adequately predicted through a deterministic approach. Furthermore, following the Reynolds hypothesis for turbulence description (Reynolds, 1895), the velocity of a particle is divided in an average and a fluctuating stochastic part (2.3): the former corresponds to the mean velocity of the local wind; the latter depends on the statistical variables of turbulent flow.

$$u_i = \overline{u_i} + u'_i \tag{2.3}$$

Taking into consideration a Cartesian frame 0xyz, *i* is one of the three axis directions (*x*, *y* or *z*). The Reynolds hypothesis leads to compute the generic component of particle velocity u_i as the sum of a mean ($\overline{u_i}$) and a stochastic term (u'_i). The mean wind velocity, which is assumed constant over a fixed time lapse, equals the mean velocity of the local wind at any single point of particle trajectory and the position of any single particle can be computed at discrete time steps (Δt) by means of the Equation (2.4), considering as before *i* as one of the three axis directions.

$$x_i(t + \Delta t) = x_i(t) + [\overline{u_i} + u'_i(t)]\,\Delta t \tag{2.4}$$

The input information needed to resolve these equations are the three-dimensional wind field, the wind speed variation around its mean value and the discrete time step Δt. The first one is usually computed externally by a meteorological model, which provides in a 3D structure the wind component for each domain cell, conversely the time step is fixed and it can be usually chosen by the model user. Finally, the fluctuation terms, due to the turbulent properties of the fluid motion, are computed internally by the model solving the Langevin Equation (2.5). This equation was introduced for the first time by Einstein in 1905 on the explanation of Brownian motion where the concept of stochastic modelling of natural phenomena was introduced for the first time. Three years later Langevin proposed an alternative method to explain Brownian motion, in which it is assumed that two forces act on each particle are divided into a

deterministic one, representing the viscous drag, and a stochastic one, accounting for the random impacts of the other molecules of the liquid.

$$\frac{\partial u'_i(t)}{\partial t} = -\beta\, u'_i(t) + \alpha\, \mu(t) \tag{2.5}$$

Where μ is a random function and β and α are two constants. In the application of turbulent dispersion the two terms in the Equation (2.5) represent the friction force exerted by the flow on the particle (the deterministic term) and the accelerations caused by pressure fluctuations (the stochastic term).

Following the Taylor approach to turbulence i.e. considering correlated particles displacements, the mean square value of the displacement is proportional both to the time elapsed from the emission in the first phase of the diffusion process and to the square root of time for "longer" times (Taylor, 1921). Therefore, the deterministic coefficient can be computed by taking into account the historical evolution of particle velocity. Let $P(u_i, t)$ be the probability density function, i.e. $P(u_i,t) \cdot du_i$ is the probability that the value for the u_i velocity component fall in the range among u_i and $u_i + du_i$. The statistical correlation function $\rho_i(t, \tau)$ between random particle velocities at time t and $t + \tau$, where τ is the elapsed time between two observations, is defined as in Equation 2.6 (Finzi, 2001):

$$\rho_i(\mathrm{t},\tau) = \frac{\overline{u_\iota(t)\, u_\iota(\mathrm{t}+\tau)}}{\overline{u'^2{}_\iota(t)}} \tag{2.6}$$

The statistical correlation values span between 0 and 1, in the first case there is no correlation and the velocity at time t and $t + \tau$ are stand-alone, by contrast on the latter case velocities are really high correlated.

In homogeneous and steady state conditions of turbulence applying the Taylor theory to the Langevin Equation (2.5), the term β^{-1} is substituted with the Lagrangian time scale T_{Li}, defined as follow:

$$T_{Li} = \int_0^\infty \rho_i(\tau)\, d\tau \tag{2.7}$$

Through the discretization of Equation (2.5), the general expression for the turbulent velocity $u'_i(t)$ is given by the Equation (2.8), where considering a Cartesian frame 0xyz, *i* and *j* are one of the three axis directions, $\boldsymbol{x} = \boldsymbol{x}(t) = [x_x(t), x_y(t), x_z(t)]$ the vector position and $\boldsymbol{u} = \boldsymbol{u}(t) = [u_x(t), u_y(t), u_z(t)]$ the velocity vector.

$$du'_j = a_i(\boldsymbol{x}, \boldsymbol{u})dt + b_{ij}(\boldsymbol{x}, \boldsymbol{u})dW_j(t) \tag{2.8}$$

In the Equation (2.8), the term $a_i(\boldsymbol{x}, \boldsymbol{u})dt$ is the deterministic term, on the other hand $b_{ij}(\boldsymbol{x}, \boldsymbol{u})dW_j(t)$ is the stochastic part and quantity $dW_j(t)$ is the incremental Wiener process with average 0 and variance *dt*. The diffusion coefficient $b_{ij} = \sqrt{C_0\varepsilon}$ (Monin and Yaglom, 1971; Du, 1997) describes the energy dissipation phenomenon due to the turbulence eddies according to the Kolmogorov theory for turbulence (1941). C_0 is a universal empirical constant, which is usually equal to 2, and ε is the dissipation rate of turbulent kinetic energy. The deterministic term $a_i(\boldsymbol{x}, \boldsymbol{u})$ depends on the probability density function of the turbulent velocity, $P(u_i,t)$. When $P(u_i,t)$ has Gaussian form the drift coefficient assumes the following general expression (Sozzi, 2003):

$$a_i(\boldsymbol{x}, \boldsymbol{u}) = -\left(\frac{C_0\varepsilon}{2\sigma_{ui}^2}\right)u'_i(t) + \frac{1}{2}\frac{\partial\sigma_{ui}^2}{\partial i} \cdot \left\{1 + \frac{[u'_i(t)]^2}{\sigma_{ui}^2}\right\} \tag{2.9}$$

In the Equation (2.9), the spatial derivatives take into account the non-homogeneity of turbulence field and σ_{ui}^2 is the variance of the speed component u'_i, where *i* is the *x*, *y*, *z* axis directions.

It can be demonstrated (Tennekes, 1979) that Lagrangian time scales T_{Li} can be expressed as in Equation (2.10):

$$T_{Li} = \frac{2\sigma_{ui}^2}{C_0\varepsilon} \tag{2.10}$$

Through the substitution of Eq. (2.9) and (2.10) in Eq. (2.8) the general expressions for the horizontal components of the stochastic particle velocity in Gaussian, stationary and non-homogeneous turbulent conditions are expressed by Equations (2.11) and (2.12). When these

equations are implemented in a Lagrangian particle model τ becomes the time step Δt of integration.

$$u'_x(t+\Delta t) = \left(1-\frac{\Delta t}{T_{Lx}}\right)u'_x(t) + \sigma_{ux}\sqrt{2\frac{\Delta t}{T_{Lx}}}u''_x(t) + \frac{1}{2}\frac{\partial\sigma^2_{ux}}{\partial x_x}\cdot\left\{1+\frac{[u'_x(t)]^2}{\sigma^2_{ux}}\right\}\cdot\Delta t \quad (2.11)$$

$$u'_y(t+\Delta t) = \left(1-\frac{\Delta t}{T_{Ly}}\right)u'_y(t) + \sigma_{uy}\sqrt{2\frac{\Delta t}{T_{Ly}}}u''_y(t) + \frac{1}{2}\frac{\partial\sigma^2_{uy}}{\partial x_y}\cdot\left\{1+\frac{[u'_y(t)]^2}{\sigma^2_{uy}}\right\}\cdot\Delta t \quad (2.12)$$

$$u'_z(t+\Delta t) = \left(1-\frac{\Delta t}{T_{Lz}}\right)u'_z(t) + \sigma_{uz}\sqrt{2\frac{\Delta t}{T_{Lz}}}u''_z(t) + \frac{1}{2}\frac{\partial\sigma^2_{uz}}{\partial x_z}\cdot\left\{1+\frac{[u'_z(t)]^2}{\sigma^2_{uz}}\right\}\cdot\Delta t \quad (2.13)$$

Where $u''_x(t)$, $u''_y(t)$ and $u''_z(t)$are random, uncorrelated, velocity terms.

These three Equations, (2.11) (2.12) (2.13) in their discretized form, combined with the position Equations (2.4) in the three axis directions (with i equal to x, y and z considering a Cartesian frame 0xyz), allow to predict the motion of a particle along its trajectory from a probabilistic point of view.

It is worth noting that, despite the Equations (2.11) and (2.12) are generally a good approximation for turbulence statistics for a wide range of atmospheric conditions, the Gaussian formulation expressed by (2.13) is a valid approximation of the reality only when high atmospheric stability occurs. Furthermore, when the atmosphere is characterized by intense convective phenomena due to the inhomogeneous thermal behavior of the terrain, unstable condition occur. During this situation the statistical distribution is asymmetric and the Gaussian formulation for the vertical motion is no longer valid, thus the probability $P(u_z, t)$ for u'_z must be a moment of the third or fourth order. In literature several non-Gaussian statistical formulations have been proposed and the most implemented are the bi-Gaussian probability density function (Weil, 1990; Anfossi et al., 1996) and the Gram-Charlier series expansion (Anfossi et al., 1997; Ferrero and Anfossi, 1998).

With the aim of solving Equations (2.11) (2.12) and the Equation for u'_z in a Gaussian (2.13) or non-Gaussian form, statistical description of the turbulence field is required and this can be achieved by estimating the Lagrangian time scales T_{Lx}, T_{Ly} and T_{Lz} and the velocity variance σ_{ux}^2, σ_{uy}^2 and σ_{uz}^2. In literature many different schemes are proposed (Hanna 1982; Irwin 1983; Hanna and Chang, 1991), and basically most of them are used to describe the turbulence at different hour of the day on the basis of parameters: z_0, u*, L, h, w* and h_{res}.
Quantities z_0, u* and L respectively represent the roughness length, friction velocity and Obukhov's length. Roughness length, is a measure of the terrain roughness, and represents the vertical level where the mean wind velocity is equal to zero, its value is about a tenth of the average height of the elements constituting the roughness of the surface (buildings, trees and so on).
Friction velocity u* is a representation form of the vertical turbulent momentum flux close to the ground, by contrast the absolute value of Obukhov's length represents the height where the production term of mechanical turbulence due to the vertical gradient of the wind velocity becomes equal to the one of thermal turbulence due to ground cooling or heating (Stull, 1989). Since it represents an assessment of the atmospheric stability/instability, it leads to a distinction between the different atmospheric conditions (stable, unstable, neutral) in order to determine the turbulence variables. w* represents the so-called vertical scale of convective velocities, i.e. a measure of the organized vertical motion (updraft and downdraft winds) taking place in days characterized by strong solar radiation inside the mixed layer, the height of which is defined by the h parameter. Finally, h_{res} defines instead the so-called height of the 'residual layer' (Stull, 1989), i.e. the height of the residual turbulent layer developed during the previous day, still existing at night-time and in the morning above the stable layer.

2.2 Modelling chain description

In order to investigate the air quality within and in the surrounding area of a city, the Chemical Transport models (CTMs) are the tool normally used to reproduce the fate of the main atmospheric pollutants and the principle physical and chemical transformations that occur between them.

Grid models are the best-suited tools to handle the regional features of the chemical reactions. However, this category of models is not designed to resolve pollutant concentrations on urban scales. Moreover, for many species of interest, having reaction time scales that are longer than the travel time across an urban area, chemical reactions can be ignored in describing local dispersion, making Lagrangian and plume-dispersion models a practical solution to study the urban pollution levels. This latter type of models are also called source-based dispersion models (Stein et al., 2007) and they use either plume, puff or particle representations of the emitted pollutants (see chapter 2.1). Typically they do not take into account atmospheric chemical reactions or they do so using simplified representations such as first-order pollutant decay. Their range of application is from a few hundred meters to a several kilometres from the source. The temporal resolutions range from an hour to several days; however, their computing cost can dramatically increase if they are applied to urban-scale domain that exceeds the range of few kilometres, involving hundreds of emission sources and taking into account the presence of buildings in the wind field reconstruction.

On the other hand, Eulerian grid-based models (such as the Weather Research and Forecasting model coupled with Chemistry) are used to simulate the transport and formation of secondary pollutants from chemical reactions not directly emitted by the ground sources. Such models may be set up to apply to a wide range of scales ranging from global to local. Typically, regional air quality models are applied over hundreds of kilometres using a regular grid with a horizontal cell resolution of few kilometres, up to tens of kilometres. These three-dimensional grid models require considerable computational resources and are usually applied only for multi-day periods to simulate long-range transports.

Unlike urban-scale models, regional-scale grid based models do not have the spatial resolution needed to correctly estimate concentrations close to the source: the primary

pollutants emitted within a model cell are homogeneously distributed throughout the same cell, hampering to simulate the effects from individual sources close to ground receptors.
One approach to mitigate this latter downside of CTM is the reduction of the grid cell size, to better correspond to the size of the area of interest (Kuik et al., 2016), but this solution can lead to highly computationally demanding simulations and currently there are technical limitations to reducing grid size below about one kilometre. In spite of this significant spatial resolution, CTMs are not the correct tool to estimate and predict pollutant concentrations at kerbsides, limiting their use since traffic areas are the most delicate city spot in regards of the air quality limits exceedance.

The idea behind this PhD project is to combine the capabilities of a chemical transport model with a source-based dispersion model into one coupled modelling system. This hybrid approach aims at describing the variability in air quality within urban areas at a high spatio-temporal resolution. This goal is pursued by using the most appropriate modelling tool to describe different scale of processes and different type of emissions sources, making a comprehensive simulation computationally possible also at high resolution. More specifically, the CTM is used to estimate the concentrations that contribute to the urban background, i.e. the part of the total concentration that is not explicitly accounted in the urban domain and may include contributions from long-range transport of pollutant from distant sources (located outside the local modelling domain), such as the part of the total concentrations produced within urban simulation but not considered with the source-based model.
Concurrently, a source-based dispersion simulation by the means of one LPDM is exploited to provide a detailed description of the concentrations variability across town, e.g. differences between kerbsides and parks, due to local emission sources at very high resolution (in the order of few meters), assuming non-reactive species. Finally, the results of both model simulations are combined to provide the total ambient air pollutant concentrations.

To date, despite the hybrid approach is a quite new approach used to estimate the air quality of a specific location, a number of papers describing this models coupling are available in the literature. Some of them focus on the combination of a CTM with a CFD model in order to estimate the effect of the building on the wind flow and on the pollution dispersion, but the size of the smallest domain and time scale considered in their application are limited,

respectively less than 1 square kilometres and a couple of hours (Kwak et al., 2015). Some others emphasize on CTM coupled with a Lagrangian model, but the investigated domain is limited to a portion of the city (e.g. 1.6 km x 1.6 km by (Pepe et al., 2016)). In other cases, notwithstanding the simulation is two weeks long, the effect of buildings on the wind flows are not taken into account (Stein et al., 2007). The ambitious goal of this PhD project was to apply a hybrid modelling system to estimate the pollution level within an entire urban area of a city located in the middle of the Po Valley, performing a two-week simulation during the first part of the thesis and a daily forecast, up to one day ahead, for an entire month in the second part.

The hybrid modelling system developed in this thesis is composed by the Weather Research and Forecasting model coupled with Chemistry (WRF-Chem), an Eulerian model and Parallel micro SWIFT SPRAY (PMSS), a Lagrangian particle dispersion model.
The choice of this modelling chain was based on the WRF-Chem ability to simulate the emissions, transport and chemical transformations simultaneously with meteorology at large scale, and on the PMSS capability to provide high resolution air quality maps over an entire urban domain characterized by large spatial and temporal concentrations gradient, with a reasonable computation time (Ghermandi, Fabbi, et al., 2015).
Figure 2.1 illustrates the interplay between WRF-Chem and PMSS. The WRF-Chem model was used to estimate NO_x concentrations on multiple domains at different grid resolutions spanning from the European domain to the Po Valley area with a nesting technique, necessary to take into account emissions at regional scale that can affect urban air quality in Modena. Then, wind streams within the city were determined by a cascade of scales from global to buildings level: synoptic and local scale meteorological conditions in the region surrounding the city of Modena were simulated by WRF-Chem taking into account the local topography and land-use data. Driven by these mesoscale flow patterns, high resolution winds were computed in the city to account for buildings and street canyons by performing the diagnostic mass-consistent Parallel-Micro-SWIFT model. Secondly, Lagrangian dispersion simulations driven by high resolution winds were carried out with Parallel-Micro-SPRAY by estimating urban traffic emission flows. As a final step of the procedure, NO_x traffic urban concentrations, simulated with Parallel-Micro-SPRAY, were added to NO_x background concentrations estimated with the WRF-Chem model.

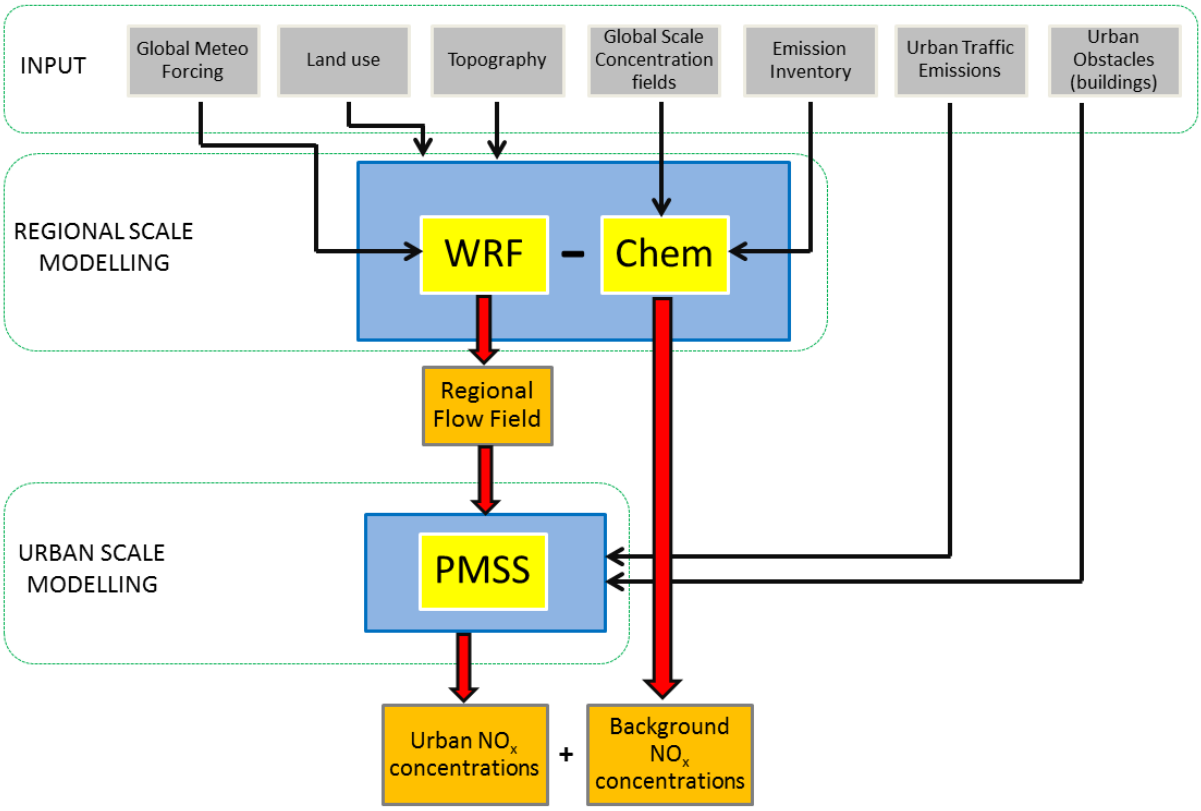

Figure 2.1: Outline of the multi-model approach implemented to generate hourly NO_x concentrations fields.

2.3 WRF-Chem model description

The simulation and prediction of air quality is a challenging task, involving both meteorological factors (such as wind speed and direction, turbulence, radiation, clouds, and precipitation) and chemical processes (such as deposition, and transformations). In the real atmosphere, the chemical and physical processes are coupled. The chemistry can affect the meteorology, for example through its effect on the radiation budget, as well as the interaction of aerosols with cloud condensation nuclei. Likewise, clouds and precipitation strongly influence chemical transformation and removal processes, and localized changes in the wind or turbulence fields continuously affect the chemical transport.

The chemical processes in air quality modelling systems are usually treated independently from meteorological phenomena adopting an "off-line" approach (as in the Community Model for Air Quality, CMAQ, Byun and Ching, 1999). Despite this approach from a computational point of view is advantageous, since offline chemical transport simulations require only a single meteorological dataset to produce several chemical scenarios, this separation can cause a loss of important information about atmospheric processes. This aspect may be especially important in air quality prediction modelling in which horizontal grid size is in the order of 1 km, as in this case study.

Since the role of the chemical transport model in this thesis project was to reproduce pollutants background concentrations within the urban area of Modena, model results need to be given at high degree of resolution (in the order of kilometre). Thus, to better integrate physical and chemical processes such as transport, deposition, chemical transformation, photolysis, and radiation the WRF-Chem suite (Grell et al., 2005) was chosen, which represent the "on-line" state of the art of the Weather Research and Forecasting (WRF) model coupled with chemical modules.

The WRF-Chem suite, as stated before, in order to describe the meteorology and meanwhile the pollutants transformation processes is composed by two main parts that run simultaneously during a simulation. The first one is performed by the numerical weather prediction model WRF, developed for research and operational activities at the National Center for Atmospheric Research (NCAR) in collaboration with many other research centres and laboratories, such as the National Centers for Environmental Prediction (NCEP), the

Earth System Research Laboratory (ESRL) of the National Oceanic and Atmospheric Administration (NOAA), the Air Force Weather Agency (AFWA), the Naval Research Laboratory (NRL) of the Department of Defence (DOD), the Center for Analysis and Prediction of Storms (CAPS) of the University of Oklahoma and the Federal Aviation Administration (FAA).

The WRF model numerically solves the Euler equations for a compressible fluid, in non-hydrostatic conditions, written in a terrain following reference system:

$$\eta = \frac{p_{dh} - p_{dht}}{\rho_d} \qquad \text{with} \qquad \rho_d = p_{dhs} - p_{dht} \qquad (2.14)$$

Where ρ_d is the dry mass per unit area (kg m^{-2}) within the column in the model domain, p_{dh} is the hydrostatic component of pressure of the dry atmosphere and p_{dhs} and p_{dht} are the values at the surface and at the top boundary respectively. η varies from a value of 1 at the surface to 0 at the upper boundary of the model domain (Figure 2.2). This vertical coordinate is also called a mass vertical coordinate.

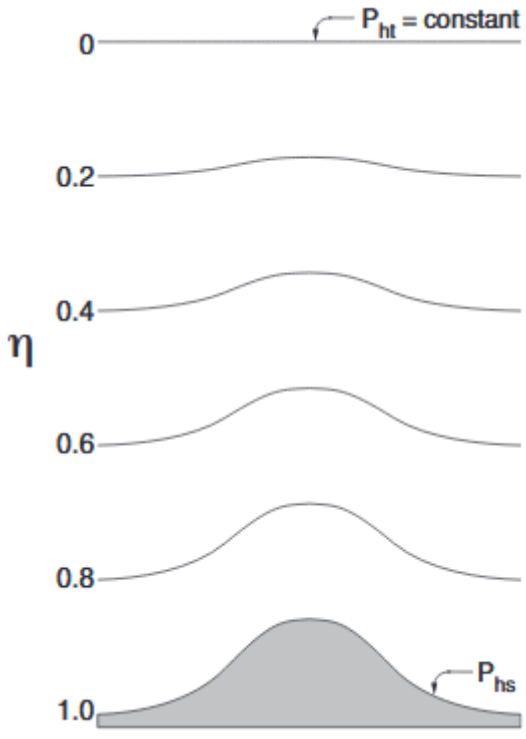

Figure 2.2: Mass vertical coordinates in presence of a mountainous relief.

The main prognostic Euler equation resolved by the WRF code, in the flux form, can be written as follow:

- ✓ Conservation equations for momentum:

$$\frac{\partial U}{\partial t} + (\nabla \cdot \boldsymbol{V}u) + \rho_d \alpha \frac{\partial p}{\partial x} + \frac{\alpha}{\alpha_d}\frac{\partial p}{\partial \eta}\frac{\partial \phi}{\partial x} = F_U \tag{2.15}$$

$$\frac{\partial V}{\partial t} + (\nabla \cdot \boldsymbol{V}v) + \rho_d \alpha \frac{\partial p}{\partial y} + \frac{\alpha}{\alpha_d}\frac{\partial p}{\partial \eta}\frac{\partial \phi}{\partial y} = F_V \tag{2.16}$$

$$\frac{\partial W}{\partial t} + (\nabla \cdot \boldsymbol{V}w) - g\left(\frac{\alpha}{\alpha_d}\frac{\partial p}{\partial \eta} - \rho_d\right) = F_W \tag{2.17}$$

- ✓ Conservation equations for energy:

$$\frac{\partial \Theta}{\partial t} + (\nabla \cdot \boldsymbol{V}\Theta) = F_\Theta \tag{2.18}$$

- ✓ Conservation equations for dry air mass:

$$\frac{\partial \rho_d}{\partial t} + (\nabla \cdot \boldsymbol{V}) = 0 \tag{2.19}$$

- ✓ Material derivative of the geopotential:

$$\frac{\partial \phi}{\partial t} + \frac{1}{\rho_d}[(\boldsymbol{V} \cdot \nabla\phi) - gW] = 0 \tag{2.20}$$

Other important equations are:

- ✓ Diagnostic relation for the inverse density:

$$\frac{\partial \phi}{\partial \eta} = -\alpha_d \rho_d \tag{2.21}$$

✓ Equation of state for moist air:

$$p = p_0 \left(\frac{R_d \theta_m}{p_0 \alpha_d} \right)^{\gamma} \tag{2.22}$$

✓ Conservation equation for moisture:

$$\frac{\partial Q_m}{\partial t} + (\nabla \cdot \boldsymbol{V} q_m) = F Q_m \tag{2.23}$$

Where $\mathbf{V} = \varsigma \boldsymbol{v}$ = (U, V, W), being ς the mass of dry air in the column and $\boldsymbol{v}$ = (u, v, w) the three-dimensional velocity vector, θ is the potential temperature and $\Theta = \rho_d \theta$, ϕ = gz is the geopotential, being g and z the gravitational acceleration and the vertical coordinate. p is the atmospheric pressure, $\alpha_d = \frac{1}{\rho_d}$ is the specific volume, p_0 is a reference pressure, R_d is the gas constant in the state equation for dry air, $\gamma = \frac{c_p}{c_v} = 1.4$ is the ratio of the specific heats for dry air. $\alpha = \alpha_d (1 + q_v + q_c + q_r + q_i + \cdots)^{-1}$ is the specific density taking into account the full parcel density for water vapour, cloud, rain, ice, etc.

$\theta_m = \theta \left(1 + \left(\frac{R_v}{R_d}\right) q_v\right) \approx (1 + 1.61 q_v)$; $\theta_m = \rho_d q_m$ with m = v,c,i,…and F_i are the external forcing such as Coriolis, curvature, missing terms and physical forcing.

The solution of the Euler equations allows the calculation of the mean wind field (u, v and w) which affect most the pollution dispersion in the atmosphere. Beside this computation, WRF implements also a series of parametrizations necessary to describe all the physical processes that cannot be explicitly resolved by the previous equation because they are too complex to be mathematically described or they occur at too small spatial-temporal scale.

Within WRF, six different categories of physics parameterizations are implemented: the microphysics, the cumulus parameterization, the planetary boundary layer (PBL), the land-surface model, the radiation and the diffusion. All these parameterizations directly influence

the main equations and interact one with each other. Further details can be found in the "*Description of the Advanced Research WRF Version 3*" user guide (Skamarock et al., 2008).

The second module that constitutes the WRF-Chem suite regards the transport, the reaction, the removal and the emissions of pollutants within the atmosphere. From a generic point of view the starting point of atmospheric transport model is the mass balance equation that for chemical specie i, can be written as follow (simplification of the Equation (2.1)):

$$\frac{\partial C_i}{\partial t} + \nabla \cdot (\boldsymbol{v} C_i) = R_i(C_1 + C_2 + \cdots + C_n) + E_i - S_i \tag{2.24}$$

Where $C_i(\boldsymbol{x}, t)$ is the concentration of *i* as a function of location $\boldsymbol{x}$ and time *t*. $\boldsymbol{v}$(**x,** t) is the velocity vector, R_i is the chemical generation term for *i*, and $E_i(\boldsymbol{x}, t)$ and $S_i(\boldsymbol{x}, t)$ are its emission and removal fluxes, respectively.
Moreover, expressing the mixing ratio of a species i at any point of the atmosphere as:

$$\xi_i = \frac{C_i}{C_{air}} \tag{2.25}$$

Where C_{air} is the total molar concentration of air ($C_{air} = \frac{p}{RT}$, with p and T the atmospheric pressure and temperature and R the gas constant in the state equation), the Equation (2.24), considering the terrain-following coordinate system (2.14), leads to the atmospheric diffusion by splitting the transport term into an advection and turbulent transport contribution in the following form:

$$\begin{aligned} &\frac{\partial \xi_i}{\partial t} + u\frac{\partial \xi_i}{\partial x} + v\frac{\partial \xi_i}{\partial y} + w\frac{\partial \xi_i}{\partial \eta} \\ &\qquad = \frac{1}{\rho}\frac{\partial}{\partial x}\left(\rho K_{xx}\frac{\partial \xi_i}{\partial x}\right) + \frac{1}{\rho}\frac{\partial}{\partial y}\left(\rho K_{yy}\frac{\partial \xi_i}{\partial y}\right) + \frac{g^2}{(\rho_d)^2}\frac{\partial}{\partial \eta}\left(\rho^2 K_{zz}\frac{\partial \xi_i}{\partial \eta}\right) \\ &\qquad + R_i(C_1 + C_2 + \cdots + C_n) + E_i(x, y, z, t) - S_i(x, y, z, t) \end{aligned} \tag{2.26}$$

Where *u*, *v* and *w* are the *x*, *y* and *z* components of the wind velocity, ρ the atmospheric mass density of the air and K_{xx}, K_{yy} and K_{zz} are the corresponding eddy diffusivity. The turbulent

fluctuation $\boldsymbol{v}'$ and ξ_i' of the velocity and mixing ratio fields relative to their average values $\overline{\boldsymbol{v}}$ and $\overline{\xi_i}$ have been approximated using the *K* theory (or mixing length or gradient transport theory) by:

$$\overline{\boldsymbol{v}'\xi_i'} = -\boldsymbol{k} \cdot \nabla\xi_i \tag{2.27}$$

During the last years the WRF-Chem model has been extensively improved and several packages have been developed to account for a large variety of pollutant processes, making it a flexible tool for a wide range of applications. The main features include:

- Dry deposition, coupled with the soil/vegetation scheme

- Four choices for biogenic emissions (including the Model of Emissions of Gases and Aerosols from Nature, a.k.a. MEGAN, (Guenther et al., 2012))

- Anthropogenic emissions

- Several choices for gas-phase chemical mechanisms (including RADM2, RACM, CB-4, SAPRC-99, MOZART, NMHC9 and CBM-Z chemical mechanisms). The Kinetic Pre-processor (KPP) is also available to generate the code for the chemical reactions for most of the chemical mechanisms.

- Photolysis schemes

- Five choices for aerosol schemes (MADE/SORGAM, MADE/VBS, MAM, MOSAIC with 4 or 8 bins and GOCART)

- The option for passive tracers transport of greenhouse gases

- A plume rise model to treat the emissions of wildfires

2.4 PMSS modelling system description

Parallel Micro SWIFT SPRAY or PMSS (Oldrini et al., 2011, 2017) is the parallelized version of the MSS modelling suite (Tinarelli et al., 2007, 2013) constituted by the individual models SWIFT and SPRAY, both used in small scale urban model (a.k.a. Micro-SWIFT and Micro-SPRAY).

Micro-SWIFT is a 3D mass-consistent diagnostic model that uses terrain-following coordinates to provide diagnostic wind, turbulence, temperature and humidity fields using data from a dispersed meteorological network. Meteorological input can be provided as measured data, like radio soundings, ground measurements and vertical profile, or as modelled data that come from a regional meteorological simulation.

The first step performed by Micro-SWIFT in the computation is the interpolation of the heterogeneous meteorological input data in order to reconstruct the three-dimensional wind field without obstacles, by applying a 2D or 3D interpolation method. Then, the first computed wind field is modified in the zones around isolated or group of buildings following the approach suggested by Röckle (1990) and Kaplan and Dinar (1996) adopting a parametrization of the recirculating flow regions around, behind, over and between obstacles. Subsequently, the mass conservation constraint is imposed through the impermeability conditions on the ground and at building surfaces. Finally, a RANS flow solver can be optionally used to simulate more accurate velocity and pressure fields in built-up environments than obtained with the pure diagnostic flow model configuration (Oldrini et al., 2014, 2016).

With the RANS approach, the momentum equation is introduced in the computation and the turbulent Reynolds stress tensor is modelled by a zero-order closure based on mixing-length theory and the momentum and pressure equations are solved using the fractional time step technique (Gowardhan et al., 2011).

A typical application of the RANS or “momentum” version of SWIFT is to compute a realistic surface pressure field on facades to evaluate infiltration inside the buildings. The momentum equation is implemented in SWIFT with an approach that allows containing the computational time, at the same time maintaining the accuracy when modelling physical processes.

The estimation of the turbulence needed by Micro-SPRAY to drive pollutants dispersion is diagnosed by Micro-SWIFT through the superimposition of the background turbulence, obtained by standard boundary layer parameterizations (Hanna et al., 1982) and the turbulence inside the flow zones modified by the obstacles. The variables that have to be calculated are: the wind standard deviations σ_{ui}, the Lagrangian time scales T_{Li} (where i is equal to the x, y and z axis considering a Cartesian frame 0xyz) and the third order statistical moment of the distribution for vertical velocities (Skewness). All these quantities directly affect the results of the Langevin equations, i.e. the velocity fluctuations that the virtual particles will experience.

The turbulence code implemented in SPRAY can build 3D arrays of the variables previous mentioned (σ_{ui}, T_{Li} and Skewness) on the basis of two dimensional arrays of land-use parameters and ground meteorological constraints given as input.

At each grid point, SPRAY compute a two dimensional fields of the u*, L, h, w* scaling variables and then identifies the atmospheric stability regime, on the basis of the value of the parameter L. By contrast h_{res} is given as input and kept constant during the whole simulation. The vertical domain is finally subdivided into three layers:

Layer 1: $z < h$

Layer 2: $h < z < h_{res}$

Layer 3: $h_{res} < z \; z_{top}$

Where z represents the height above the ground and z_{top} is the top of domain level. If h_{res} is lower than the height of the boundary layer, the Layer 2 is absorbed. Inside of the first layer (Layer 1), profiles are determined as follows, on the basis of the actual stability condition:

<u>Stable conditions:</u> $0 < L < +300$

$$\sigma_u(z) = 2.0\, u^* \left(1 - \frac{z}{h}\right) \tag{2.28}$$

$$\sigma_u(z) = 1.3\, v^* \left(1 - \frac{z}{h}\right) \tag{2.29}$$

$$\sigma_{ux}(z) = \sigma_{uy}(z) = \sqrt{0.5({\sigma_u}^2 + {\sigma_v}^2)} \tag{2.30}$$

$$\sigma_w(z) = 1.3\, u^* \left(1 - \frac{z}{h}\right) \tag{2.31}$$

$$T_{Lx}(z) = T_{Ly}(z) = 0.11\left(\frac{h}{\sigma_{ux}}\right)\left(\frac{z}{h}\right)^{0.5} \tag{2.32}$$

$$T_{Lz}(z) = 0.10\left(\frac{h}{\sigma_{ux}}\right)\left(\frac{z}{h}\right)^{0.8} \tag{2.33}$$

Skewness = 0

<u>Neutral conditions:</u> L $\geq$ +300 or L $\leq$ -300

$$\sigma_u(z) = 2.0\, u^* e^{-3\frac{fz}{u*}} \tag{2.34}$$

$$\sigma_v(z) = 1.3\, u^* e^{-2\frac{fz}{u*}} \tag{2.35}$$

$$\sigma_{ux}(z) = \sigma_{uy}(z) = \sqrt{0.5({\sigma_u}^2 + {\sigma_v}^2)} \tag{2.36}$$

$$\sigma_w(z) = 1.3\, u^* e^{-2\frac{fz}{u*}} \tag{2.37}$$

$$T_{Lx}(z) = T_{Ly}(z) = T_{Lz}(z) = 0.5\left(\frac{z}{[\sigma_w(1 + 15\,\frac{fz}{u^*})]}\right) \tag{2.38}$$

Skewness = 0

Unstable conditions: -300 < L < 0

$$\sigma_{ux}(z) = \sigma_{uy}(z) = u^* \left(12 - 0.5\frac{h}{L}\right)^{\frac{1}{3}} \tag{2.39}$$

$$\sigma_w(z) = \begin{cases} 0.763\frac{z}{h}, & z \leq 0.4h \\ 0.722\, w^* \left(1 - \frac{z}{h}\right)^{0.207}, & 0.4h < z \leq 0.96h \\ 0.722\, w^*, & 0.96h < z \leq h \end{cases} \tag{2.40}$$

$$\overline{w'^3}(z) = w^*(1.4\frac{z}{h})e^{-2.5\frac{z}{h}} \tag{2.41}$$

$$T_{Lx}(z) = T_{Ly}(z) = 0.15\left(\frac{h}{\sigma_{ux}}\right) \tag{2.42}$$

$$T_{Lz}(z) = \begin{cases} 0.1\left(\frac{z}{[\sigma_w(0.55 + 0.38\,\frac{(z - z_0}{L})]}\right), & z \leq 0.1h,\ z < z_0 - L \\ 0.59\left(\frac{z}{\sigma_w}\right), & z \leq 0.1h,\ z \geq z_0 - L \\ 0.15\left(\frac{h}{\sigma_w}\right)\left[1 - e^{-5\frac{z}{h}}\right], & z > 0.1h \end{cases} \tag{2.43}$$

Inside the Layer 2 (whenever existing), the SPRAY code proceeds as in the neutral case, interpolating the equations with the results obtained on the layer below in the region between Layer 1 and Layer 2. Into Layer 3 variances are linearly brought to 0 at the domain top level, whereas Lagrangian time scales are kept constant.

In presence of buildings, with the aim of accounting the contribution of urban canopy, the description of turbulence features requires the turbulent diffusion coefficients K_x, K_y, K_z and the dissipation rate of turbulent kinetic energy ε. Such parameters depend on how urban obstacles affect the diffusion conditions and energy transfer between turbulent eddies at different spatial scales, according to the Kolmogorov theory (Kolmogorov, 1941).

In this case a three-dimensional field of local turbulence, following the approach suggested by Rodean (AMS, 1996) and considering a Cartesian frame 0xyz where *i* can be x, y and z (the

references axis), the local wind standard deviation due to the presence of obstacles and the Lagrangian time scales can be computed as follow:

$$\sigma_{ui\_local} = \frac{1}{2}\, C_0 K_i \varepsilon^{\frac{1}{4}} \tag{2.44}$$

$$T_{Li} = 2\frac{{\sigma_{ui}}^2}{C_0 \varepsilon} \tag{2.45}$$

Sum of local and background turbulence kinetic energy can also be computed either on the whole domain, either only in the zones affected by obstacles in the following way:

$$\sigma_{ui} = \sqrt{{\sigma_{ui\_local}}^2 + {\sigma_{ui\_inflow}}^2} \tag{2.46}$$

Where σ_{ui_inflow} are computed through Hanna profile as described before.

Micro-SPRAY is a 3D Lagrangian Particle Dispersion Model (Rodean, 1996) able to simulate the advection and the diffusion of gaseous species or fine aerosol by accounting for the presence of obstacles. The dispersion of an airborne contaminant is modelled by virtual particles that follow the turbulent motion of the air as passive tracers and their spatial distribution at a certain time represents the concentration of an emitted substance.

The trajectories of the particles emitted by a source are obtained by integrating in time their velocity (see chapter 2.1). This can be considered as the sum of a transport component, defined by the local averaged wind, usually provided by Micro-SWIFT, and a stochastic component, standing for the dispersion due to the atmospheric turbulence. The stochastic component is obtained by solving a 3D form of the Langevin equation for the random velocity, following Thomson's approach (Thomson, 1987).

The PMSS modelling system has been validated (Oldrini et al., 2017; Oldrini and Armand, 2019; Trini Castelli et al., 2017, 2018) and applied (Carlino et al., 2016, Moussafir et al., 2016) to several experiments and real cases. In this study, the performances of the PMSS modelling system are exploited to estimate urban air quality in the city of Modena in a real case scenario.

3. Traffic emissions

Vehicular emissions are becoming increasingly important in urban centres (Borrego et al., 2000; Carslaw, 2005; Ghermandi et al., 2019) and measurements have shown that compounds emitted from exhausts can be highly reactive in the atmosphere, contributing to critical episodes of photochemical smog (Moussiopoulos et al., 1995; Rani et al., 2011; Tiao et al., 1975). However, finding detailed information regarding traffic emissions is not easy at all, since obtaining precise traffic fluxes estimation within urban and rural street network can be complicated, as well as estimating a representative emission factor of the vehicle fleet composition. This can be a challenge, especially in developing countries, due to the lack of information about the vehicle type, technology, age, motor size, fuel, speeds, accelerations, street type and environmental temperatures. The most common aspects are the accuracy and complexity related to the exact contribution of the different pollutant sources, for these reasons provide an accurate emission inventory can be crucial for the representation of measured concentrations.

There are two different methods that can be used to estimate and validate emissions. One is the "top-down" approach, which rely on statistical information that must be homogeneously available for large territories such as the fuel consumption, resident population and registered vehicles fleet. The other one is the "bottom-up" approach, based on traffic counts, vehicle composition and speed recording (Ntziachristos and Samaras, 2016). In both the methodologies the accuracy of the emissions inventory will reflect the representation of the pollutants in the atmosphere. Indeed, it is not always related to the complexity of the model. For instance, a meta-analysis of several studies on vehicular emissions (Smit et al., 2010) concluded that there is no evidence that the more complex models perform better than the less complex ones and that emissions estimation techniques must be chosen according to the available traffic data.

A first guess of estimating vehicular emission for the Emilia-Romagna region was performed by the local environmental agency, ARPAE (Agenzia regionale per la prevenzione, l´ambiente e l´energia), which computed the annual total emissions for 2015 combing linear traffic emissions, due to the vehicle flows within the main street of the Emilia-Romagna

region, such as high-way and ring roads, and diffuse traffic emissions based on urban fuel consumption and vehicles averaged emission factors.

Despite the inventories developed by ARPAE being useful, they still suffer from limitations as they use surrogates to produce spatial and temporal distributions, hence limiting the representation of the emissions. Therefore, in order to account for more accurate emissions estimation, in particular for NO_x ($NO + NO_2$) emissions, was developed a bottom-up vehicular emission model aiming to generate directly the input files needed by PMSS model to simulate related dispersion in urban environment. The model was named Vehicular Emissions from Road Traffic (VERT) and it is coded into an R (R Core Team, 2018) package. The main feature of the model include the capability to produce high spatial and temporal vehicular emissions using the emission factors suggested by Ntziachristos and Samaras (2016), updated in 2018. It allows also the classification of vehicles into categories and pollutants, and it can compute the emissions for a specific vehicle category or for the entire fleet by considering its real composition. According to the computational platform availability, the parallel computing can be also enabled by the user.

The R package VERT is largely inspired by the Vehicular Emissions IN-ventory (VEIN) model, developed by Ibarra-Espinosa et al. (2018), which include the emission factors related to previous version of COPERT (IV) and the related vehicle classification. Most of the functions originally available in VEIN were re-written in order to enable the computation of the total emissions considering the actual fleet composition in Modena.

3.1 Exhaust Emissions Overview

Exhaust emissions from road transport arise from the combustion of fuels such as petrol, diesel, liquefied petroleum gas (LPG) and compressed natural gas (CNG) in internal combustion engines. This combustion process produces CO_2 and H_2O as the main products, unfortunately, other secondary products are also generated from incomplete fuel oxidation (CO, hydrocarbons (THC), particulate matter (PM)) or from the oxidation of non-combustible species present in the combustion chamber (NO_x from N_2 in the air, SO_x from S in the fuel and lubricant, etc.).

With the aim of reducing the secondary harmful combustion products, the emissions from road vehicles have been controlled by European legislation since the 1970s. In order to meet the increasingly stringent requirements of the legislation, vehicle manufacturers have continually improved engine technologies, by reducing the energy consumption, and have also introduced various emission-control systems. As a result, modern vehicles have emission levels for regulated pollutants (CO, NO_x, THC and PM) which are more than an order of magnitude lower than those of vehicles entering service two decades ago.

Road vehicles are usually classified according to their level of emission control technology, which is actually defined in terms of the emission legislation with which they are compliant. Table 3.1 (Ntziachristos and Samaras, 2016) summarize the different levels of technologies with their respective year of introduction, according to the fuel and vehicle category.

Table 3.1: List of the European emission standards implemented for Passenger cars, Light Duty Vehicles, Heavy Duty Trucks and L-category, according to the fuel type.

Vehicle category	Type	Euro Standard	Start Date	End Date
Passenger Car	Petrol	PRE ECE		Up to 1971
		ECE 15/00-01	1972	1977
		ECE 15/02	1978	1980
		ECE 15/03	1981	1985
		ECE 15/04	1985	1992
		Improved Conventional	1985	1990
		Open Loop	1985	1900
		Euro 1	1992	1996
		Euro 2	1996	1999

		Euro 3	2000	2004
		Euro 4	2005	2009
		Euro 5	2010	2014
		Euro 6 up to 2016	2015	2016
		Euro 6 2017-2019	2017	2019
		Euro 6 2020+	2020 and on	
	Diesel	Conventional		up to 1992
		Euro 1	1992	1996
		Euro 2	1996	2000
		Euro 3	2000	2005
		Euro 4	2005	2010
		Euro 5	2010	2014
		Euro 6 up to 2016	2014	2016
		Euro 6 2017-2019	2017	2019
		Euro 6 2020+	2020 and on	
	LPG	Conventional		up 1991
		Euro 1	1992	1996
		Euro 2	1996	1999
		Euro 3	2000	2004
		Euro 4	2005	2009
		Euro 5	2010	2014
		Euro 6 up to 2016	2015	2016
		Euro 6 2017-2019	2017	2019
		Euro 6 2020+	2020 and on	
	CNG	Euro 4	2005	2009
		Euro 5	2010	2014
		Euro 6 up to 2016	2015	2016
		Euro 6 2017-2019	2017	2019
		Euro 6 2020+	2020 and on	
	2 stroke	Conventional		
Light Duty Vehicles	Petrol	Conventional		up to 1993
		Euro 1	1993	1997
		Euro 2	1997	2001
		Euro 3	2001	2006
		Euro 4	2006	2010
		Euro 5	2011	2015
		Euro 6 up to 2017	2016	2017
		Euro 6 2018-2020	2018	2020
		Euro 6 2021+	2021 and on	
	Diesel	Conventional		up to 1993
		Euro 1	1993	1997
		Euro 2	1997	2001
		Euro 3	2001	2006
		Euro 4	2006	2010

		Euro 5	2011	2015
		Euro 6 up to 2017	2016	2017
		Euro 6 2018-2020	2018	2020
		Euro 6 2021+	2021 and on	
Heavy Duty Trucks	Diesel	Conventional		
		Euro I	1992	1995
		Euro II	1996	2000
		Euro III	2000	2005
		Euro IV	2005	2008
		Euro V	2008	2013
		Euro VI	2013 and on	
L-category	Mopeds and Mini-cars	Conventional		up to 1999
		Euro 1	1999	2002
		Euro 2	2002	2006
		Euro 3	2006	2016
		Euro 4	2016	2020
		Euro 5	2020 and on	
	Motorcycles	Conventional		up to 1999
		Euro 1	1999	2002
		Euro 2	2002	2006
		Euro 3	2006	2016
		Euro 4	2016	2020
		Euro 5	2020 and on	

3.2 Exhaust Emissions Computation

According to the guidelines provided by the European Environmental Agency (Ntziachristos and Samaras, 2016), depending on the level of detail available for the data, the approach adopted for the calculation of emissions can be divided into three different approaches: Tier 1, Tier 2 and Tier 3. If the kilometre travelled per vehicle and the mean travelling speed are available for each type and vehicle technology, the Tier 3 approach is suggested. By contrast, if the mean travelling speed is not available, the use of the emission factors based on vehicle kilometre for different technologies are advised (Tier 2). Finally, in case the total fuel consumption is the only resource accessible, default emission factors are applied (Tier 1).

More specifically, the Tier 1 approach for exhaust emissions uses the following general equation:

$$Emission_i = \sum_j \left(\sum_m \left(FC_{j,m} \cdot EF_{i,j,m} \right) \right) \tag{3.1}$$

Where $Emission_i$ is the emission of pollutant i (g), $FC_{j,m}$ the fuel consumption of vehicle category j using fuel m (kg) and $EF_{i,j,m}$ is the fuel consumption-specific emission factor of pollutant i for vehicle category j and fuel m (g kg^{-1}).

The Equation (3.1) requires the fuel consumption/sales statistics to be split by vehicle category, as national statistics do not provide vehicle category details. This information can be obtained by combining the local fleet composition with the typical fuel consumption per vehicle category, which is possible to find in literature. Following the same methodology, the Tier 1 emission factors ($EF_{i,j,m}$), one for every broad vehicle category (Passenger cars, Light Duty vehicles, Heavy Duty Trucks and L-category), are calculated assuming a typical European (EU-15) fleet and related activity data. Tier 1 emission factors for all vehicle categories are available in the European Environmental Agency Guidebook (Ntziachristos and Samaras, 2016).

The Tier 2 approach considers the fuel used by different vehicle categories and their emission standards. Hence, the four broad vehicle categories used in Tier 1 are sub-divided into

different technologies *k* according to emission-control legislation. The user needs to provide the number of vehicles and the annual mileage per technology (or the number of vehicle-km per technology). Then, these vehicle-km data are multiplied by the Tier 2 emission factors and the relative equation is the following:

$$Emission_{i,j} = \sum_k (< M_{j,k} > \cdot EF_{i,j,k}) \quad or \quad Emission_{i,j} = \sum_k (N_{j,k} \cdot M_{j,k} \cdot EF_{i,j,k}) \qquad (3.2)$$

Where $< M_{j,k} >$ is the total annual distance driven by all vehicles of category *j* and technology *k* (veh-km), $EF_{i,j,k}$is the technology-specific emission factor of pollutant *i* for vehicle category *j* and technology *k* (g (veh-km)$^{-1}$), $M_{j,k}$ is the average annual distance driven per vehicle of category *j* and technology *k* (km veh^{-1}) and $N_{j,k}$ is the number of vehicles in the considered fleet of category *j* and technology *k*. Emission factors for different vehicle categories, fuels, vehicle technologies and for the principal pollutants are reported by Ntziachristos and Samaras (2016) in the reference guidebook.

The Tier 3 approach is also known as the detailed methodology, since it requires more information with respect to Tier 1 and 2 approaches. The exhaust emissions are calculated using a combination of activity data, such as the total vehicle kilometre and technical data, for example emission factors. Moreover, total exhaust emissions are calculated as the sum of hot emissions (which occur when the engine is at its normal operating temperature) and emissions during transient thermal engine operation (known as cold-start emissions). This distinction is necessary because there is a substantial difference in vehicle emission performance during the two conditions: concentrations of some pollutants during the warming-up period are many times higher than during hot operation and a different methodological approach is required to estimate the additional emissions during this period.

Vehicle emissions are heavily dependent on the engine operation conditions, for this reason different driving situations impose different engine operation conditions, and therefore a distinct emission performance. In this respect, a distinction is made between urban, rural and highway driving. By contrast, cold-start emissions are attributed mainly to urban driving (and secondarily to rural driving), as it is expected that a limited number of trips start at highway conditions. Therefore, the total emissions can be calculated by means of the following equation:

$$Emission_{total} = Emission_{HOT,urban} + Emission_{COLD,urban} + Emission_{HOT,rural} + Emission_{COLD,rural} + Emission_{HOT,highway} \quad (3.3)$$

Hot exhaust emissions depend upon a variety of factors, including the distance that each vehicle travels, its speed (or road type), its age, its engine size and its weight. The general formula for estimating hot emission is:

$$Emission_{HOT;i,k,r} = N_k \cdot M_{k,r} \cdot e_{HOT;i,k,r} \quad (3.4)$$

Where $Emission_{HOT;i,k,r}$ is the hot exhaust emissions of the pollutant *i* (g), produced in the period concerned by vehicles of technology *k* driven on roads of type *r* (urban, rural or highway), N_k is the number of vehicles of technology *k* in operation in the period concerned, $M_{k,r}$ is the total mileage per vehicle in vehicle technology *k* and $e_{HOT;i,k,r}$ is the hot emission factor in (g km^{-1}) for pollutant *i*, relevant for the vehicle technology *k*, operated on roads of type *r*.

As introduced before, cold start emissions take place under all driving conditions, however they seem to be most likely related to urban and rural cycles, as the number of starts in highway conditions is relatively limited. They occur for all vehicle categories, but emission factors are only available, or can be reasonably estimated, for petrol, diesel and LPG cars, and light commercial vehicles. Moreover, they are not considered to be a function of vehicle age. Cold-start emissions are introduced into the calculation as additional emissions per km using the following formula:

$$Emission_{COLD;i,k} = \beta_{i,k} \cdot N_k \cdot M_{k,r} \cdot e_{HOT;i,k} \cdot \left(\frac{e_{COLD;i,k}}{e_{HOT;i,k}} - 1\right) \quad (3.5)$$

Where $Emission_{COLD;i,k}$ is the cold-start emissions of pollutant *i* produced by vehicle technology *k*, $\beta_{i,k}$ is the fraction of mileage driven with a cold engine or catalyst operated below the light-off temperature for pollutant *i* and vehicle technology *k*. N_k is the number of

vehicles of technology k in circulation, $M_{k,r}$ is the total mileage per vehicle in vehicle technology k, $e_{HOT;i,k}$ is the hot emission factor for pollutant i and vehicles of k technology. Finally, $\frac{e_{COLD;i,k}}{e_{HOT;i,k}}$ is the cold/hot emission quotient for pollutant i and vehicle of k technology, available on guidebook (Ntziachristos and Samaras, 2016) for different vehicle types.

The β-parameter depends upon ambient temperature T_a and on the average trip length l_{trip}, and can be estimated with the following experimental formulation:

$$\beta_{i,k} = 0.6474 - 0.02545 \cdot l_{trip} - (0.00974 - 0.000385 \cdot l_{trip}) \cdot T_a \qquad (3.6)$$

Where l_{trip} is the mean travel distance, i.e. the mean travel segment defined between a key-on and a key-off event. Trip for passenger cars can occur at any distance between a few meters (urban local trip) to several hundred kilometres (interurban trips). Usually for urban area the mean travel distance is limited between 1 and 3 kilometres, for example for the city of Modena the 45% of the trips are less than 2.5 km and the 32% of the trips are less than 2 km.

Hot emission factors are speed dependent and are expressed in (g km^{-1}), their formulation depends on seven coefficients (*Alpha*, *Beta*, *Gamma*, *Delta*, *Epsilon*, *Zeta* and *Eta*) that differ by fuel, vehicle class and engine technology. Considering v the vehicle velocity, the general formula can be expressed in this way:

$$EF = \frac{\left(Alpha \cdot v^2 + Beta \cdot v + Gamma + \frac{Delta}{v}\right)}{(Epsilon \cdot v^2 + Zeta \cdot v + Eta)} \qquad (3.7)$$

3.3 VERT (Vehicular Emission from Road Traffic) model

The development of VERT started in 2018 as a collection of several R script written during this PhD, aiming at estimating high spatial and temporal vehicular emissions using the latest emission factors suggested by the European Environmental Agency in 2018 (Ntziachristos and Samaras, 2016), which later evolved into an R package, largely inspired by VEIN (Vehicular Emissions IN-ventory, Ibarra-Espinosa et al., 2018).

VERT implements the detailed methodology for estimating NO_x exhaust emissions (Tier 3 approach) and it is designed to directly perform cold and hot emissions estimation using as activity data the number of vehicles simulated by a traffic model within a road network, in a specific time step (usually one hour). Thus, it is able to handle input and output spatial data.

In Figure 3.1 is shown an example of traffic flow simulation that the VERT package is able to ingest as "activity data" in the emission computation. VERT uses objects of the class "Spatial", including `SpatialLinesDataFrame` available through different packages, such as `rgdal` (Bivand, Keitt, et al., 2019) or `maptools` (Bivand, Lewin-Koh, et al., 2019), both based on the `sp` package (Pebesma et al., 2019) which work like a GIS (Geographic Information System) software in order to visualize layers, coverages, rasters or geometries.

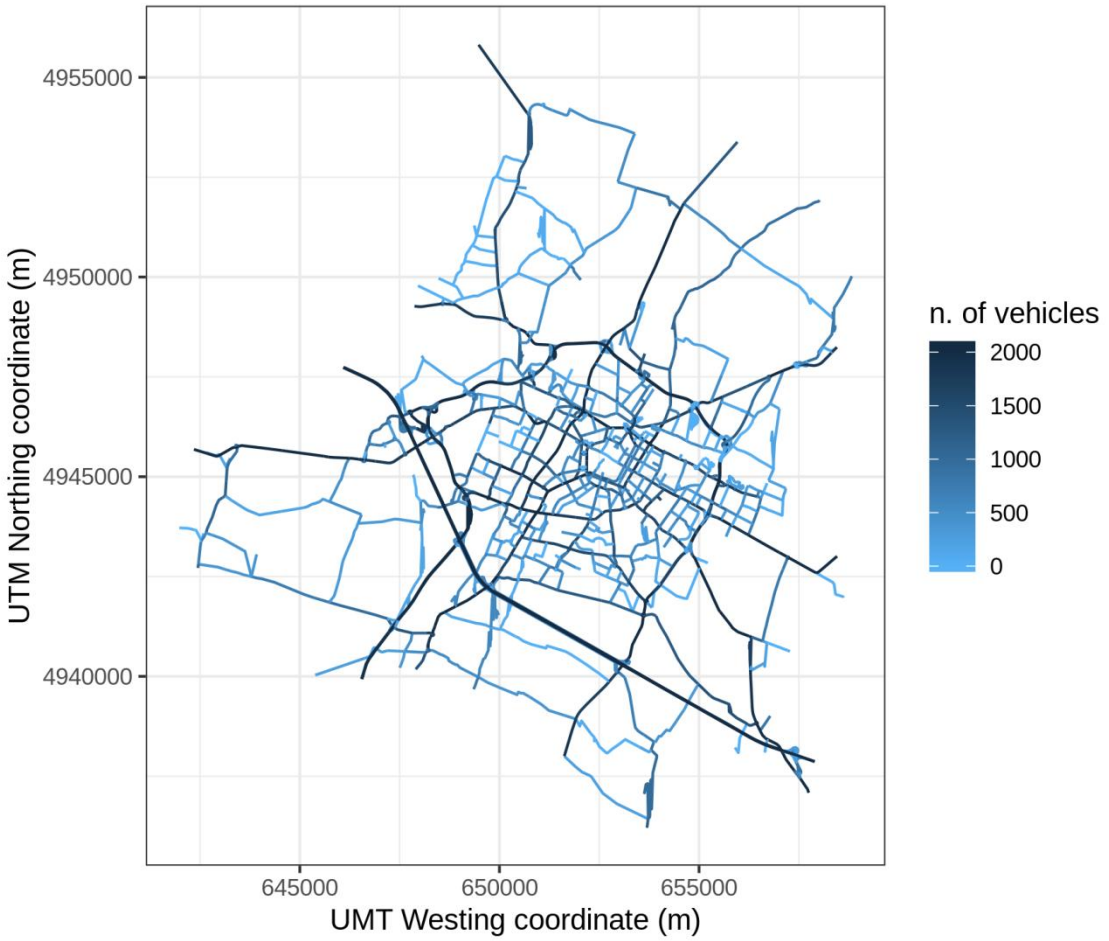

Figure 3.1: Example of Modena traffic flow simulation for all vehicle categories which can be used as input for VERT emission model.

The diagram process for estimating emissions is shown in Figure 3.2. The boxes in this figure refer to the functions inside the model and circles refer to the input or output data. Circles filled with light blue colour are spatial data, while blank circles refer to scalar or vector data.

The emissions computation starts with the air temperature and with the mean travel distance (l_{trip}), which are used by the function *beta_param* to estimate the fraction of mileage driven with a cold engine or catalyst operated below the light-off temperature (Equation (3.6)), also known as β-parameter. At the same time by selecting a specific pollutant (for this project NO_x), the user can select which vehicle category need to be introduced in the emission computation. The "Capture" functions (*Capture_hot_EF* and *Capture_cold-hot_EF*) select which of the hot and cold-hot quotient emission factors need to be considered in the computation (respectively $e_{HOT;i,k,r}$ in the Equation (3.4) and $\frac{e_{COLD;i,k}}{e_{HOT;i,k}}$ in the Equation (3.5)),

according to the vehicle type selected by the user. The common way to proceed is to consider all the vehicle types in the fleet composition.

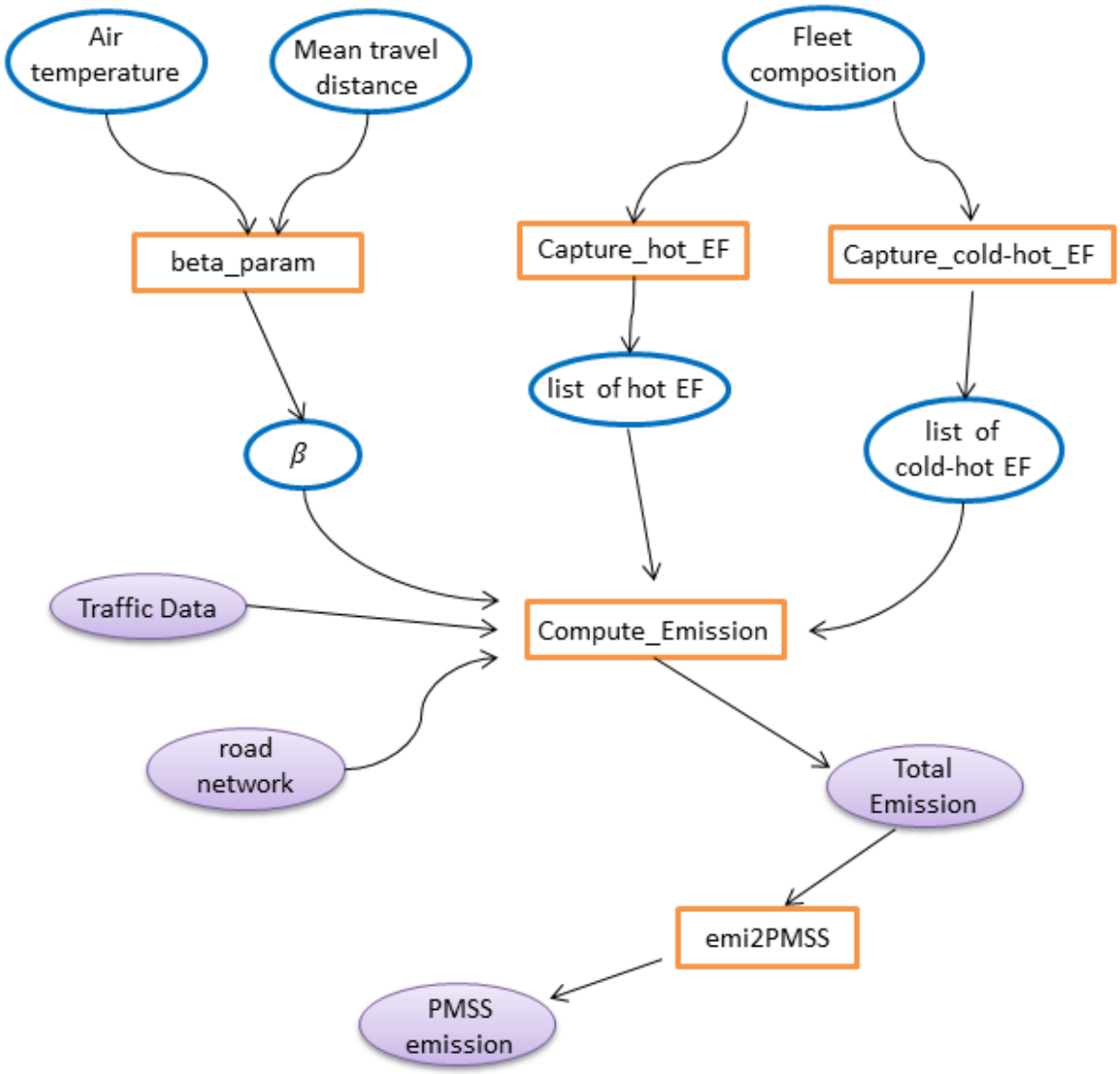

Figure 3.2: VERT flow chart. Orange boxes represent the functions implemented into VERT and Circles are the input/output data in spatial format (filled by light blue) or scalar/vector format (empty circles).

Moreover, the "Capture" functions determine the emission degradation due to vehicle age by estimating the mileage of each selected category (for Passenger Cars and petrol Light Duty Vehicles only), based on vehicles age. Actual average annual mileage (AAAM) for gasoline and diesel cars in the Italian vehicle stock, respectively $AAAM_{gasol}$ and $AAAM_{diesel}$, are estimated with the formulas suggested by Caserini et al. (2013). Considering *age* as the

number of years between the current year and the year of vehicle purchase, the formulas can be written as follow:

$$AAAM_{gasol} = 20.817 \cdot age^2 - 1124.3 \cdot age + 15651 \qquad if\ age \leq 30\ years \qquad (3.8)$$

$$AAAM_{gasol} = 20.817 \cdot 30^2 - 1124.3 \cdot 30 + 15651 \qquad if\ age > 30\ years \qquad (3.9)$$

$$AAAM_{diesel} = 35.072 \cdot age^2 - 1811.2 \cdot age + 23942 \qquad if\ age \leq 30\ years \qquad (3.10)$$

$$AAAM_{diesel} = 35.072 \cdot 30^2 - 1811.2 \cdot 30 + 23942 \qquad if\ age > 30\ years \qquad (3.11)$$

Baseline hot emission factor ($e_{HOT;i,k,r}$) are then corrected by applying the following multiplication factor ($MC_{c,i}$):

$$MC_{c,i} = A_m \cdot AAAM_* + B_m \qquad (3.12)$$

Where $MC_{c,i}$ is the mileage correction factor for a given mileage and pollutant i, $AAAM_*$ is the mileage of vehicles for which correction is applied, A_m is the degradation of the emission performance per kilometre and B_m is the emission level of a fleet of brand new vehicles.

The second types of input needed by VERT are the spatial data, which indicate the geometry, the length, the number of vehicles and their travelling speed for each road of the network, for a specific time step (usually the morning rush hour).

Once the emission factors, the β-parameter, the road network and traffic data are ready, the *Compute_Emission* function estimate the total emission of each street by using the Equations (3.3), (3.4) and (3.5), where the streets length represents the total mileage driven per vehicle ($M_{k,r}$ factor), the traffic data are the number of vehicles N_k, and vehicles travelling speed enter in the formulation of the hot emission factors in Equation (3.7). In Figure 3.3 is shown the total NO_x emissions produced by the traffic flows reported in Figure 3.1 for the morning rush hour, between 07:30 a.m. and 08:30 a.m..

Finally, the total emission can be post-processed by the *emi2PMSS* function in order to produce the emission file needed by the PMSS dispersion model.

The code of the VERT package will be made available as soon as possible after the end of the PhD through a dedicated journal paper.

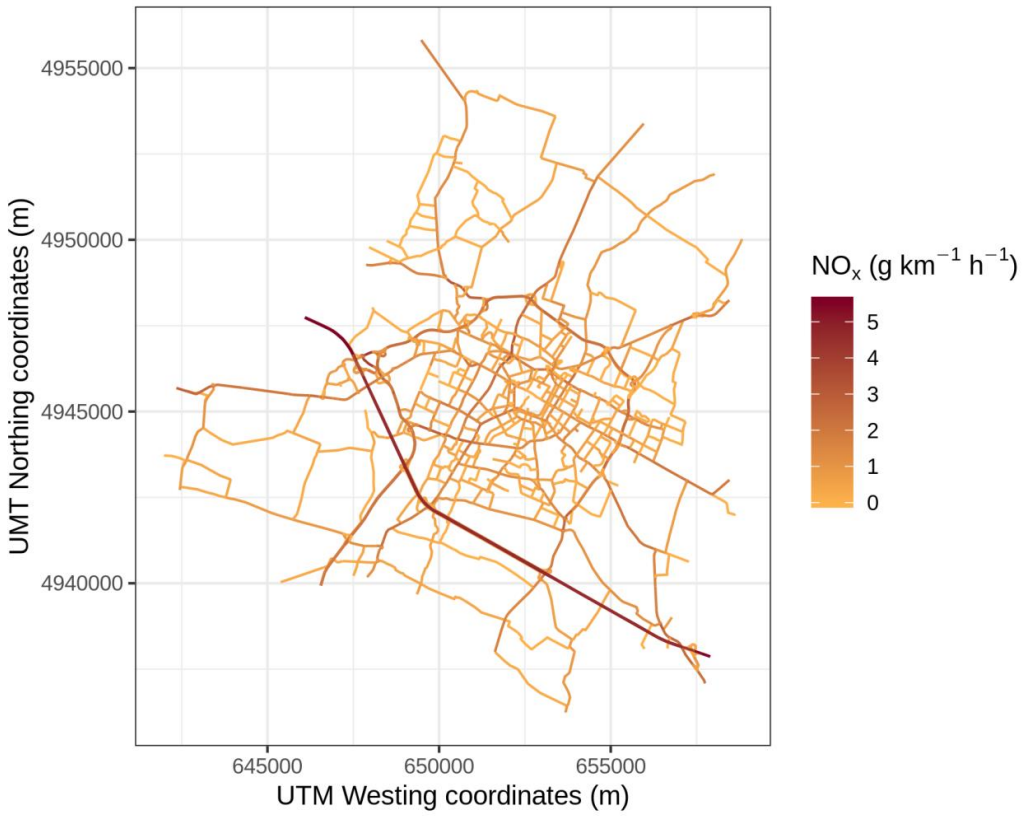

Figure 3.3: Example of VERT output. Modena NO_x emissions from traffic sources related to the morning rush hour.

4. Case study area

The case study area is the urban area of Modena, Italy. Modena is a city located in the Northern part of Italy at 44.65° latitude and 10.93° longitudes at an elevation of 34 meters above the sea level, with a population of about 185 700 inhabitants. It lies on the centre of the Po Valley and it is bounded by the two rivers Secchia and Panaro, both affluent of the Po River. The Adriatic Sea is situated about 100 km to the Est of the city, the same distance to the Liguarian Sea (located to the South-West of Modena) but respect to the previous one, the Apennine chain (40 km South of the town) greatly limits its influence on temperature and wind recirculation. By contrast the air masses coming from the Adriatic Sea can enter without encountering any obstacles along their path causing local weak land-sea breeze phenomena.
Based on its location, Modena has a humid subtropical climate, with continental influences, i.e. is characterized by hot and humid summer with low rainfall rate and by cold and mild winter, featuring damp and chilly with sudden bursts of frost.

Figure 4.1: Overview of the location of the city of Modena in the middle of the Po Valley. The Alps are situated to the North and to the West. Apennines chain is to the South of the city. Adriatic Sea is about 100 km to the East and the Ligurian Sea is also about 100 km to the South-West.

The anemometric regime of Modena is affected by the general breeze winds, mainly caused by the nearby Apennine chain and, as said before, in part also by the Adriatic Sea when the Po Valley is characterized by a strong heating, low baric gradients (less than 0.01 hPa km^{-1}), lack of significant synoptic winds and clear sky (Whiteman, 2000). The resulting process during daytime is the presence of East-Northeast thermal upslope winds to the Apennine hills combined also with the Adriatic breeze. On the other hand, during nighttime the sea influence on local winds is negligible and the prevailing phenomena are the wind from South-West, progressively rotating to the North-West in the early morning and from East in the afternoon when the speed velocity reaches its maximum intensity.

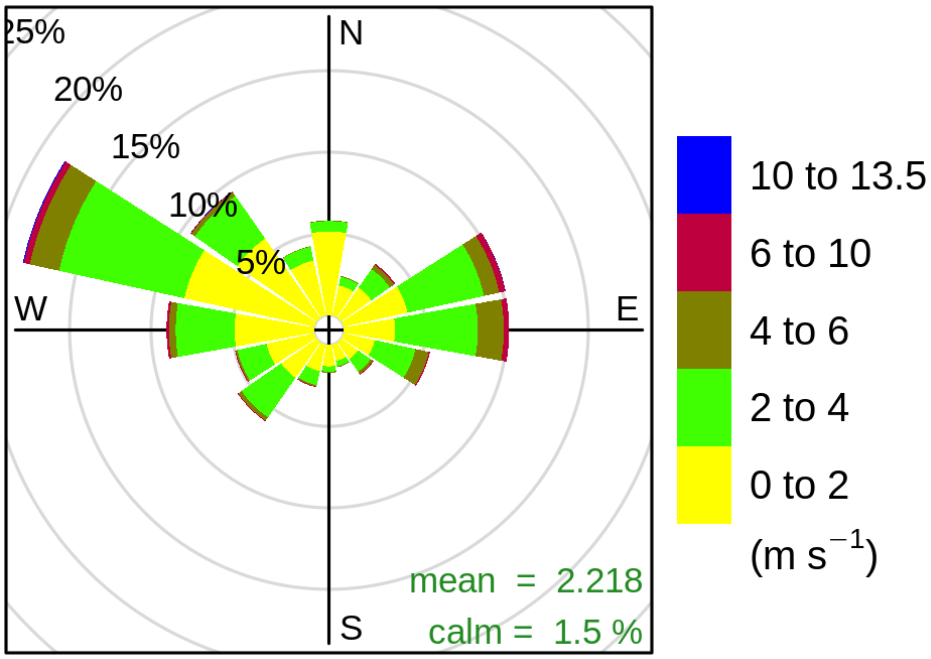

Figure 4.2: Wind-rose computed between January 2015 and December 2018 at the station placed on top to the tower of the Geophysical Observatory of Modena (42 m height above the ground) and located in the historical part of the city of Modena.

Summary statistics for wind in Modena are based on the meteorological station placed on top to the tower of the Geophysical Observatory of of Modena, sited at 42 m above the ground in the centre of the urban area of Modena and in the centre of the simulation domain of the study area. The wind rose from these latter data (figure 4.2) is in line with the prevailing winds of the central Po Valley: western winds are the most frequent, followed by eastern winds. Despite the low wind speed and the poor influence of the breezes compared to the mountain

areas or to the sea coasts, the frequency of thermal and convective winds is still not negligible, since they affect the wind direction distribution depending on the season and the time of the day. Only the winds coming from the South present very low frequency, therefore the transport to Modena of natural or anthropic emissions from the South occurs very rarely, while it is more common from the West or from the East. In particular the direction that had the highest frequency in the period January 2015 – December 2018 was West-Northwest (about 18% of occurrence), followed by East and East-Northeast (both 10% of occurrence), North-West (9.5% of occurrence) and West (9% of occurrence) (Figure 4.2).

Typical meteorological conditions in Modena and in the whole Po Valley are often unfavourable to atmospheric pollutant removal, due to the high frequency of thermal inversion and low wind events, i.e. wind speed values less than 2 m s^{-1}, or calms. The most critical meteorological conditions in the Po Valley are experienced in winter season (Ferrero et al., 2011).

As reported in Figure 4.3, the monthly average wind speed measured at the Geophysical Observatory of Modena between January 2015 and December 2018 reaches its minimum value during winter time, especially in October, November and December, respectively equal to 1.84, 1.86 and 1.74 m s^{-1}. By contrast the monthly mean maximum occur in spring time, with values close to 2.5 m s^{-1} (2.60 m s^{-1} in March and 2.48 m s^{-1} in April).

Along with wind speed, Figure 4.3 shows also the monthly mean temperature in Modena (computed from the daily mean) observed in the same time range (between January 2015 and December 2018): minimum values are reached in January and December respectively equal to 3.7 and 4.4 °C and maximum in July with the average monthly mean temperature equal to 25.2 °C.

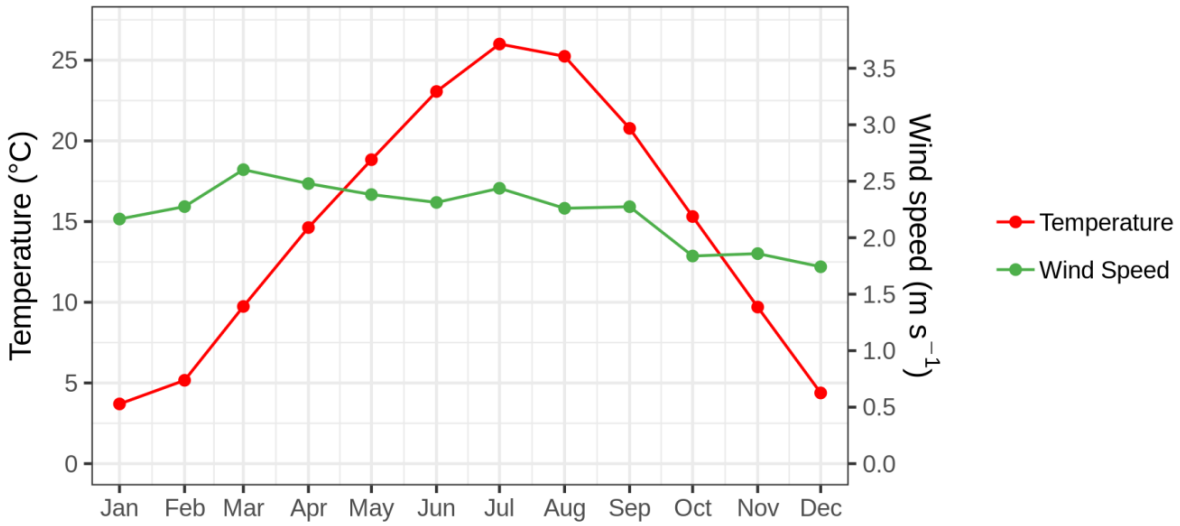

Figure 4.3: Observed monthly average of daily wind speed and temperature between January 2105 and December 2019 at the Geophysical Observatory tower in Modena

During colder months the Alps and Apennines surrounding the valley strongly limit the maximum mixing layer height and prevent the development of moderate or strong winds, leading to recurrent thermal inversion both at daytime and at night time. Monthly average mixing height in winter is generally below 250 m (Figure 4.4), with minimum value in January and December (about 150-200 m): this meteorology along with the large fuel consumption for domestic heating and industry that strong characterizes the area, finally resulting in the build-up of pollutant concentrations in the valley and making the local air quality one of the worst in Europe (Bigi et al., 2017; Bigi and Ghermandi, 2016; Ghermandi et al., 2019).

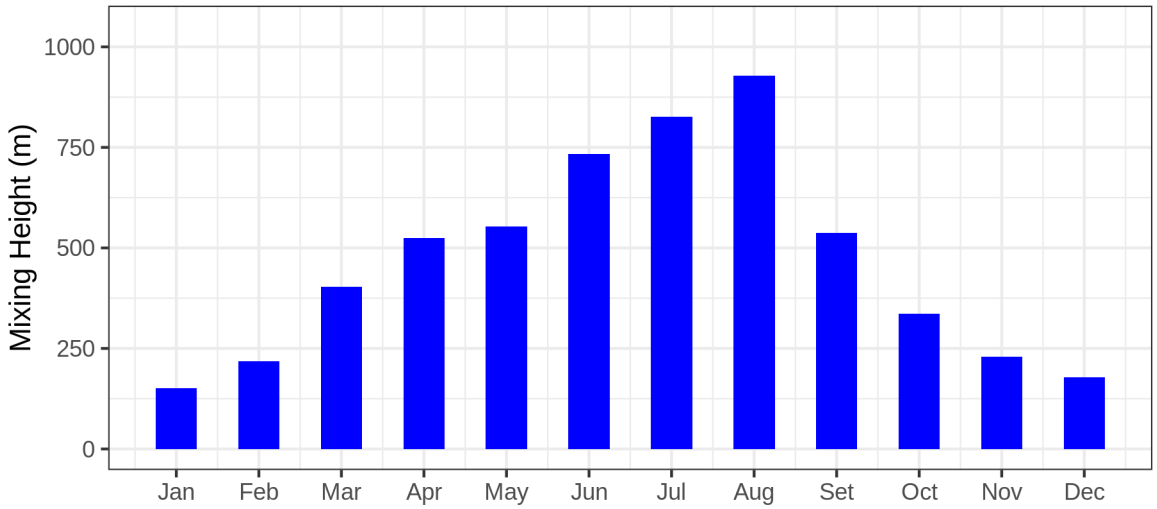

Figure 4.4: Monthly average Mixing height in Modena estimated by the COSMO meteorological model (Arpae Emilia-Romagna) during the whole 2016.

5. Testing the hybrid modelling system in analysis mode

The first part of thesis was focused on the application of the hybrid modelling system described into chapter 2.2 to reproduce hourly NO_x concentrations over the urban area of Modena for the period between 28 October 2016 and 8 November 2016, the same period whereby a traffic measurement campaign was carried out. These days were characterized by weather condition typical for autumn in the central Po Valley (Bigi et al., 2012, Thunis et al., 2009) with a very little atmospheric circulation due to recurrent thermal inversions at low altitude, low mixing layer heights and persistent foggy and hazy events which lasted also during day time. Recurrent wind calm episodes and high-pressure conditions facilitate persistence and homogenization of air masses on a regional scale: the characteristic climate conditions, along with the strong anthropic pressure in the area, lead to long-lasting high concentrations of pollutants also at remote rural sites (Bigi et al., 2017; Masiol et al., 2015; Tositti et al., 2014).

Low rainfall rate (cumulative precipitation lower than 10mm), mean wind speed lower than 2 m s^{-1} (Figure 5.1) and daily average temperature from 7.4 to 13.6 °C characterized the meteorological condition in Modena during the investigated period.

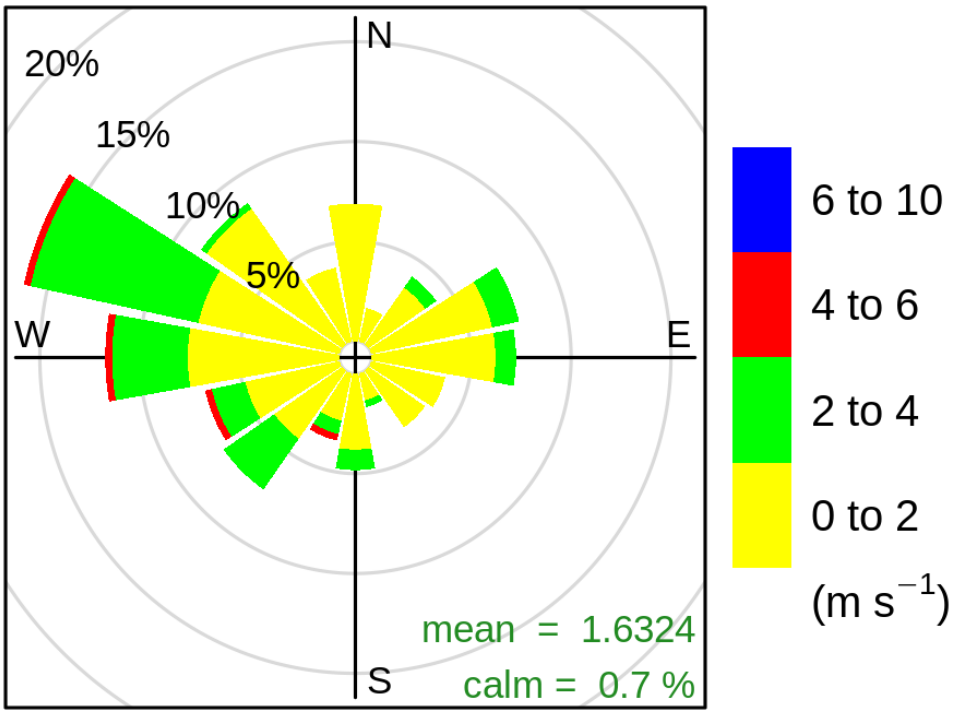

Figure 5.1: Wind-rose of the observed wind between 28 October and 8 November 2016 at the station placed on top to the Geophysical Observatory tower.

As it is possible to see in Figure 5.1, mean observed wind speed between 28 October and 8 November 2016 at the station located on the top the Geophysical observatory tower in the urban centre of the city, was 1.6 m s^{-1}, and the direction that had the highest frequency of occurrence was the wind from the West-Northwest (about 16%), followed by the West (11.5%), the other wind directions had a frequency of occurrence lower than 10% and origins typical of the area: East, East-Northeast and North-West.

Following the multi-model approach (chapter 2.2), WRF-Chem provided the contribution to the Modena urban background concentration generated by the sources located outside the urban area as well as the emissions from industry, waste management and other production processes within the urban area, on which is the base of the PMSS domain. On the other hand PMSS reproduced the hourly field concentration produced by vehicular traffic in the urban domain. The final NO_x concentration field was computed adding the local traffic contribution to the WRF-Chem background concentration. Further explanations regarding the methodology used to avoid double counting of traffic emissions within Modena urban domain are reported in chapter 5.3.

In sections 5.1 and 5.2 are reported the main configurations of WRF-Chem and PMSS models, while in section 5.3 is described the methodology chosen to account for the anthropogenic emissions within and outside the urban area of Modena. Finally section 5.4 highlights the results obtained by applying the multi-model approach in terms of both NO_x atmospheric concentrations and wind field evaluation.

5.1 WRF-Chem set-up

The Weather Research and Forecasting model with chemistry (WRF-Chem), version 3.9.1, was applied over three one-way nested domains, centred in the urban area of Modena. The outer domain (d01) covers most of Europe with 150 x 150 grid cells at 15 km horizontal resolution, the intermediate domain (d02) covers the North of Italy with a resolution of 3 km (150 x 150 grid cells) and the innermost domain (d03) focuses on the Po Valley area with a spatial resolution of 1 km with 175 x 175 grid cells (Figure 5.2). The model was configured with 35 vertical levels with the first layer approximately at 30 m and the model top set at 50 hPa.

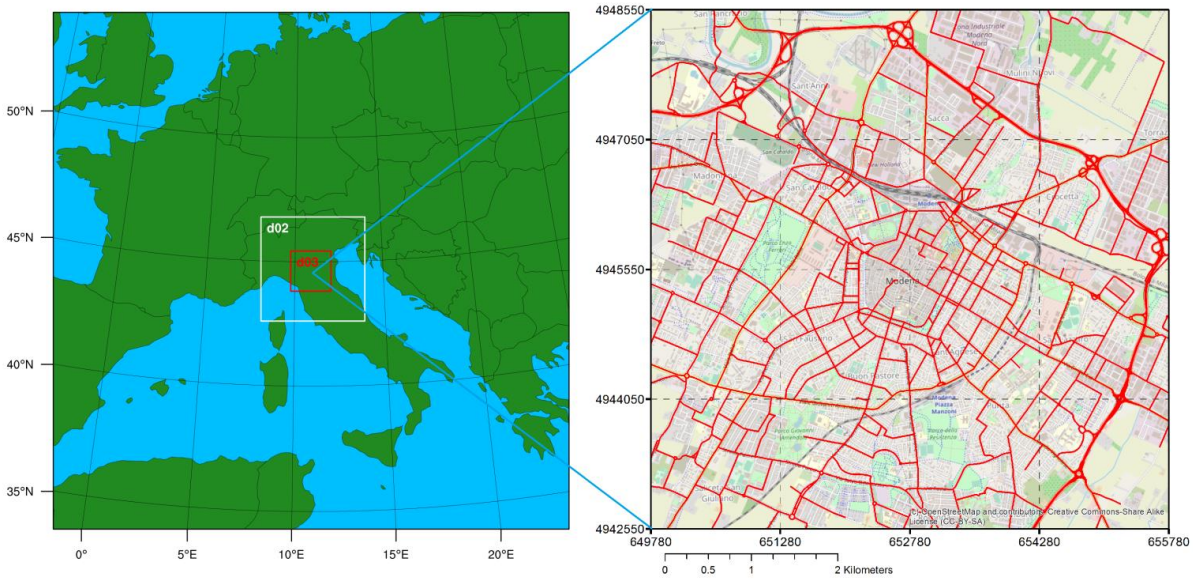

Figure 5.2: Overview of the WRF-Chem model domains on the left (Geographic coordinate system-WGS84) and PMSS investigation domain with the considered Modena street network represented as red lines on the right (UTM32-WGS84).

The main options for physical and chemical schemes adopted here are reported in Table 5-1. These include the Noah Land Surface Model (Chen and Dudhia, 2001), the Yonsei University Planetary Boundary Layer scheme (Hong, 2010), the Grell-Freitas cumulus parameterization (Grell and Freitas, 2014) activated only for the outer domain, the Lin microphysics scheme

(Lin et al., 1983), and the Rapid Radiative Transfer Model (RRTM) radiation scheme (Mlawer et al., 1997) aimed to represent both shortwave and longwave radiation.

Table 5-1: WRF-Chem model set-up and parameterisation.

Process	WRF-Chem option
Land-surface model	Noah Land Surface Model
Boundary layer scheme	YSU
Cumulus parameterization	Grell-Freitas (only for the outer domain)
Microphysics	Lin
Short-wave radiation	RRTM with MCICA method
Long-wave radiation	RRTM with MCICA method
Gas-phase mechanism	MOZART
Aerosol model	MOSAIC 4 bins
Meteo initial/boundary condition	ECMWF - ERA5
Chemical initial/boundary condition	MOZART-4 model

The global Model for OZone And Related chemical Tracers output (MOZART-4; Emmons et al., 2010) and the MOSAIC aerosol model (Zaveri et al., 2008) were used to simulate airborne pollutants over the nested domains. The first one includes 85 chemical species, 196 reactions and is consistent with the chemistry used in the global model that provides the chemical input and boundary conditions for the nested simulations. MOSAIC uses a sectional bin approach for the representation of the aerosol size distribution. The MOSAIC model predicts several aerosol species, such as sulfate, nitrate, ammonium, elemental carbon, and primary aerosols (POAs). Processes involving secondary organic aerosols (SOAs) formation were represented by the scheme based on Hodzic and Jimenez, (2011).

Meteorological initial and boundary conditions were provided by the 6-hourly ECMWF analysis field (ERA5 dataset) with a horizontal resolution of 0.25° x 0.25°, interpolated to 37 pressure levels from 1000 to 1 hPa. Data included 3D fields of temperature, specific humidity and wind speed components. 2D surface parameters such as mean sea level pressure, sea surface temperature, soil temperature and volumetric soil water content were also considered.

A grid nudging on temperature and wind field has been also performed within the boundary layer in all three model configurations using as input data the ECMWF analysis.

As to land use, the Corine Land Cover (CLC) dataset was adopted after reclassifying it into the 33 USGS classes to match the WRF land use tables. Chemical initial and boundary conditions were provided by the MOZART-4 model (Emmons et al., 2010). Biogenic emissions were calculated online by the Model of Emissions of Gases and Aerosols from Nature version 2.1 (MEGAN2.1) by Guenther et al., (2012). In addition, sea salt and dust emissions are calculated online.

5.2 PMSS Set-up

A 3D wind and turbulence field and air pollution dispersion reconstruction was performed on a 6 km x 6 km square domain covering the city of Modena (Figure 5.2) with the PMSS modelling suite. Given the low altitude difference between different areas of the city, a flat domain was considered and a 3D reconstruction of buildings was made by using a pre-processor: 25,600 polygons contained in the ESRI shapefile (provided by Geoportale Regione Emilia-Romagna) were transformed into approximately 146 000 triangular prisms directly usable by Micro-SWIFT.

In order to guarantee both flow and pollutant dispersion fields at a high resolution in each part of the domain, a horizontal grid step of 4 m (square cells) was chosen for both Micro-SWIFT and Micro-SPRAY models. To represent the flow entering the Micro-SWIFT computational domain, vertical profiles of temperature, humidity, wind speed and direction from the innermost domain (d03) of the WRF-Chem simulation were extracted on an hourly basis. In addition, mixing height values and main background turbulence parameters (i.e. friction velocity, Obukhov length and convective scale velocity) were estimated with the Mesoscale Model Interface Program v3.4 (MMIF, https://www.epa.gov/scram/air-quality-dispersion-modeling-related-model-support-programs), which converts prognostic meteorological WRF output fields into turbulence scale parameters.

3D fields of wind, temperature and turbulence were obtained for 20 vertical levels from 3 m up to 200 m above the ground using the Micro-SWIFT model (version 2.1.1) with the RANS flow solver option activated. The 2D Cressman interpolation method wind field was also considered in the configuration.

Regarding the Micro-SPRAY model simulations the horizontal grid was chosen to be identical to that of the Micro-SWIFT model computation and the vertical grid structure consisted of 10 levels with a linear progression up to 200 m above the ground level with 3 m height for the first layer close to the soil. This arrangement leads to a configuration of 1504 x 1504 x 10 nodes and a total number of $2.26 \cdot 10^7$ cells. The main SPRAY parameters also included an emissions time step of 5 seconds and a synchronisation time step of 10 seconds. The version of Micro-SPRAY used in the analysis case study was 3.7.3.

Concentrations are computed every hour and sampled every 10 seconds. Since the cumulative precipitation for all the examined period was less than 10 mm, the wet deposition was not included in the set-up. The main PMSS set-up parameters are reported in Table 5-2.

Table 5-2: Micro-SWIFT and Micro-SPRAY set-up

Micro-SWIFT		**Micro-SPRAY**	
Parameters	Value	Parameters	Value
Horizontal resolution	4 m	Horizontal resolution	4 m
Horizontal grid	1504 x 1504 points	Horizontal grid	1504 x 1504 points
Vertical grid	from 3 up to 200m	Vertical grid	from 3 up to 200m
	20 vertical levels		10 vertical levels
Interpolation method	Cressman 2D	Emission time step	5 s
RANS flow solver	Activated	Averaging period for concentrations	3600 s

5.3 Anthropogenic emissions

Following the regional emissions inventory database produced by Arpae Emilia-Romagna, the local environmental agency (INEMAR 2013), the road traffic in Modena contributes up to the 60% of the total emissions in terms of NO_x, while the domestic heating and industrial combustion represent only the 15% and 14% of the total amount. Based on this percentage distribution, the methodology employed to account for anthropogenic emissions rely on two different strategies: a city-tailored emission estimate, to describe traffic emissions at micro-scale resolution in the urban area of Modena, and an emission inventory estimate, more suitable to account for emissions at large-scale area, used as an input for the chemical transport model in order to estimate the contribution of all the SNAP (Selected Nomenclature for Air Pollution) emission categories throughout Europe.

The anthropogenic emissions used for the parent and the nested WRF-Chem domains were taken from the TNO-MACC III inventory, available on a regular grid with a horizontal resolution of 0.125° x 0.0625°, which contains emissions for air pollutants such as NO_x, SO2, NMVOC, NH3, CO and primary particulate matter (PM2.5 and PM10). The inventory is based on nationally reported emissions for specific sectors and spatially distributed with proxy data such as the population density for urban emissions or the road network for non-urban emissions. The main developments with respect the version II of the inventory (Kuenen et al., 2014) includes improved emissions and trends for the international sea shipping, improved wood consumption estimation and more detailed spatial distribution, as well as improved industrial emissions apportioning achieved through the use of CORINE land cover data instead of population density data as a default item.

TNO-MACC III emissions are provided as annual totals, therefore each SNAP category was scaled to take into account monthly, daily variation (weekend or weekday) and hour of the day (diurnal cycle), as suggested by Kuik et al., (2018). A vertical emissions distribution was also taken into account by distributing the emissions of industrial sources, airports, extraction and distribution of fossil fuel into seven vertical layers, up to 750 m.

In order to avoid the double counting of the traffic emissions placed inside the urban area of Modena and to better represent the spatial distribution of traffic sources in the nearby territory, a downscaling procedure was conducted for the SNAP sectors 71-75. The original

TNO dataset (resolution ca. 14 km x 7 km) covering the inner most WRF-Chem domain was subdivided to a finer grid with a horizontal resolution of 1 km x 1 km.

Traffic fluxes of light (passenger cars and L-category vehicles) and duty (light commercial vehicle and heavy-duty trucks) vehicles on the main roads of the province of Modena at morning rush hour (07:30 – 08:30 a.m., local time) for the year 2010 were provided by the Municipality of Modena and proceed from a simulation study by means of the PTV VISUM model (PTV Group, Karlsruhe, Germany http://vision-traffic.ptvgroup.com/en-us/products/ptv-visum/). These data were used as a proxy variable to assign TNO-MAC III traffic emissions over the province of Modena to the portion of the land interested by PTV VISUM road network: the more traffic fluxes were estimated for a specific road segment, the more emissions were assigned to the corresponding grid (1 km x 1 km) (Figure 5.3).

Once the downscaled grid dataset was created, a spatial surrogate function was implemented to identify the TNO-MACC III traffic emissions within the PMSS domain. This function returns zero if the territory cell is completely inside the PMSS domain, one if the territory cell is completely outside and a value between zero and one (proportional to the area outside the PMSS domain) if the territory cell crosses the domain boundaries. Finally, to exclude TNO-MACC III emissions from the PMSS domain, the spatial mask created with the surrogate function was multiplied by the downscaled traffic emission inventory. The same traffic simulation obtained with the PTV VISUM model includes also vehicle fluxes in the urban area of Modena, providing the number and the average speed for light and duty vehicles at rush hour for each segment of the urban road network, which encompasses about 1100 sections with a total length of 210 km (Figure 5.4).

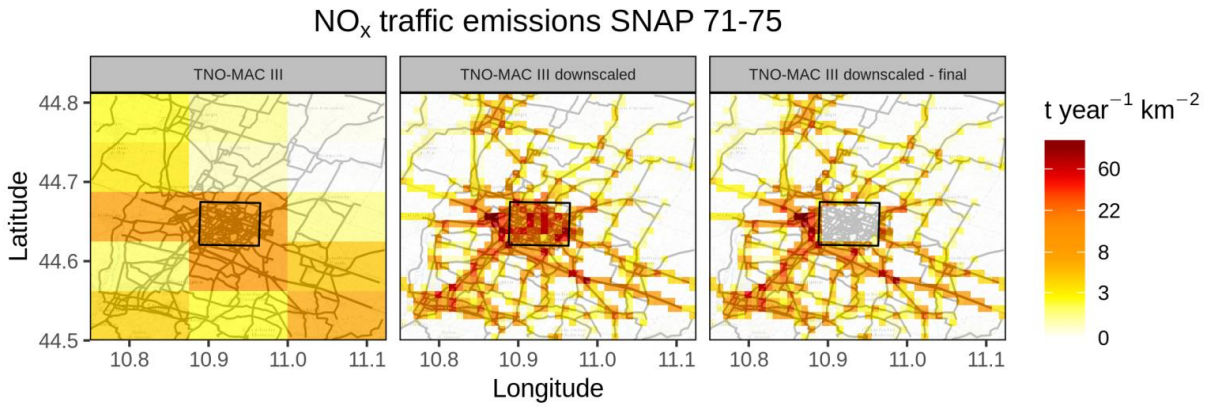

Figure 5.3: Total NO_x traffic emissions (SNAP sector 71-75) in the province of Modena. On the left the original TNO-MACC III inventory emissions (resolution ca. 14 km x 7 km). At the centre the TNO-MACC III inventory emissions downscaled to a resolution of 1 km x 1 km and distributed according to the street traffic flow estimated by PTV VISUM. On the right the TNO-MACC III inventory emissions downscaled to a resolution of 1 km x 1 km without the emissions by road traffic in the urban area of Modena.

The methodology chosen to estimate traffic emissions in the urban area of Modena was based on a bottom-up approach: traffic flow data simulated by PTV VISUM model were employed as "activity factor" and specific Emission Factors (EF) were used to estimate total emissions according to the fleet composition, vehicle type, fuel, engine capacity, load displacement, slope of the road, Euro emission standard and average traveling speed.

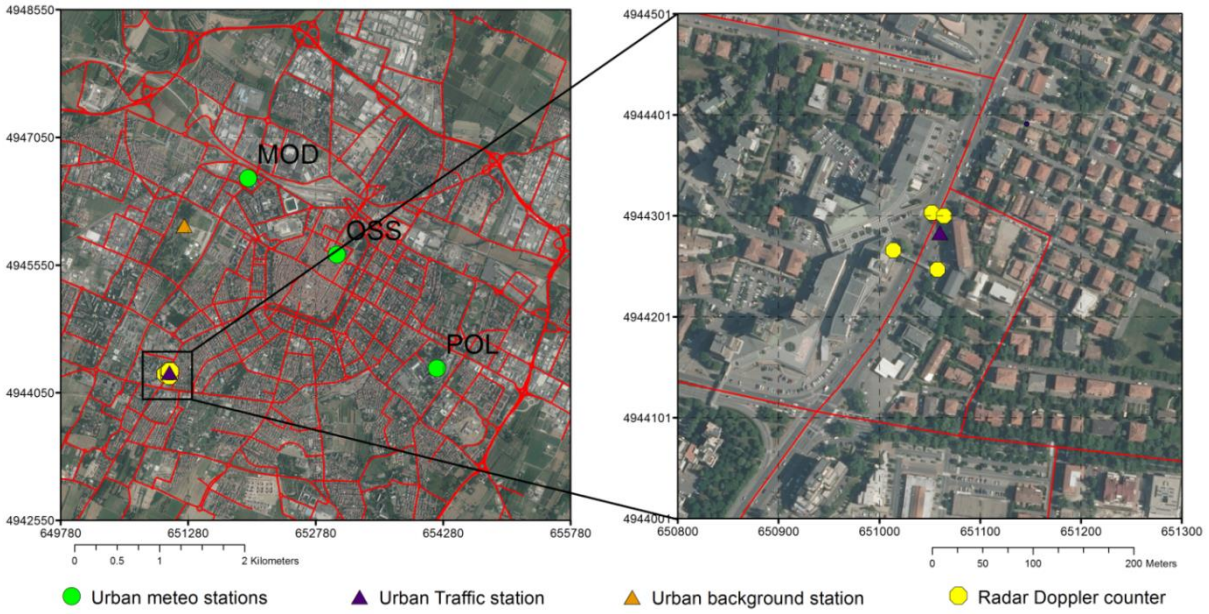

Figure 5.4: PMSS computational domain (left side) and view of the radar traffic counters position (right side). Radars are represented by yellow dots, air quality urban background station by orange triangle and urban traffic station by blue triangle. Urban meteorological stations are also depicted by green dots along with their label names.

With aim of estimating for each road segment the NO_x atmospheric emissions in terms of pollutant mass per trip unit, the R package VERT (Vehicular Emissions from Road Traffic), see chapter 3.3, was employed. The Emission Factors suggested by Ntziachristos and Samaras (2016) were used and a series of functions to automatically compute for each road of the network the total NO_x emissions were implemented.

The Tier 3 methodology, defined in the European guidelines EMEP/EEA (Ntziachristos and Samaras, 2016) for the estimate of exhaust emissions from road transport was adopted, and total exhaust emissions were calculated as the sum of hot emissions (when the engine is at its normal operating temperature) and emissions during transient thermal engine operation (termed 'cold-start' emissions). As stated before, the road network considered in the micro-scale simulation is contained in the urban area of Modena, therefore only urban driving situation was considered in the emissions estimation.

EF values were computed for each vehicle fleet category considering the flow speed estimated by PTV VISUM, and then EFs were mathematically weighted according to fleet composition to obtain for each road two EFs, one representing the light vehicles and one on behalf of duty vehicles.

Hot emissions computation included also correction values applied to the baseline emission factors to account for different vehicle age for passenger cars and light commercial vehicles, also called emissions factors degradation due to vehicle age (Ntziachristos and Samaras, 2016).

In addition to the traffic model data, a direct vehicle flow measurement campaign was carried out continuously over two weeks between October 28 and November 8, 2016, with 4 Doppler radar counters (one for each road lane) in a four-lane road in the proximity of the intersection with the urban ring road (Ghermandi et al., 2019) (Figure 5.4). The radar traffic counters recorded the time, the length and the velocity for each passing vehicle. The captured vehicles were subdivided into two different groups according to the vehicle classes modelled by PTV VISUM: light vehicles, with measured length less or equal to 6 m and duty vehicles, with measured length greater than 6 m. Finally, to appropriately describe NO_x emissions under typical vehicle flux conditions, recorded flow data were used to reproduce hourly modulation rates for the entire road network.

In order to test the reliability of the hot EFs computed with the methodology previously described and to check how far these EFs are with respect the one computed considering recently emission data, based on new PEMS tests (Hausberger et al, 2019, Sjödin et al., 2018), the weighted EFs for Passenger Cars (PC), Light Commercial Vehicle (LCV), Heavy Duty Trucks (HDT) and Motorcycle in Modena were compared with the weighted average hot EFs calculated following the handbook of emission factors (HBEFA, 2019) for different European countries (Germany, Austria, Switzerland, France, Norway and Sweden).

Since the HBEFA desktop application is not available for free, an extensive analysis relied on the real vehicle fleet composition in Modena was not possible. Despite this limitation, an indicative comparison between the actual hot EFs considered in the emission computation for the city of Modena and the average hot EFs for the respective vehicles category between the 6 European countries mentioned before is shown in Figure 5.5. The green rectangles indicate the EFs used in study, while the red rectangles represent the average EFs computed between Germany, Austria, Switzerland, France, Norway and Sweden, when available. The black horizontal segments below and above the red rectangles upper limit indicate respectively the minimum and the maximum EF for each respective vehicle category.

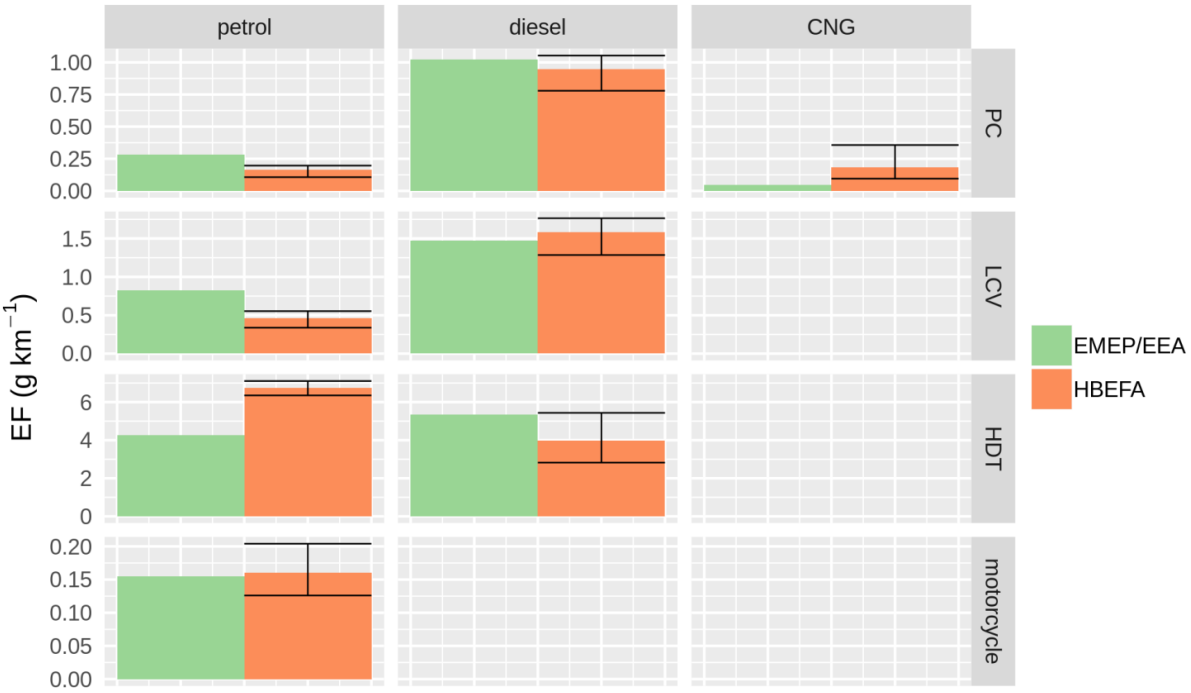

Figure 5.5: Comparison between weighted NO_x hot EFs used in this study, computed following the EMEP/EEA guidelines (green rectangles) and the corresponding average NO_x hot EFs computed between Germany, Austria, Switzerland, France, Norway and Sweden following the handbook of emission factors (HBEFA) version 4.1 (red rectangles). With horizontal black segment are also indicated the minimum and maximum HBEFA EF for the same six European countries. Please note the difference in the scale on the y-axis in each panel.

The hot EFs obtained following the EMEP/EEA guidelines for the city of Modena are in general in line with the hot EFs computed using the HBEFA methodology (v4.1) for similar European countries. The main differences in absolute terms regard the Heavy Duty Truck category, where the HDT EFs estimated in Modena are 4.28 and 5.34 g km^{-1} for petrol and diesel respectively, while the average hot EFs for the same vehicles category are 6.75 and 3.97 g km^{-1}. The variability between diesel HDT EF for the six European countries considered is also large and the maximum of these EFs is greater than the EF considered in Modena. On the other hand, diesel LDV EFs are very similar to each other and equal to 1.47 g km^{-1} for Modena and 1.58 g km^{-1} for the average EF between the six countries. By contrast, petrol LDV EFs differ of about 0.37 g km^{-1} (0.83 g km^{-1} for Modena and 0.46 g km^{-1} for the average of the other countries). Finally, Motorcycle and Passenger Cars EFs estimated in Modena agree very well with the average EFs estimated following the HBEFA methodology: 0.28 (petrol), 1.02 (diesel) and 0.05 (CNG) g km^{-1} are the PC EFs estimated in Modena, while the

HBEFA respective average is 0.16, 0.94 and 0.18 g km^{-1}. Motorcycle EFs are almost the same, 0.15 g km^{-1} for Modena and 0.16 g km^{-1} for the HBEFA average.

5.4 Model evaluation

The statistical performance analysis considered multiple statistical indicators regardless of the model's application since each one has its advantages and disadvantages and it is not possible to identify a unique exhaustive index of quality.

The main statistical metrics employed in this thesis are Pearson correlation coefficient (*r*), Mean Bias (MB), Normalized Mean Bias (NMB), Root Mean Square Error (RMSE), Mean Absolute Error (MAE) and the fraction of predicted values within a factor of two of observations, also referred as Factor of two (FAC2). These statistical indicators are defined as follows, with *n* the number of model–observation pairs, *M* the modelled values (with $\bar{M} = \frac{\sum_{i=1}^{n} M_i}{n}$ the averaged modelled value) and *O* the observations (with $\bar{O} = \frac{\sum_{i=1}^{n} O_i}{n}$ the averaged observed value):

$$r = \frac{\sum_{i=1}^{n}(M_i - \bar{M})(O_i - \bar{O})}{\sqrt{\sum_{i=1}^{n}(M_i - \bar{M})^2}\sqrt{\sum_{i=1}^{n}(O_i - \bar{O})^2}}$$

$$MB = \frac{1}{n}\sum_{i=1}^{n} M_i - O_i$$

$$NMB = \frac{\sum_{i=1}^{n} M_i - O_i}{\sum_{i=1}^{n} O_i}$$

$$RMSE = \sqrt{\frac{1}{n}\sum_{i=1}^{n}(O_i - M_i)^2}$$

$$MAE = \frac{\sum_{i=1}^{n} DWD_i}{n}$$

$$where\ DWD(\text{difference of the wind direction}) is\ calculated\ from:$$

$$DWD_i = \begin{cases} \min(M - O, O - M + 360), & for\ M > O \\ \min(O - M, M - O + 360), & for\ M < O \end{cases}$$

$$FAC2\ (fraction\ where\ 0.5 < \frac{M}{O} < 2\ )$$

In order to evaluate the performance of the models in urban environment, the Fractional Mean Bias (FB), Normalized Absolute Difference (NAD) and Normalized Mean Square Error (NMSE) were also considered. They can be defined as follow:

$$FB = 2\frac{\overline{O - M}}{\bar{O} + \bar{M}}$$

$$NAD = \frac{\overline{|O - M|}}{\bar{O} + \bar{M}}$$

$$NMSE = \frac{\overline{(O - M)^2}}{\bar{O} \cdot \bar{M}}$$

5.5 Results and discussion

5.5.1 Meteorology

2 m temperature (T2), 10 m wind speed (ws10) and 10 m wind direction (wd10) meteorological fields predicted by WRF-Chem were compared against corresponding surface observations of these variables provided by 33 stations within the d03 domain (see Table 5-3 and Figure 5.6): 18 stations (with 16 of them for T2, ws10 and wd10) belong to the RIRER (Rete idro-meteo-pluviometrica integrata) Arpae-Simc network, 11 stations (with 7 for T2, ws10 and wd 10) belong to the Archivio dati idro-nivo-meteorologici ARPA Lombardia network, 4 stations belong to the Osservatorio Meteo Idrologico della Regione Liguria (OMIRL) ARPAL network. Other two stations belonging to the Geophysical Observatory of Modena weather network were considered for the micro-scale wind field evaluation. All the meteorological stations mentioned before are automated and realized according to WMO (World Meteorological Organization) directive. On the other hand, NO_x concentrations at air quality stations are measured using chemiluminescence. With this method all the NO_2 contained in an air sample is converted to NO with a molybdenum converter, then the sample gas goes straight to the reaction chamber where NO (both the original NO contained in the air sample and the NO_2 converted to NO) will react with O_3 to form NO_2 and O_2 while emitting light. Finally, the measure of the emitted light will be proportional to the NO_x concentrations in the air sample.

Table 5-3: Observation sites. Locations are provided in Geographic coordinates (WGS84). Available parameters are: "T2" for temperature at 2 m height above the ground, "ws10" for wind speed and "wd10" for wind direction at 10 m above the ground and "NO_x" for NO_x concentrations.

Station name	Label	Network	Longitude (°)	Latitude (°)	Type	Parameters
Bologna urbana	BOL	Arpae-Simc	11.32879	44.50075	Meteorology	T2, ws10, wd10
Colorno	COL	Arpae-Simc	10.34959	44.94378	Meteorology	T2, ws10, wd10
Ferrara urbana	FER	Arpae-Simc	11.621138	44.832498	Meteorology	T2
Finale Emilia	FIN	Arpae-Simc	11.284	44.839	Meteorology	T2
Granarolo Faentino	GRA	Arpae-Simc	11.95861	44.36013	Meteorology	T2, ws10, wd10
Imola	IMO	Arpae-Simc	11.74953	44.3332	Meteorology	T2, ws10, wd10
Loiano	LOI	Arpae-Simc	11.32646	44.26093	Meteorology	T2, ws10, wd10

Malborghetto di Boara	MAL	Arpae-Simc	11.66134	44.85799	Meteorology	T2, ws10, wd10
Modena urbana	MOD	Arpae-Simc	10.91699	44.65639	Meteorology	T2, ws10, wd10
Panocchia	PAN	Arpae-Simc	10.29584	44.6837	Meteorology	T2, ws10, wd10
Parma urbana	PAR	Arpae-Simc	10.33049	44.808	Meteorology	T2, ws10, wd10
Reggio Emilia urbana	REG	Arpae-Simc	10.6337	44.69781	Meteorology	T2, ws10, wd10
Rolo	ROL	Arpae-Simc	10.874	44.88481	Meteorology	T2, ws10, wd10
S.Pietro Capofiume	SPC	Arpae-Simc	11.62264	44.65378	Meteorology	T2, ws10, wd10
San Pancrazio	SPA	Arpae-Simc	10.27245	44.80806	Meteorology	T2, ws10, wd10
Sasso Marconi	SAS	Arpae-Simc	11.24125	44.43967	Meteorology	T2, ws10, wd10
Sivizzano	SIV	Arpae-Simc	10.35704	44.6482	Meteorology	T2, ws10, wd10
Vignola	VIG	Arpae-Simc	11.00414	44.50405	Meteorology	T2, ws10, wd10
Bigarello	BIG	ARPA Lombardia	10.8874	45.18783	Meteorology	T2, ws10, wd10
Cremona	CRE	ARPA Lombardia	10.04414	45.14188	Meteorology	T2, ws10, wd10
Gambara	GAM	ARPA Lombardia	10.29949	45.24903	Meteorology	T2, ws10, wd10
Gonzaga	GON	ARPA Lombardia	10.7678	44.96381	Meteorology	T2
Mantova Lunetta	MAL	ARPA Lombardia	10.82421	45.15733	Meteorology	T2, ws10, wd10
Mantova Tridolino	MAT	ARPA Lombardia	10.86007	45.15135	Meteorology	T2, ws10, wd10
Mantova Virgilio	MAV	ARPA Lombardia	10.79293	45.11438	Meteorology	T2
Persico Dosimo	PED	ARPA Lombardia	10.1041	45.1851	Meteorology	T2
Pieve S.Giacomo	PSG	ARPA Lombardia	10.19548	45.12107	Meteorology	T2, ws10, wd10
Ponti sul Mincio	PSM	ARPA Lombardia	10.68363	45.41211	Meteorology	T2, ws10, wd10
Spinadesco	SPI	ARPA Lombardia	10.05912	45.16297	Meteorology	T2
La Spezia	LAS	ARPAL	9.82819	44.10703	Meteorology	T2, ws10, wd10
Luni	LUN	ARPAL	10.00899	44.07491	Meteorology	T2, ws10, wd10
Monte Rocchetta	MOR	ARPAL	9.93842	44.07129	Meteorology	T2, ws10, wd10
Porto Venere	POV	ARPAL	9.83594	44.052	Meteorology	T2, ws10, wd10
Badia	BAD	Arpae Emilia-Romagna	10.28937	44.65823	Air Quality	NO_x
Besenzone	BES	Arpae Emilia-Romagna	10.0192	44.9895	Air Quality	NO_x
Febbio	FEB	Arpae Emilia-Romagna	10.43104	44.30071	Air Quality	NO_x
Gherardi	GHE	Arpae Emilia-Romagna	11.96125	44.83975	Air Quality	NO_x
Ostellato	OST	Arpae Emilia-Romagna	11.94194	44.7409	Air Quality	NO_x
Parco Ballirana	PAB	Arpae Emilia-Romagna	11.98236	44.52743	Air Quality	NO_x
San Pietro	SCA	Arpae Emilia-	11.62482	44.65423	Air Quality	NO_x

Capofiume		Romagna				
San Rocco	SAR	Arpae Emilia-Romagna	10.66478	44.87373	Air Quality	NO_x
Schivenoglia	SCH	ARPA Lombardia	11.0761	45.01688	Air Quality	NO_x
Spinadesco	SPN	ARPA Lombardia	9.930599	45.15047	Air Quality	NO_x
Policlinico	POL	Geophysical Observatory MO	10.94429	44.63580	Meteorology	ws10, wd10
Geophysical Observatory	OSS	Geophysical Observatory MO	10.92981	44.64809	Meteorology	ws10, wd10
"Parco Ferrari"	VGA	Arpae Emilia-Romagna	10.90731	44.65157	Air Quality	NO_x
"via Giardini"	PFE	Arpae Emilia-Romagna	10.90572	44.63699	Air Quality	NO_x

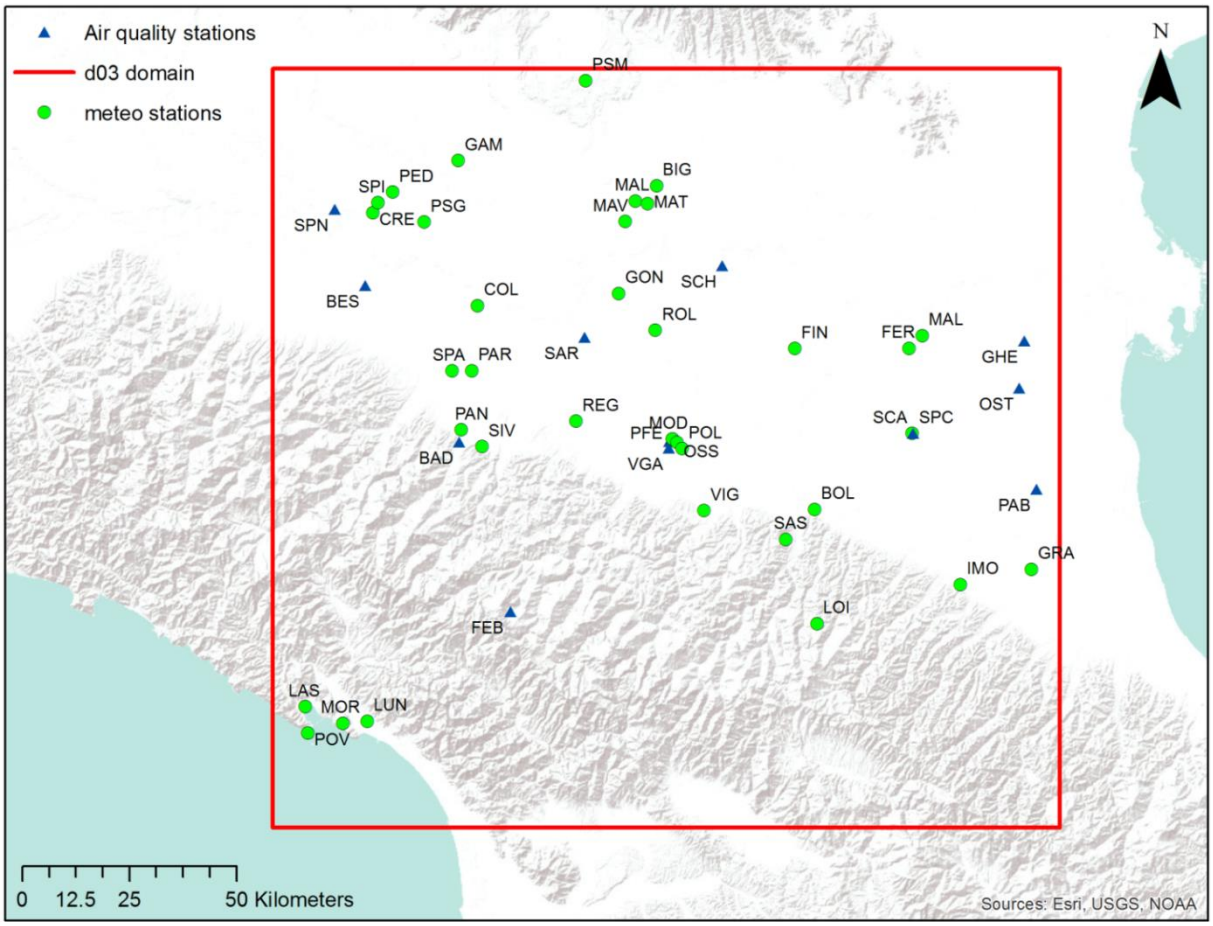

Figure 5.6: Map of the stations inside the WRF-Chem d03 domain. Site of the meteorological stations are reported by the green dots and site of air quality station are reported by the blue triangles.

Generally, modelled hourly 2 m temperatures reproduced by WRF-Chem at 1 km resolution (d03 domain) are consistent with observations at all the stations: *r* is between 0.68 and 0.87, except for two stations, Persico Dosimo and Bologna urbana, where the correlation is respectively very good (0.96) and not particularly high (0.59). The minimum value can be attributed to the difficulties of the model in representing urban meteorological dynamics where land use data for a large urban area may not be extremely accurate and some local phenomena can be missed. This could be the case of the Bologna city environment. By contrast, the maximum correlation observed at the Persico Dosimo station could in this case reached by a chance where hourly measurements were available only for one fourth of the investigated period. However, the good correlation between modelled 2 m temperature and observations for a large number of stations shows that the WRF-Chem model represented the observed meteorological variability quite well.

The model on average tends to be positively biased with a MB smaller than +1°C for most of the stations where only two of them exceed +2°C of MB, respectively at the Reggio Emilia urbana and Colorno stations. On the other hand, the minimum MB is -1.6°C, achieved at the Porto Venere station on to the Ligurian Sea shore. These results are in the same range as the MB that Gsella et al., (2014) found using MM5, WRF and TRAMPER meteorology models for the same area.

Figure 5.7 shows the statistical performance of WRF-Chem in reproducing 2 m temperature. *r* is plotted as a function of MB for the three different model resolutions: 15 km (d01), 3 km (d02) and 1km (d03). The variability of MB tends to increase by increasing the model resolution, conversely, the average *r* including all the stations is 0.78 for the d01 WRF-Chem domain, 0.80 for the d02 domain and 0.81 for the d03 domain, showing that the increase of the model resolution from 15 km to 1 km generally leads to slightly improve the performance of the model in reproducing 2 m temperature.

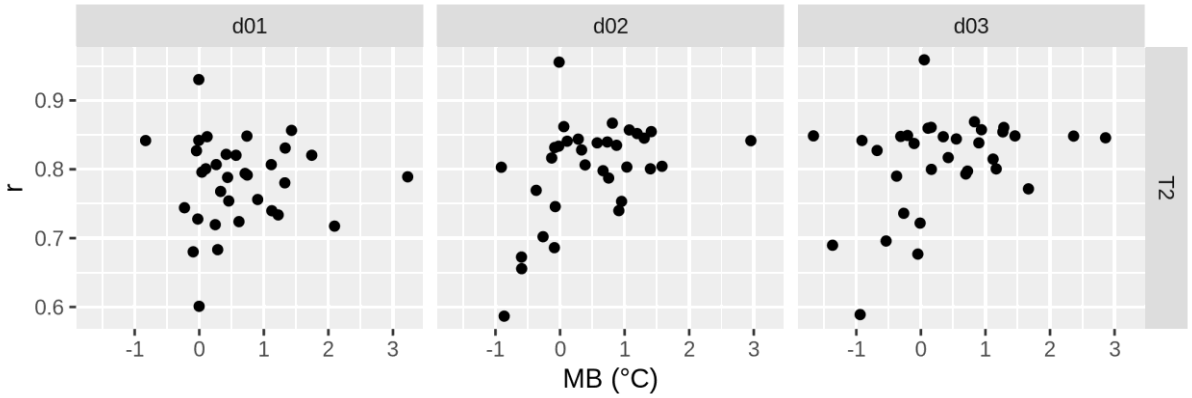

Figure 5.7: Pearson correlation coefficient (r) reported as function of the Mean Bias (MB) between modelled hourly 2 m temperature (T2) and observation at 33 measurements sites for the three WRF-Chem resolutions: 15 km (d01), 3 km (d02) and 1 km (d03).

Simulated hourly wind speed at the d03 domain generally express performance in line with similar case study in literature (Gsella et al., 2014; Kuik et al., 2016; Mar et al., 2016) since the great majority of the stations exhibits a MB between -0.5 m s^{-1} and +0.5 m s^{-1}, range suggested by Malm et al. (2009) and by European Environmental Agency (EEA) guidelines (EEA, 2011). Only the stations of Loiano and La Spezia are outside these limits with respectively a MB of -0.99 m s^{-1} and +1.43 m s^{-1}: the former is located in the Tuscan-Emilian Apennines at about 700 m above the sea level and the latter is close the Ligurian sea and then characterized by a strong influence of land-sea breeze, similarly to the temperature monitoring station of Porto Venere. The large bias found at these two stations suggests that the model might have difficulties in simulating the wind field in mountainous areas and close to the sea where complex orography and local breeze characterize the territory, however for the rest of the stations the MB values are consistent with the reference benchmarks proposed in literature.

Another statistical indicator suggested by the EEA guidelines (2011) and by Malm et al. (2009) is the Root Mean Square Error, for which the recommended benchmark for wind speed is less than 2 m s^{-1}. As for the MB, RMSE of modelled wind speed values are below 2 m s^{-1} at all stations besides Loiano and La Spezia, where RMSE are 3.76 m s^{-1} and 2.14 m s^{-1}, respectively. Nonetheless, modelled wind speed at the vast majority of the stations is in line with the benchmark for a mesoscale meteorological reconstruction.

In Figure 5.8 the performance of WRF-Chem in reproducing wind speed for the three different resolutions is shown: RMSE is plotted as a function of the MB. As the resolution is

increased, the model tends to show lower MB in absolute terms. Similarly, the RMSE generally tends to moderately decrease as well with increasing resolution. It is therefore possible to conclude that in increasing model resolution from 15 km to 1 km there is a slight improvement of performance also for wind speed reconstruction.

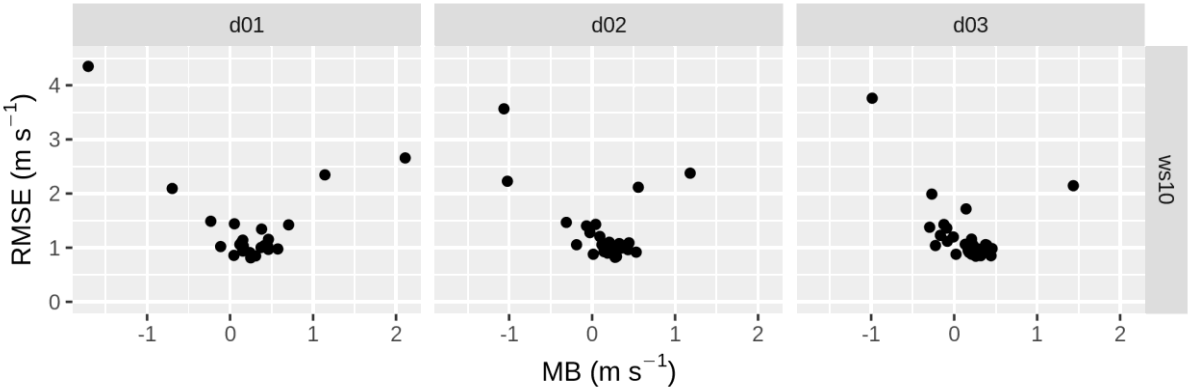

Figure 5.8: Root Mean Square Error (RMSE) reported as function of the Mean Bias (MB) between modelled hourly 10 m wind speed (ws10) and observation at 27 measurements sites for the three WRF-Chem resolutions: 15 km (d01), 3 km (d02) and 1 km (d03).

Despite the WRF-Chem performance in reproducing observed wind speed were satisfactory, wind direction at the same locations were in general poorly reproduced by the model in all the three domains. The MAE statistical indicator, modified as indicated in section 5.4 to meet the special requirement for circular data, was used to quantify the model capability to capture measured wind direction. In Figure 5.9 MAE is plotted in function of RMSE, where nevertheless this later one ignores the particularities of circular data, it has been applied in several previous studies for wind direction evaluation. WRF-Chem captured particularly well wind direction at Loiano station where RMSE is around 85° for all the three domains and MAE is 33° for domain d01 and 38° for domain d02 and d03. By contrast wind direction at Parma urbana and Reggio Emilia urbana stations the model expressed the maximum MAE with values respectively equal to 80° (domain d01) and 82° (for both d02 and d03 domains), with RMSE about 140° at Parma urbana station for all the three domains and equal to 127° (domain d01) and 137° (domain d02 and d03) at Reggio urbana.

Although the model performances in reproducing the wind directions are not outstanding, they are in line with other case studies within the Po Valley, where MAE was between 42° and 93° (Gsella et al., 2014, de Meij et al., 2009) and RMSE was between 127° and 148°

(Gsella et al., 2014), confirming the difficulties in modelling the wind fields in this area characterized during winter and fall time by stagnant conditions and low wind speed.

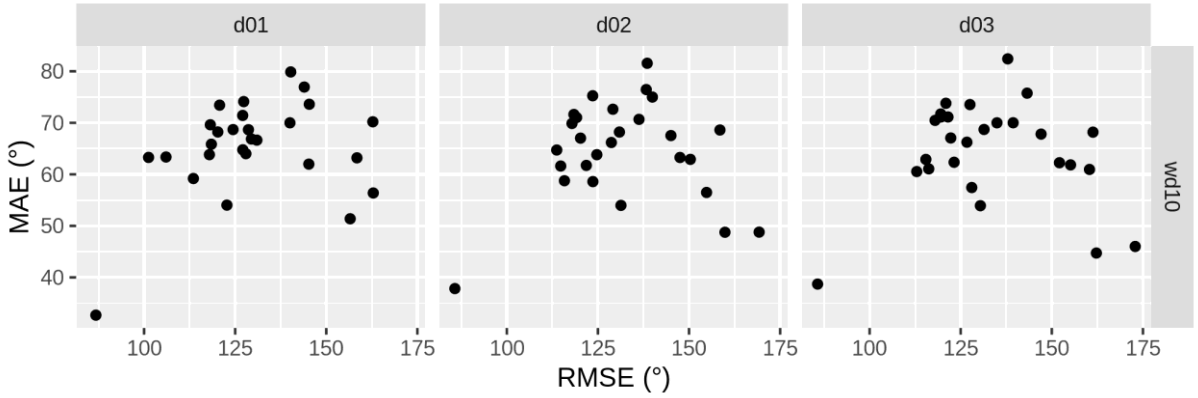

Figure 5.9: Mean Absolute Error (MAE) reported as function of the Root Mean Square Error (RMSE) between modelled hourly 10 m wind direction (wd10) and observation at 27 measurements sites for the three WRF-Chem resolutions: 15 km (d01), 3 km (d02) and 1 km (d03).

5.5.2 WRF-Chem nitrogen oxides

Since the role of WRF-Chem in this study was to estimate NO_x ($NO + NO_2$) concentrations due to emissions on the regional scale that may affect the background air quality in Modena, modelled hourly NO_x concentrations were compared with observations at 10 rural background sites (8 of them from the Arpae Emilia-Romagna network and 2 of them from Arpa Lombardia network, see Table 5-3 and Figure 5.6) within the d03 WRF-Chem domain.

Modelled NO_x concentration at 1 km resolution is biased negatively for 8 stations with a minimum MB equal to -18.1 µg m^{-3} (-62% of NMB) and biased positively for 2 stations with a maximum MB of +7.8 µg m^{-3}(+30% of NMB). In addition, for each reference station, the fraction of predicted values within a factor of two of observations was computed, also referred as FAC2. The corresponding average value over all stations is 56% (minimum 30% at the station of Ostellato and maximum 76% at the stations of Schivenoglia), in accordance with the reference value suggested by Chang and Hanna, (2004), greater or equal to 50%.

In order to test which level of model spatial resolution gives better results, observed NO_x concentrations were compared with modelled concentrations at 15 km (d01) and 3 km (d02) resolutions in terms of FAC2 and NMB (Figure 5.10). The model at 15 km resolution presents on average the highest FAC2 with respect other configuration, 62% (maximum equal to 82% at the stations of Schivenoglia and minimum equal to 39% at the station of Ostellato), conversely the NMB presents its higher variability, from -58.9% to +122.2% (respectively -17.5 µg m^{-3} and +5.7 µg m^{-3} of MB).

Among the other configurations, WRF-Chem at 3 km resolution shows better performance with an averaged FAC2 between all the stations equal to 61% (79% of maximum at Langhirano station and 37% of minimum at the station of Ostellato) and the smallest variability between all the stations in terms of NMB, from -56.6% to +28.7% (respectively -16.8 µg m^{-3} and +1.3 µg m^{-3} of MB).

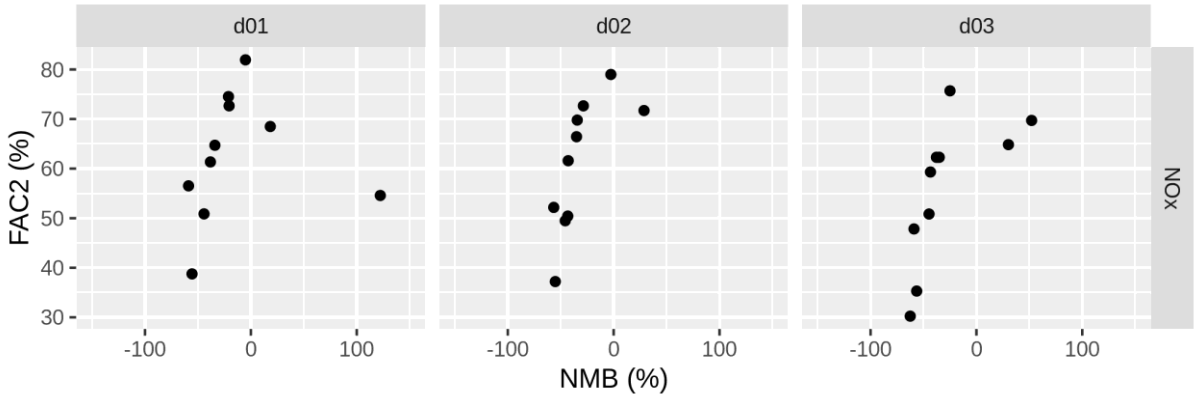

Figure 5.10: Factor of two (FAC2) reported in function of the Normalized Mean Bias (MB) between modelled hourly NO_x concentrations and observation at 10 rural background sites for the three WRF-Chem resolutions: 15 km (d01), 3 km (d02) and 1 km (d03).

The comparison showed that generally the WRF-Chem model with a horizontal resolution of 3 km is better suited to reproduce NO_x concentrations at rural background sites considering an emission inventory of 14 km x 7 km resolution. Increasing resolution to 1 km, the model tends to decrease the number of predicted concentrations within a factor of two of observations, despite the variability of the NMB being approximately the same as the configuration at 3 km. It is also worth remarking that nonetheless the modelled NO_x concentrations are on average in agreement with the values suggested by Chang and Hanna (2004) for model performance evaluation in terms of NMB and FAC2, not all considered stations satisfy these statistical indicators, this might mean that a more detailed emissions estimation such as an improved emissions distribution in the area should be implemented to achieve better results.

5.5.3 WRF-Chem combined with PMSS

5.5.3.1 Micro-scale wind field

High resolution winds in the urban area of Modena were estimated by the means of Micro-SWIFT (the 3D mass-consistent diagnostic model that composes PMSS), initialised with the meteorological fields reproduced by WRF-Chem at hourly time step. Simulated winds reproduced by Micro-SWIFT were compared with observation at three different meteorological sites located within the urban centre of the city. These stations are respectively placed on top to the Geophysical Observatory tower, at 42 m height above the ground and placed in the historical part of the city (referred as OSS), above the public hospital to the Est of the historical city centre at about 20 m height (referred as POL), and on top to the municipality building at 40 m height, to the West of the historical city centre (MOD station), the latter used also to validate the WRF-Chem meteorology. Figure 5.4 depicts the position of these three stations.

The time series reported in Figure 5.11 show the comparison between modelled and measured hourly wind speed for the three urban meteorological sites. Notwithstanding a few remarkable overestimations on November 3, 5 and 7, mostly visible at the OSS and MOD stations, modelled data reproduced observed trend quite well for all the three locations. MOD and OSS modelled time series show also a very similar behaviour (with a general less pronounced overestimation for MOD on November 3, 5 and 7) due to the location of the sensor, both above 40 m and thus characterized by the same meteorological input and not affected by the presence of buildings.

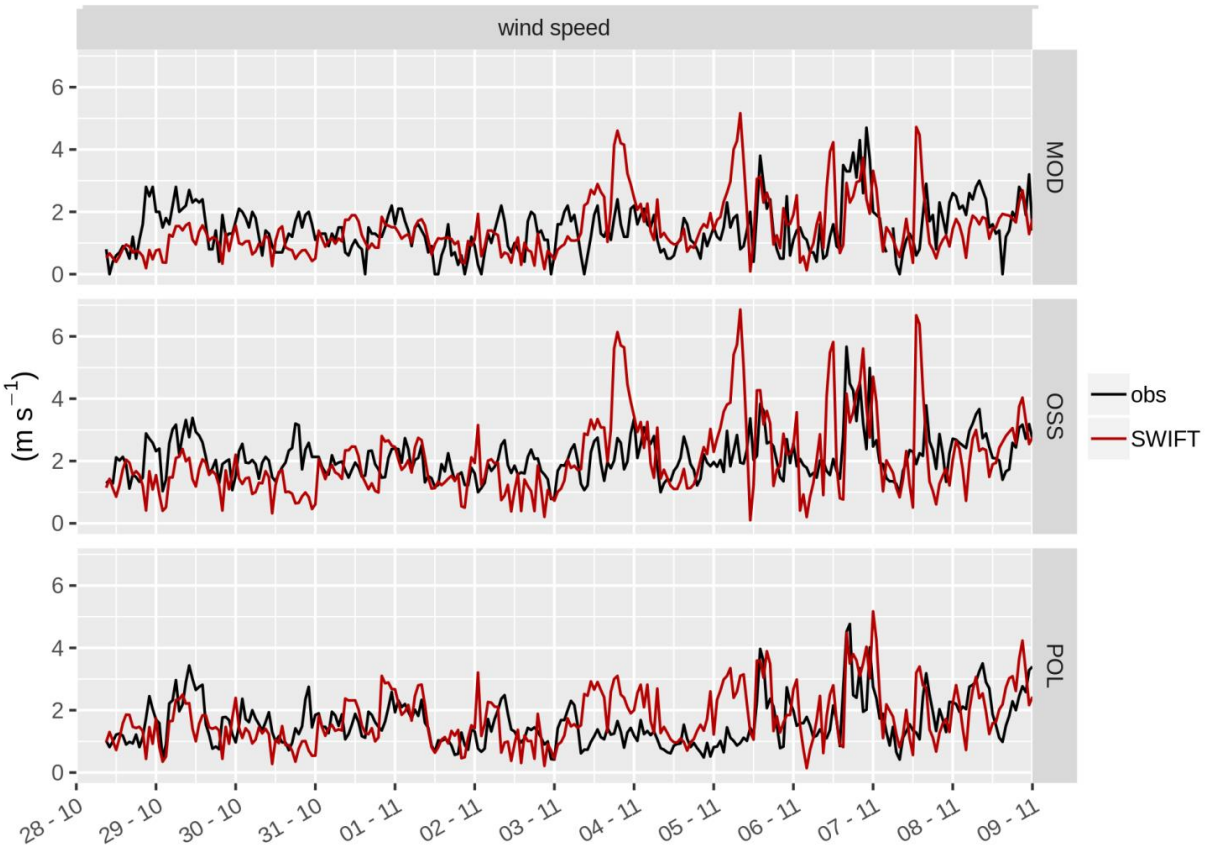

Figure 5.11: Hourly observed wind speed at MOD (on top), at OSS (in the middle) and at POL (on bottom) meteorological site along with hourly simulated wind speed by Micro-SWIFT, from October 28 to November 8, 2016.

The satisfactory performances showed by the time series regarding wind speed are also confirmed by the statistical metrics. The MB is less than 0.2 m s^{-1} for all the three stations and the RMSE is between 0.93 and 1.24 m s^{-1}. FB and FAC2 are also in line with the values found during the validation of the PMSS modelling suite in urban environment (Oldrini and Armand, 2019). Table 5-4 summarizes computed metrics.

Table 5-4: Statistics of hourly wind speed computed for the period between October 28 and November 8 at three urban meteorological stations. MB and RMSE are expressed in m s^{-1}.

Station	FB	MB	NMB	RMSE	FAC2
MOD	0.003	-0.005	-0.3%	1.05	0.67
OSS	0.03	-0.05	2%	1.24	0.76
POL	-0.10	0.17	11%	0.93	0.76

In Figure 5.12 hourly simulated wind directions are compared with hourly observed wind for the same three locations. As for regional wind field evaluation, wind directions were poorly reproduced by Micro-SWIFT, respectively with MAE equal to 125° for the MOD station, 124° for OSS and 114° for POL. By contrast the performance of Micro-SWIFT evaluated in terms of FB and NMSE are similar to the results obtained in urban environment by Oldrini et al. (2019) using the same model: for MOD site the FB and NMSE are respectively equal to 0.21 and 0.76, FB is 0.23 for both OSS and POL locations and NMSE is 0.80 and 0.70 at OSS and POL stations.

This poor behaviour in wind direction reconstruction can be partly attributed to the input data used by Micro-SWIFT, which reflects the bias given by the regional forecast model in wind direction estimation. This is mainly due to the difficulty of the meteorological models in reproducing wind fields during the situations with very little atmospheric circulation (stagnant condition) and low wind speed, as often occurred during this case study (Gsella et al., 2014, de Meij et al., 2009).

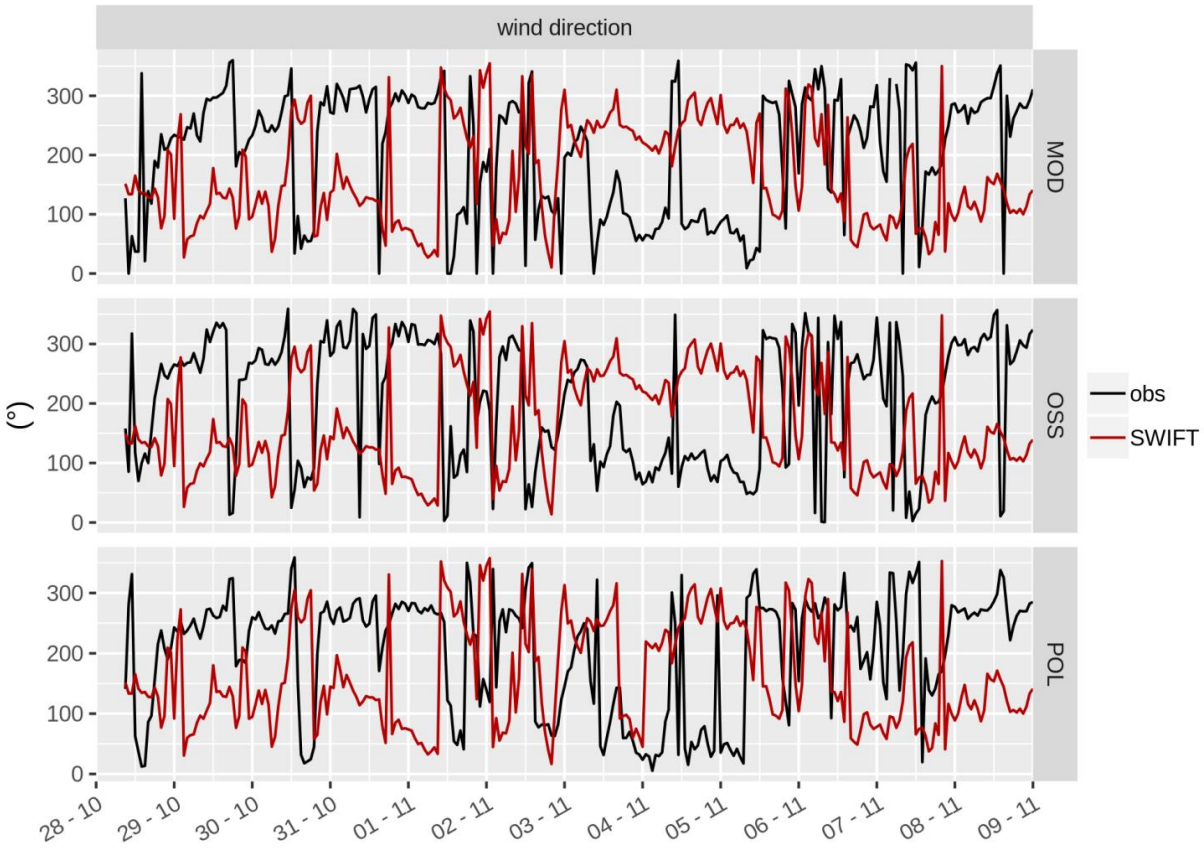

Figure 5.12: Hourly observed wind direction at MOD (on top), at OSS (in the middle) and at POL (on bottom) meteorological sites along with hourly simulated wind direction by Micro-SWIFT, from October 28 to November 8, 2016.

5.5.3.2 Micro-scale NO_x concentrations

NO_x background concentrations estimated with WRF-Chem in the urban area of Modena were added to the NO_x simulated concentrations reproduced with PMSS modelling system performed considering exclusively road traffic emissions. Modelled concentrations were compared with observations at two urban stations: the first one at a traffic site, located in the proximity of a busy street close to the urban ring road, named "via Giardini", and the second one at background site, within a public park to the West of the historical city centre, named "parco Ferrari" (Figure 5.4).

In Figure 5.13, the hourly NO_x concentrations predicted by PMSS in combination with WRF-Chem at 3 km and 1 km resolutions (labelled as "d02+ PMSS" and as "d03+ PMSS") are compared through scatter plots for both urban traffic and background stations. In this figure, the solid line represents perfect agreement with observations and within the dashed lines modelling results and observations agree with a factor of two.

Most of the modelled data are within a factor of two of observations, especially for the urban traffic site in both WRF-Chem configurations, whereas for the urban background station an under estimation is more noticeable. It is also worth noting that the results of PMSS combined with WRF-Chem at 3 km and at 1 km resolution depict similar behaviour and relative scatter plots are very comparable to each other, with a slightly less pronounced underestimation for WRF-Chem at 3 km resolution.

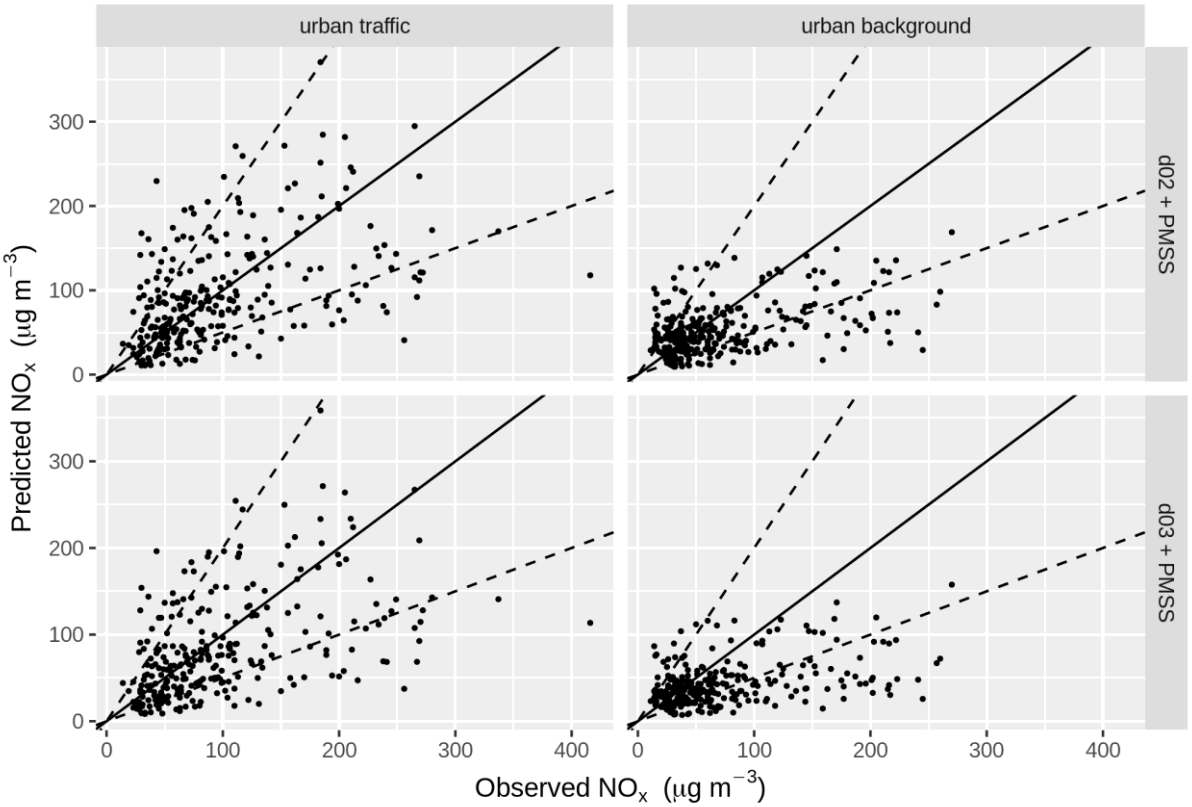

Figure 5.13: Scatter plots of predicted NO_x concentrations at urban traffic ("via Giardini") and urban background ("parco Ferrari") stations for different models configurations: PMSS combined with WRF-Chem at 3 km resolution (labelled as "d02+PMSS") and PMSS combined with WRF-Chem at 1 km resolution (labelled as "d03+PMSS").

Modelled hourly NO_x concentrations are biased negatively in both urban stations: at the "via Giardini" traffic site the MB of simulated NO_x by PMSS and WRF-Chem at 1 km resolution is -15 µg m^{-3}, which corresponds to -15% of NMB, for the same model configuration the MB at the "parco Ferrari" background site is -30 µg m^{-3} (-41% NMB). Modelled hourly concentrations correlate reasonably well with observations in both sites, with *r* equal to 0.48 at the traffic station and 0.43 at the background station.

The performance of the models generally increases when hourly NO_x concentrations reproduced by PMSS are combined with the results of WRF-Chem at 3 km resolution, the MB at the "via Giardini" traffic station is -4 µg m^{-3} (-4% NMB) and -18 µg m^{-3} (-25% NMB) at the "parco Ferrari" measurement station.

Despite an improvement in term of MB with WRF-Chem at 3 km, its combination with PMSS does not particularly affect the *r* between modelled and observed concentrations (0.47 at "via Giardini" traffic station and 0.44 at "parco Ferrari" background site).

A quantitative estimation of the agreement between simulated and observed concentrations was also assessed following the statistical metrics proposed by Hanna and Chang, (2012) for urban dispersion model evaluation. FB, NMSE, FAC2 and NAD were computed for both the urban stations located in Modena and for both the combination of WRF-Chem (3 km and 1 km resolution) with PMSS. Table 5-5 summarizes all the computed statistics.
Following Hanna and Chang (2012) the reference acceptance criteria for the aforementioned metrics in urban dispersion model evaluation are as follows:

- |FB| < 0.67, i.e. the relative mean bias is less than a factor of ~2
- NMSE < 6, i.e. the random scatter is less than 2.4 times the mean
- FAC2 > 0.30, i.e. the fraction of predicted concentrations within a factor of two of observed concentrations exceeds 0.30
- NAD < 0.50, i.e. the fractional area for errors is less than 0.5

Table 5-5: Statistics of hourly NOx concentrations computed for the period between October 28 and November 8, considering two different model configurations.

Configuration	Station	FB	NMSE	FAC2	NAD
PMSS + d02	urban traffic	0.04	0.48	0.72	0.24
	urban background	0.29	0.75	0.62	0.29
PMSS + d03	urban traffic	0.16	0.54	0.68	0.26
	urban background	0.52	1.15	0.59	0.35

The statistical analysis shows that PMSS combined with WRF-Chem at both d02 and d03 domains fulfill the acceptance criteria defined by Hanna and Chang (2012). Regarding the FB, the results are always less than the threshold of 0.67, in particular at urban traffic site the outcomes of this metric are particularly good with values equal to 0.04 (PMSS + d02) and 0.16 (PMSS + d03). At urban background station the results are larger than the previous one (0.29 for PMSS + d02 and 0.52 for PMSS + d03) indicating that the models tend to underestimate more the mean concentrations but nevertheless in well agreement with the reference benchmark. As far as the NMSE is concerned, the models show their best performances with scores largely lower than the acceptance benchmark (6), with a maximum

value of 1.15 at urban background station for PMSS + d03 (minimum value at traffic station for PMSS + d03 equal to 0.48), meaning that predicted values very rarely differ strongly from observations.

Regarding the FAC2 and the NAD there is a significant agreement between model results and relative acceptance criteria at both urban stations and for both model configurations. Minimum and maximum FAC2 are equal to 0.59 and 0.72 achieved respectively at the urban background station for PMSS + d03 and at urban traffic station for PMSS + d02 (the lower limit proposed by Hanna and Chang is 0.30). For the same locations and model configuration the maximum and the minimum NAD are 0.35 and 0.24 respectively (upper limit proposed by Hanna and Chang is 0.50).

The statistical analysis, despite supporting a moderately better behaviour when the resolution of WRF-Chem is 3 km, also shows that the metrics of modelled NO_x concentrations are comparable between the two WRF-Chem resolutions (1 km and 3 km), without a clear difference of one of the two.

Time series analysis (Figure 5.14) shows that modelled NO_x concentrations agree quite well with observations. In particular for the first five days of simulations (considering the combination with WRF-Chem at 3 km resolution as a reference), between October 28 and November 1st observations are reproduced well and daily peaks are modelled with quite good accuracy, especially for urban traffic station where the MB between October 28 and November 1 is +7µg m^{-3} and NMB is about 1% (at the background station the MB is -14 µg m^{-3} and NMB is -1%).

By contrast, between November 1 and 2 observed NO_x concentrations tend to be overestimated since the WRF-Chem contribution during the central hour of days exceeds observed NO_x concentrations. This situation is particularly evident at the "parco Ferrari" station. Furthermore, between November 2 and 3, PMSS failed to capture the diurnal cycle in observed concentrations: on November 2 in the central hours of the day observations are largely overestimated with an increasing trend up to the afternoon peak. A possible explanation to this episode can be addressed to an underestimation of the PBL height during the central hours of the day, where its modelled value doesn't exceed 190 m (average daily maximum during the whole simulation is 600 m) and during only 6 hours the modelled PBL height is greater than 100 m.

On the other hand, on November 3, when observed concentrations reach values over 200 µg m^{-3}, the models underestimate the observed values. Between November 4 and November 6 observed NO_x concentrations were lower than in the previous days (hourly maximum always lower than 200 µg m^{-3}) mostly due to the rainfall which occurred on November 5 (8 mm) and 6 (1 mm), where the combination of the two models was able to reproduce the hourly pattern well, with a slight overestimation at the traffic station.

On November 7 and 8 extremely high peaks occurred with values that exceeded 400 µg m^{-3} at urban traffic station and 250 µg m^{-3} at urban background station. Despite an underestimation of absolute observed NO_x concentrations experienced on these two days, the shape of the diurnal cycle was captured quite well by the models.

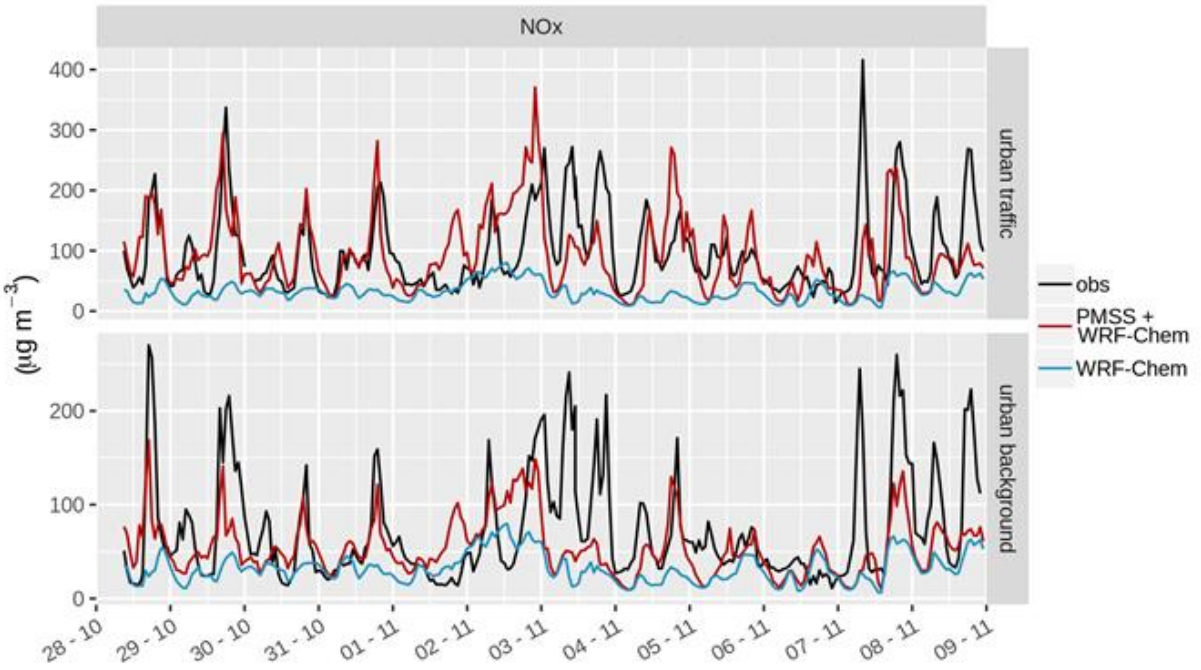

Figure 5.14: Hourly observed concentrations of NO_x at urban traffic (on top) and urban background (on bottom) measurements stations along with hourly simulated concentrations by WRF-Chem at 3 km resolution and PMSS combined with WRF-Chem at the same resolution, from October 28 to November 8, 2016. Please note the difference in the scale on the y-axis in each panel.

Finally, in order to study which part of day primarily affected the general underestimation of the models and to investigate the WRF-Chem contribution to the total NO_x concentrations during the day, the variation of observed and predicted NO_x concentrations by hour of the day was assessed. The comparison of mean observed NO_x daily cycle shows very similar behaviour between the "via Giardini" and "parco Ferrari" stations (Figure 5.16): two main

peaks occur on average during the day, one between 08:00 and 09:00 a.m. (equal to 150 µg m^{-3} at traffic site and 105 µg m^{-3} at background site) and the second, on average greater of about 20-30 µg m^{-3} than the former, around 07:00 p.m. (about 170 µg m^{-3} at traffic site and 140 µg m^{-3} at background site). At "parco Ferrari" station another peak occurs in the early morning (around 01:00 a.m.) less pronounced than the other two, with a mean concentration of about 70 µg m^{-3}.

For the purpose of further investigate the modelled concentrations, in Figure 5.15 is shown the diurnal cycle of traffic emissions used for WRF-Chem and the average diurnal cycle used for PMSS in working and non-working days. There is a large correspondence between the traffic temporal cycle of WRF-Chem and PMSS in working days. For the former, the afternoon peak (which occurs at 06.00 p.m.) is a little more pronounced than the morning maximum (08:00 and 09:00 a.m.), while for PMSS is the opposite. During non-working days WRF-chem presents the same hourly behaviour of for working days but absolute values are quite decreased. By contrast, as far PMSS is concerned, the morning peak is at 10:00 a.m. and the afternoon maximum is at 07:00 p.m., both delayed by one hour compared to WRF-Chem.

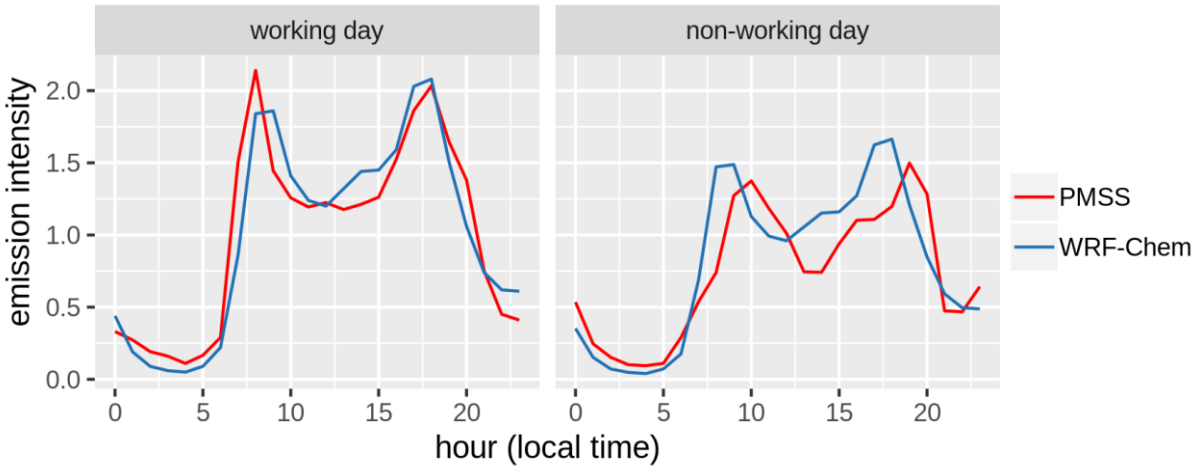

Figure 5.15: Overview of the diurnal cycle of the traffic emission intensity for WRF-Chem (light blue) and the average diurnal cycle for PMSS (red) for working and non-working days.

Modelled daily NO_x concentrations present a good agreement with observed daily cycle for traffic station: the first peak of the day on average tending to be underestimated and despite the second peak is anticipated of about two hours, its magnitude is captured very well,

especially when the WRF-Chem model is used at 3 km resolution (Figure 5.16). This confirms the advantages obtained using a detailed traffic modulation recorded on a street in the proximity of the traffic station.

On the other hand, at urban background site, the modelled daily pattern is acceptable, but absolute concentrations are generally underestimated in particular in the morning peak. This behaviour might be explained looking at the PBL height simulated by WRF-Chem and used to drive the micro-scale dispersion (Figure 5.16): during the night the boundary layer is stable due to surface longwave cooling and a shallow temperature inversion strong characterizing the area with a mean PBL height during night time hours for the whole simulation around 100 m. After dawn, surface heating builds up a shallow mixed layer, which deepens during the central hours of the day inducing a rising of the PBL height, on average up to 600 m. During this situation, at the background site, where the traffic emissions are less pronounced compared to the traffic site, modelled NO_x concentrations tend to be limited by the mixing phenomenon that occurs from around 07:30 a.m. onwards, causing a strong underestimation of the morning observed peak.

In the late afternoon (between 04:00 and 05:00 p.m.), the solar heating is no longer sufficient to maintain an upward surface buoyancy flux and the boundary layer becomes restricted to a shallow layer, around 100 m deep, as in the night. Under this condition NO_x concentrations increase, generating the second daily peak more pronounced than the first one and anticipated of about two hours. A more detailed description of the PBL evolution during the day, through for example ceilometer observation, could help to improve the concentration estimation.

At urban traffic site the mechanism seems to be the same but large traffic emissions affected less the underestimation during the morning peak.

The NO_x underestimation could also be associated to the aged traffic fluxes estimated by the PTV VISUM model, which simulation reference year is 2010 and then affected by economic recession whereby all western countries have fallen since 2007. The economic crisis caused a slower growth of gross national product and an increase in unemployment which, among the other consequences, led to a reduction in traffic fluxes in the European business centres. For these reasons traffic fluxes estimated by PTV VISUM in the city of Modena may be affected by an underestimation with respect the real traffic occurred during the simulated period.

It is also worth noting that the PTV VISUM simulation doesn't include traffic fluxes of urban public transport, therefore the vast majority of urban buses emissions are not taken into

account in the simulation. Due to the presence of schools nearby the "via Giardini" monitoring station, the morning rush hours (especially between 08:00 and 09:00 a.m.) are characterized by an intense flow of public buses and the consequent omission of public transport emissions can influence and contribute to the morning NO_x underestimation.

In addition, traffic fluxes in secondary streets seem to be modelled worse than busier roads and at the urban background station the NO_x underestimation can also be attributed to a rough estimation of NO_x sources around the area where traffic emissions are modulated according the measurement data collected at "via Giardini" street. Moreover, other NO_x emissions sources are simulated by the WRF-Chem model through the use of the TNO-MACC inventory which level of detail is about 7 km and thus not as exhaustive as the traffic emissions, and these other NO_x sources are expected to have larger influence at urban background than at urban traffic sites. Besides this, looking at the NO_x concentrations daily cycle, the contribution of WRF-Chem to the total simulated concentrations seems to be modest compared to direct effect of traffic emissions. In particular, when the resolution of WRF-Chem is 1 km, its share does not present a strong hourly trend but it is rather flat, with an average contribution during each hour of simulation in the order of 20 μg m^{-3}, at both traffic and background sites. On the other hand, when the resolution of WRF-Chem is 3 km, its rate to the total concentrations is greater than the one a 1 km resolution (average hourly contribution about 30 μg m^{-3}), with an hourly trend more marked during the two daily peaks. This difference in contribution estimate could be explained considering the position of the WRF-Chem computational cells. In the case of 1 km resolution the computational cells over "parco Ferrari" and "via Giardini" stations, even if they present very similar concentrations, are different and located both inside the PMSS domain. Conversely, for d02, both the stations are within the same computational cell and the cell itself is no longer entirely contained in the PMSS domain but it extends to the West, beyond the PMSS borders. This latter configuration leads to account within the PMSS domain part of the TNO traffic emissions occurring outside the Modena urban area, originally excluded from the PMSS computation, causing a homogenization and an increasing in NO_x concentrations over the entire WRF-Chem cell. The final outcome is that the contribution of WRF-Chem using d02 to the urban concentrations is larger and also the daily trend during the two daily peaks appears more pronounced.

More accurate traffic modulation across the city and a finer spatial resolution of non-traffic related exhaust emissions, as well as a more accurate description of the planetary boundary

layer height during the day, would better fit the 1km grid of WRF-Chem used in d03 and can certainly contribute to achieve better results also at urban background station.

The results presented in chapter 5 have been submitted as a paper to the *Atmospheric Environment* journal and at the moment of writing (4 January 2019) is under review (Veratti et al.).

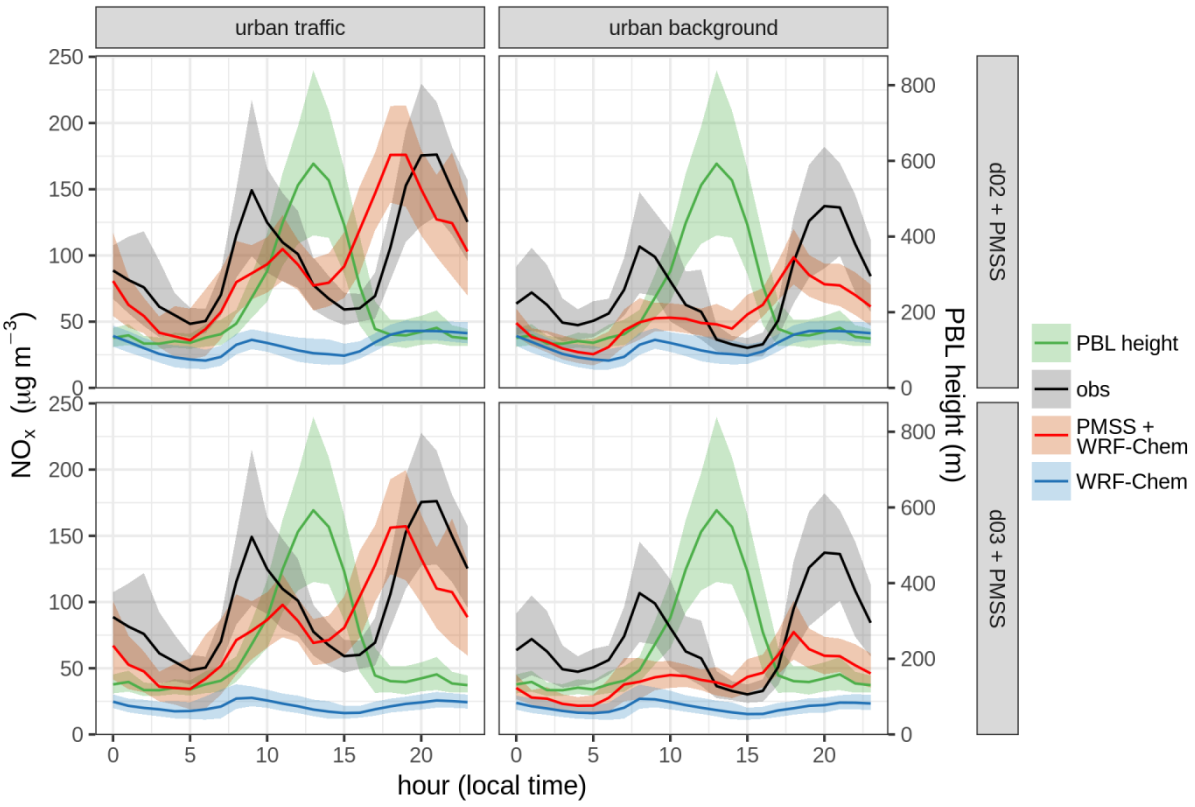

Figure 5.16: Mean daily cycle of observed NO_x concentrations (black), modelled by the combination of WRF-Chem and PMSS model (red) and the only contribution of WRF-Chem (light blue), by station type (traffic or background) and by WRF-Chem resolution (3 km or 1 km). Green lines show the mean daily cycle of planetary boundary layer height modelled by WRF-Chem and used in the micro-scale dispersion. Solid lines represent the daily mean cycle, meanwhile shaded area show the variability between 25th and 75th percentiles.

6. Testing the hybrid modelling system in forecast mode

In second section of the thesis the hybrid modelling system was set-up with the aim of produce hourly forecast of NO_2 and NO (as well as their sum, NO_x) concentrations, up to one day ahead. This set up was tested for the entire month of February 2019 for the urban area of Modena. The WRF-Chem model was run for every day of February 2019 in order to provide synoptic meteorological forecast and background concentrations of NO and NO_2, produced by the sources located outside the urban area of Modena as well as the emissions from all the other sectors a part from traffic emissions within PMSS domain, up to one day ahead from the time of initialization. By contrast, primary NO and NO_2 (and their sum, NO_x) from vehicular exhaust emissions were forecasted by the PMSS modelling suite in the urban area of Modena at very high resolution (4m), using as meteorological input the wind and temperature field modelled by WRF-Chem. The final concentration fields were computed adding the local traffic contribution to the WRF-Chem background concentration.
Hourly NO and NO_2 urban traffic emissions were estimated with the VERT model using as "activity data" the light and duty traffic fluxes modelled with PTV VISUM (see chapter 5.3). Due to the inability of the traffic models to forecast vehicles trips for the future, an historical analysis of traffic pattern in the city was undertaken. Predicted traffic modulation during the days of the month and the hours of the day were calculate through a cluster analysis performed considered traffic measurements by induction loop spires located at 50 cross roads under road pavement in the urban area of Modena, from November 1, 2018 and January 31, 2019. In addition, data recorded in the monitoring traffic campaign carried out between October 28 and November 8, 2016, with 4 Doppler radar counters (chapter 5.3) were also considered.

The days of February 2019 were characterized in general by low rainfall rate, with cumulative precipitation equal to 37 mm, which occurred only in the first three days of the month (8 mm on February 1, 11 mm on February 2 and 18 mm on February 3); all the other days were characterized by no rainfall. Daily average temperatures were in general slightly greater than the monthly average for February in Modena (about 5 °C) (see Figure 6.1), especially on

February 22 (mean daily temperature equal to 12.2 °C) and between February 25 and February 28 (mean daily equal to 11.1 °C on February 25, 13.6 °C on February 26, 15 °C on February 27 and 12.5 °C on February 28).

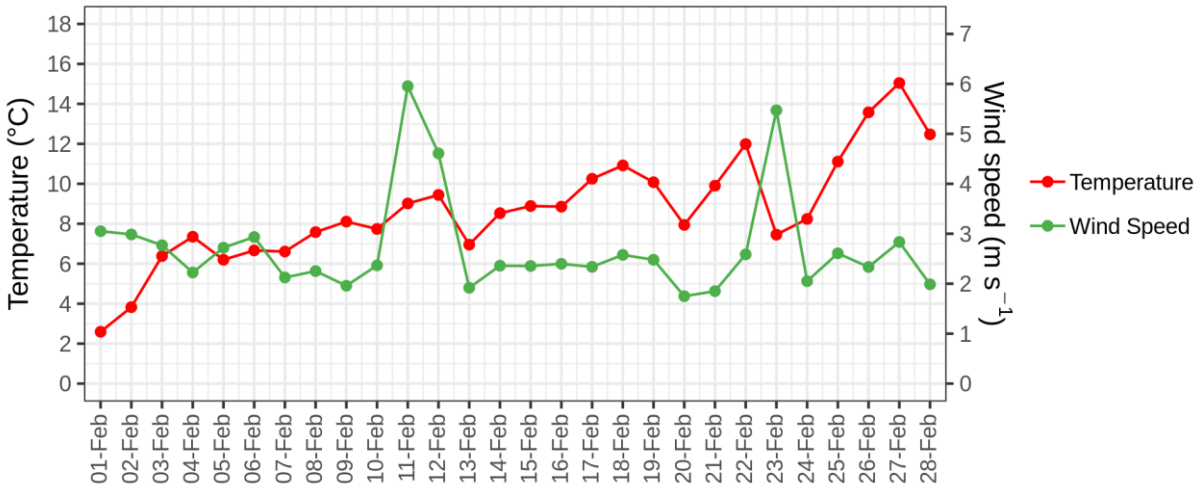

Figure 6.1: Observed mean daily temperature and mean daily wind speed at Geophysical Observatory tower between February 1 and February 28, 2019.

Observed wind speed at the Geophysical Observatory tower was also greater than mean wind speed for the period. Indeed, mean wind speed for February 2019 was equal to 2.7 m s^{-1} (Figure 6.3), with a daily average above 2 m s^{-1} for all the days of the month except on February 13 (daily mean equal to 1.9 m s^{-1}), on February 20 (daily mean equal to 1.7 m s^{-1}) and on February 21 (daily mean equal to 1.7 m s^{-1}) (Figure 6.1). Moreover, on February 11, 12 and 23 mean daily wind speed presented very high values with respect typical weather condition for winter in the central Po Valley, with respective daily mean equal to 5.9, 4.6 and 5.5 m s^{-1}. As it is possible to see in Figure 6.2 high wind speed on February 11 and 12 was caused by a strong wind blowing from the West with a frequency of occurrence on both days around 50% (hourly data). On the other hand the high speed recorded on February 23 was due to a wind blowing from the East, with a frequency of occurrence slightly less than 60% (hourly data).

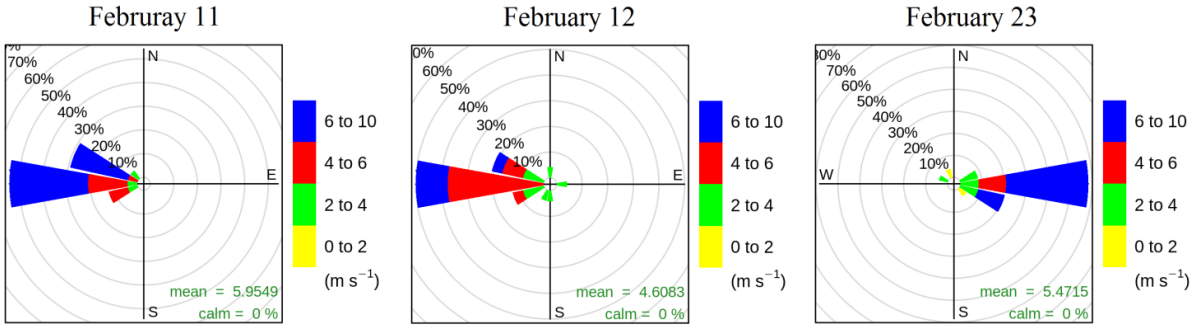

Figure 6.2: Wind rose of hourly wind on February 11 (on the left), 12 (in the centre) and 23 (on the right), observed at the Geophysical Observatory tower.

As it is possible to see in Figure 6.3, the wind directions that had the highest frequency of occurrence for the entire month of February 2019 (hourly data) were the westerly winds, in particular from the West and from the West-Southwest (both about 18%), followed by West-Northwest (12%), South-West and North-West (both around 10%). Wind from the South and from the North very rarely occurred, as well as easterly winds, which had only a strong occurrence on February 23 (Figure 6.2). Furthermore the directions that presented highest wind speed were the West, the West-Northwest and the East.

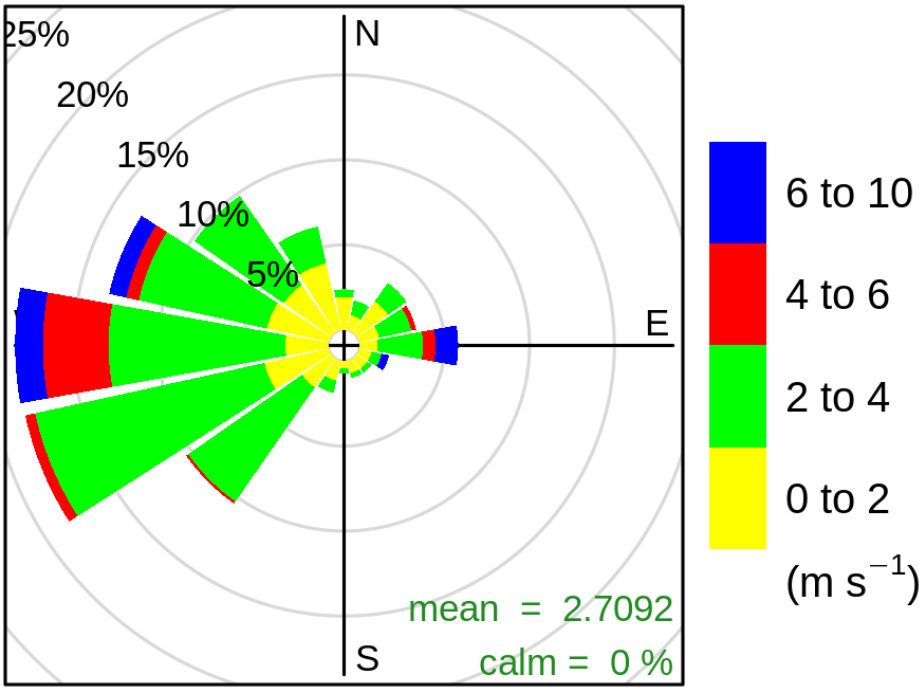

Figure 6.3: February 2019 wind-rose observed at the Geophysical Observatory tower

6.1 WRF-Chem set-up

The same version (3.9.1) of the Weather Research and Forecasting model with chemistry (WRF-Chem) used for the analysis case study, was employed also to forecast the meteorological field and the NO, NO_2 and NO_x background concentrations. In order to limit the computing resources required by the model and to keep the simulation of the multi-model chain affordable in less than one day, WRF-Chem was applied over two one-way nested domains, centred in the urban area of Modena. The outer domain (d01) covers most of Europe with 150 x 150 grid cells at 15 km horizontal resolution and the innermost domain (d02) covers the North of Italy with a resolution of 3 km (150 x 150 grid cells), (Figure 6.4). The model was configured with 35 vertical levels with the first layer approximately at 30 m and the model top set at 50 hPa.

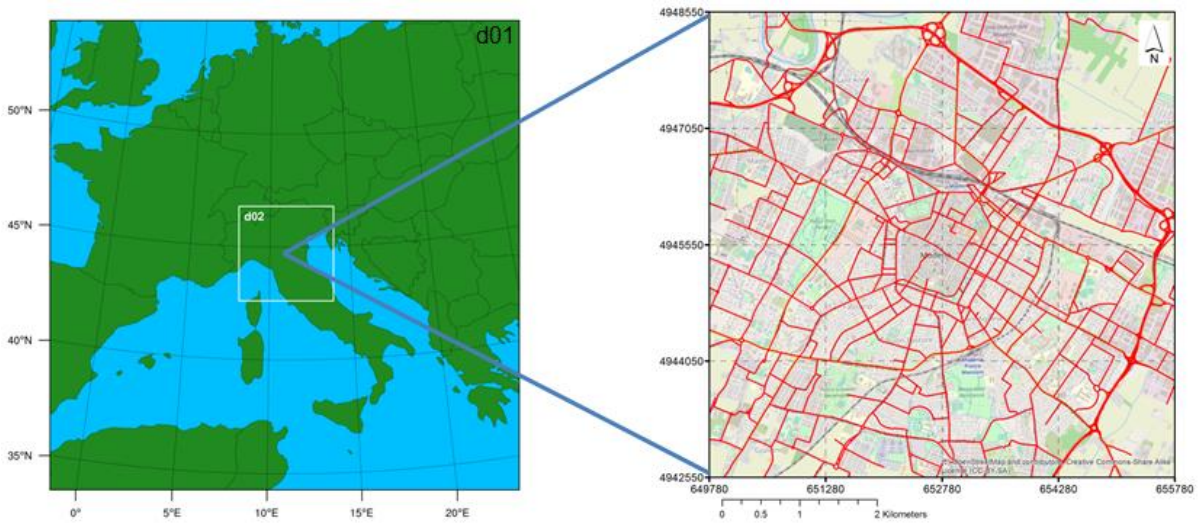

Figure 6.4: Overview of the WRF-Chem model domains on the left (Geographic coordinate system-WGS84) and PMSS investigation domain with the considered Modena street network represented as red lines on the right (UTM32-WGS84).

The main differences in the WRF-Chem configuration with respect to the one applied for the analysis case study regard the meteorological and chemical initial and boundary conditions. They were provided respectively by the Global Forecast System (GFS) model (https://www.ncdc.noaa.gov/data-access/model-data/model-datasets/global-forcast-system-gfs) (Han and Pan, 2011), which is able to forecast up to 16 days ahead dozens of atmospheric and land-soil variables at 28 km resolution. On the other hand chemical initial and boundary

came from the daily forecast of the Whole Atmosphere Community Climate Model (WACCM) (Beres et al., 2005; Garcia, Yue, et al., 2019), which forecast 10 days ahead global atmospheric concentrations exploiting the NASA/GMAO GEOS-5 meteorological forecasts.

Other configuration parameters include the Noah Land Surface Model (Chen and Dudhia, 2001), the Yonsei University Planetary Boundary Layer scheme (Hong, 2010), the Grell-Freitas cumulus parameterization (Grell and Freitas, 2014) activated only for the outer domain, the Lin microphysics scheme (Lin et al., 1983), and the Rapid Radiative Transfer Model (RRTM) radiation scheme (Mlawer et al., 1997) aimed to represent both shortwave and longwave radiation.

The MOZART gas-phase chemical mechanism developed by Emmons et al., (2010), and the MOSAIC aerosol model (Zaveri et al., 2008) were used to simulate airborne pollutants over the nested domains. As to land use, the Corine Land Cover (CLC) dataset was adopted and the biogenic emissions were calculated online by the MEGAN model (Guenther et al., 2012). Table 6-1 summarize the main options for physical and chemical schemes as well as initial/boundary input.

WRF-Chem was re-initialized every seven days with a one day spin-up to ensure consistency with meteorological and chemical fields.

Table 6-1: WRF-Chem model set-up and parameterisation.

Process	WRF-Chem option
Land-surface model	Noah Land Surface Model
Boundary layer scheme	YSU
Cumulus parameterization	Grell-Freitas (only for the outer domain)
Microphysics	Lin
Short-wave radiation	RRTM with MCICA method
Long-wave radiation	RRTM with MCICA method
Gas-phase mechanism	MOZART
Aerosol model	MOSAIC 4 bins
Meteo initial/boundary condition	Global Forecast System model
Chemical initial/boundary condition	WACCM model

The anthropogenic emissions used for the parent and the nested WRF-Chem domains were taken from the TNO-MACC III inventory, available on a regular grid with a horizontal resolution of 0.125° x 0.0625°, which contains emissions for air pollutants such as NO_x, SO_2, NMVOC, NH_3, CO and primary particulate matter ($PM_{2.5}$ and PM_{10}).

In order to avoid the double counting of the traffic emissions placed inside the urban area of Modena and to better represent the spatial distribution of traffic sources in the nearby territory, the emissions from sectors 71-75 were downscaled and excluded from the PMSS domain as described in chapter 5.3.

6.2 PMSS Set-up and urban traffic emissions estimation

The version of PMSS used for the forecast case study was the 3.8.4 for Micro-SPRAY and 2.1.7 for Micro-SWIFT. Pollutant dispersion were performed using six hours of spin-up on a 6 km x 6 km square domain covering the city of Modena (Figure 5.2), with a horizontal grid step of 4 m (square cells) for both Micro-SWIFT and Micro-SPRAY models. Since the goal of this experiment was to produce a daily forecast, up to one day ahead, it was not possible to run a continuous simulation. Thus, in order to avoid a cold restart for each day of simulation or a spin-up period which would cause a loss in terms of computing hours, was activated a particular function in the SPRAY code called Restart. Restart procedures allowing to save all the information at a given simulation time in a binary file that can be used as starting points for future simulations. In this way the position of each virtual particle in the last simulation time step is saved into a specific file and the simulation of the following day will restart with that distribution of particles in the domain.

With the aim of representing the flow entering the Micro-SWIFT computational domain, nine vertical profiles of temperature, humidity, wind speed and direction forecasted by WRF-Chem in d02 domain were extracted in the nearby area of Modena on an hourly basis and used as input for Micro-SWIFT. In addition, mixing height values and main background turbulence parameters (i.e. friction velocity, Obukhov length and convective scale velocity), necessary to estimate the wind standard deviation, the Lagrangian time scale and the third moment order (Skewness) of the distribution for vertical velocity (see chapter 2.4), were estimated with SURFPRO (SUR-face-atmosphere interFace PROcessor). SURFPRO is a tool developed by Arianet S.r.l. able to estimate gridded fields of the PBL turbulence scaling parameters, horizontal and vertical eddy diffusivity according to land cover type exploiting the atmospheric circulation (e.g. wind speed, temperature, stability, solar radiation) provided by a meteorological model such as WRF-Chem.

Regarding Micro-SPRAY, the horizontal grid was chosen to be identical to that of the Micro-SWIFT model computation and the vertical grid structure consisted of 20 levels with a logarithmic progression up to 200 m above the ground level with 3 m height for the first layer close to the soil. The main PMSS set-up parameters are reported in Table 6-2.

Table 6-2: Micro-SWIFT and Micro-SPRAY set-up for the forecast case study

Micro-SWIFT		**Micro-SPRAY**	
Parameters	Value	Parameters	Value
Horizontal resolution	4 m	Horizontal resolution	4 m
Horizontal grid	1504 x 1504 points	Horizontal grid	1504 x 1504 points
Vertical grid	from 3 up to 200m	Vertical grid	from 3 up to 200m
	20 vertical levels		20 vertical levels
Interpolation method	Cressman 2D	Emission time step	5 s
RANS flow solver	Activated	Averaging period for concentrations	3600 s

Traffic emissions in the urban area of Modena were estimated with a bottom-up approach: traffic flows within the main urban streets were simulated with the PTV VISUM model at morning rush hour between 07:00 a.m. and 08:00 a.m. and exploited as "activity factor". On the other hand, the R package VERT was used to estimate primary NO and NO_2 emissions at rush hour taking into account the number of light and duty vehicles simulated by the PTV VISUM model and considering cold and hot emissions factors (Ntziachristos and Samaras, 2016) weighted according to the local fleet composition, as defined by the *Automobile Club d'Italia* (ACI, http://www.aci.it/laci/studi-e-ricerche/dati-e-statistiche.html). Moreover, the NO_2 mass fraction of total NO_x (primary NO_2) was computed following the suggested values by Ntziachristos and Samaras (2016) and reported in table 6-3, where f-NO_2 express the percentage of NO_x emitted as primary NO_2.

Table 6-3: Mass fraction of NO_2 in NO_x emissions (f-NO_2) expressed for different Emission Standard and Category

Category	**Emission Standard**	**f-NO_2**
Petrol PCs	Pre-Euro	4
	Euro 1 – Euro 2	4
	Euro 3 – Euro 4	3
	Euro 5	3
	Euro 6 up to 2016	2

	Euro 6 2017-2019	2
	Euro 6 2020+	2
Diesel PCs	Pre-Euro	15
	Euro 1 – Euro 2	13
	Euro 3	27
	Euro 3 with DPF	51
	Euro 4	46
	Euro 5	40
	Euro 6 up to 2016	30
	Euro 2017-2019	20
	Euro 2020+	20
LPG PCs	Pre-Euro	5
	Euro 1 – Euro 3	5
	Euro 4	5
	Euro 5	5
	Euro 6	5
CNG PCs	Euro 4	3
	Euro 5	3
	Euro 6	2
Petrol LCVs	Pre-Euro	4
	Euro 1 – Euro 2	4
	Euro 3 – Euro 4	3
	Euro 5	3
	Euro 6 up to 2017	2
	Euro 6 2018-2020	2
	Euro 6 2021+	2
Diesel LCVs	Pre-Euro	15
	Euro 1 – Euro 2	13
	Euro 3	27
	Euro 4	46
	Euro 5	33
	Euro 6 up to 2017	30
	Euro 6 2018-2020	20
	Euro 6 2021+	20
HDVs	Pre-Euro	11
	Euro I – Euro II	11
	Euro III	14
	Euro IV	14
	Euro V	10
	Euro VI	10
	Euro III+CTR	35

Since the traffic flows simulation provided by the PTV VISUM model was related only to the rush hour for a typical working day, and since it is not possible to predict the exact number of vehicles within each streets for the following day (forecast simulation), traffic flows had to be modulated during the hours of the day based on historical data. To accomplish this task, traffic flows were recorded by 230 inductive loop spires located under the road pavement at the main cross roads of the urban area of Modena, from November 1, 2018 and January 31, 2019. In Figure 6.5 is shown the position of each spire. Secondly, since the numbers of streets are greater than the maximum number of traffic modulation that is possible to give as input to Micro-SPRAY model, a cluster analysis of recorded traffic data was performed in order to identify which are the typical modulations that characterize Modena urban area for each day of the week..

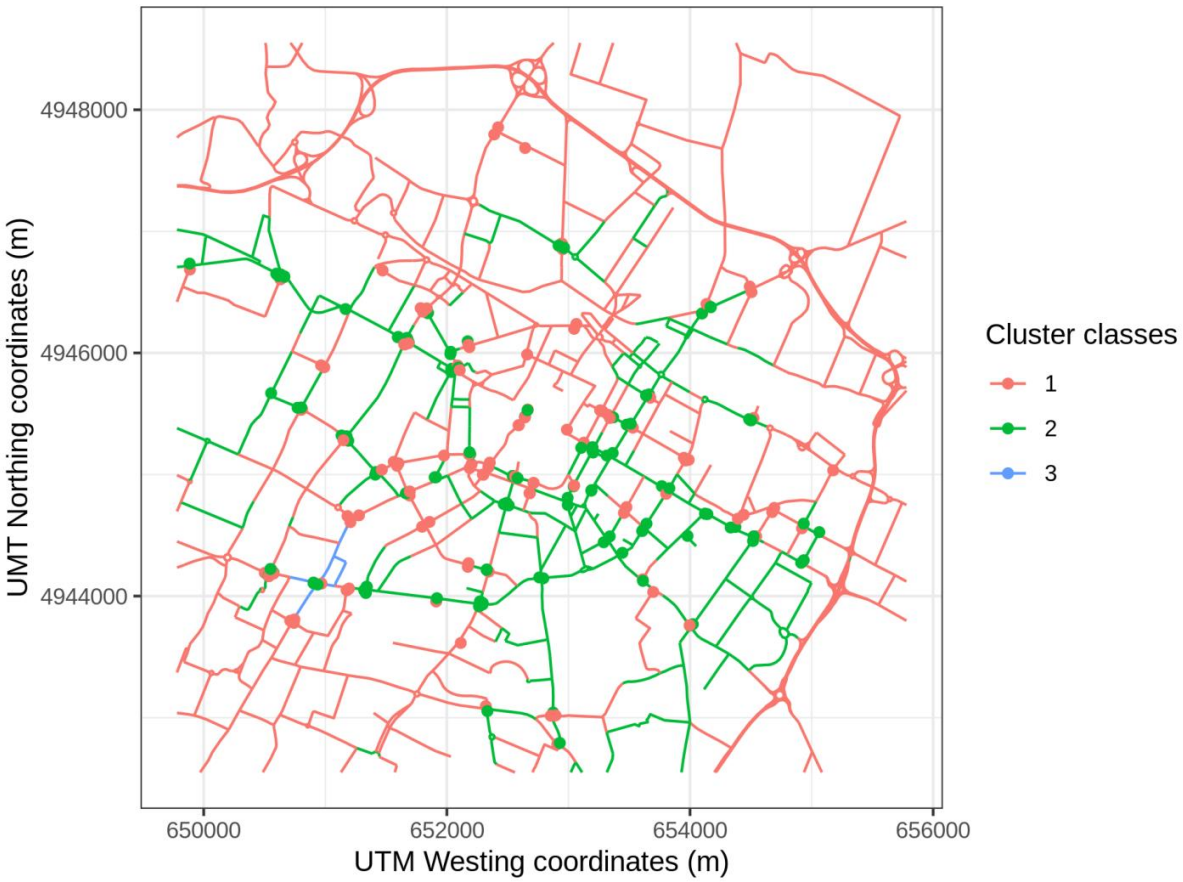

Figure 6.5: Location of the inductive loop spires (dots) and road streets network (segment). The colours represent the respective modulation computed from the cluster analysis and assigned to each spires and then to each roads according to the proximity between the road took as a reference and the nearest inductive loop sensor.

The goal of a cluster analysis is to identify pattern or groups of similar objects within a dataset of interest. Each group contains observations with similar profile according to a specific criterion. Similarities between observations are defined using some intra-observation distance measures such as Euclidian or correlation-based methodology. In this case study, since the number of clusters to be produced was not known a priori, but was one of the goals of the procedure, the Hierarchical clustering method was chosen for grouping objects (daily traffic modulation) based on their similarity. In particular the Agglomerative clustering was considered the most suited, since each observation is initially considered as a cluster of its own (leaf) and then the most similar clusters are successively merged until a single big cluster (root) is created.

The result of the hierarchical clustering can be presented as a tree-based representation of traffic modulation, which is called dendogram. Starting from the bottom each leaf represent a single traffic modulation recorded at one measurement point, moving up to the top, traffic modulations are merged together based on their similarities until to reach a single root, where all the clusters are merged together into only one traffic modulation. In Figure 6.6 is shown the dendogram related to the traffic modulation recorded by the 230 inductive loop spires.

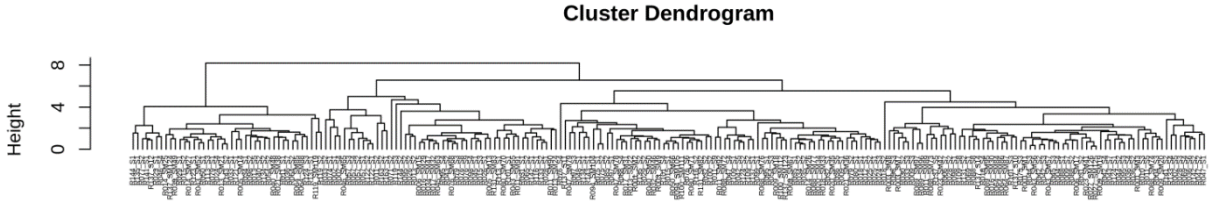

Figure 6.6: Cluster Dendogram related to the traffic modulation recorded by 230 inductive loop spires. At the bottom there are single clusters (leafs) and on top all the clusters are merged together in only one modulation (root).

With the aim of deciding the level at which to cut the three for generating suitable groups of a data objects, were computed sixteen types of indices considering for each of them four different distance methods: Euclidean (Equation 6.1), Maximum (Equation 6.2), Manhattan (Equation 6.3) and Canberra (Equation 6.4). Table 6-4 summarize the scores (number of suited cluster classes) for each statistical test and distance method.

Considering *x* and *y* as two vectors and *n* the number of elements that form each vector, their similarities can be calculated with these distance measures:

Euclidean distance

$$d_{euc}(x,y) = \sqrt{\sum_{i=1}^{n}(x_i - y_i)^2} \quad (6.1)$$

Maximum distance

$$d_{max}(x,y) = max_{i=1}^{n}|x_i - y_i| \quad (6.2)$$

Manhattan distance

$$d_{man}(x,y) = \sum_{i=1}^{n}|(x_i - y_i)| \quad (6.3)$$

Canberra distance

$$d_{can}(x,y) = \sum_{i=1}^{n}\frac{|x_i - y_i|}{(|x_i| + |y_i|)} \quad (6.4)$$

Table 6-4: Number of clusters suggested by sixteen different indices computed considering four different distance methods.

Indeces name	Distance Method			
	Euclidean	Maximum	Manhattan	Canberra
kl	13	4	2	9
ch	2	6	2	2
hartigan	4	4	6	9
mcclain	2	2	2	2
gamma	20	2	20	18
gplus	20	2	20	20
tau	12	5	4	7
dunn	20	2	20	18
sdindex	14	3	2	7
sdbw	19	3	20	18
cindex	2	20	3	2
silhouette	2	2	2	2
ball	3	3	3	3
ptbiserial	12	5	4	7
gap	2	2	2	2
frey	1	3	1	2

The number of clusters that had the most frequency of occurrence between the sixteen considered indices and the four distance methods was equal to two. For this reason all the traffic modulation recorded by 230 inductive loop spires were aggregate into two groups (clusters) according to their similarity (distance) and averaged within the same group. The two final modulations are reported in Figure 6.7 (Cluster Class 1 and Cluster Class 2). In addition, an average modulation rate was computed from the traffic measurement campaign data carried out between October 28 and November 8, 2016, with 4 Doppler radar counters (chapter 5.3), one for typical working days and one for non-working days (Cluster Class 3 in Figure 6.7 and in Figure 6.5). These additional modulations were added to the two clusters and assigned to the roads close to the measurement point.

The two modulations obtained with the cluster analysis were assigned to the roads according to the proximity between the road took as a reference and the nearest inductive loop sensor. A final adjustment was also performed in order to keep the same modulation for similar type of road and continuous streets. The final result is shown in Figure 6.5.

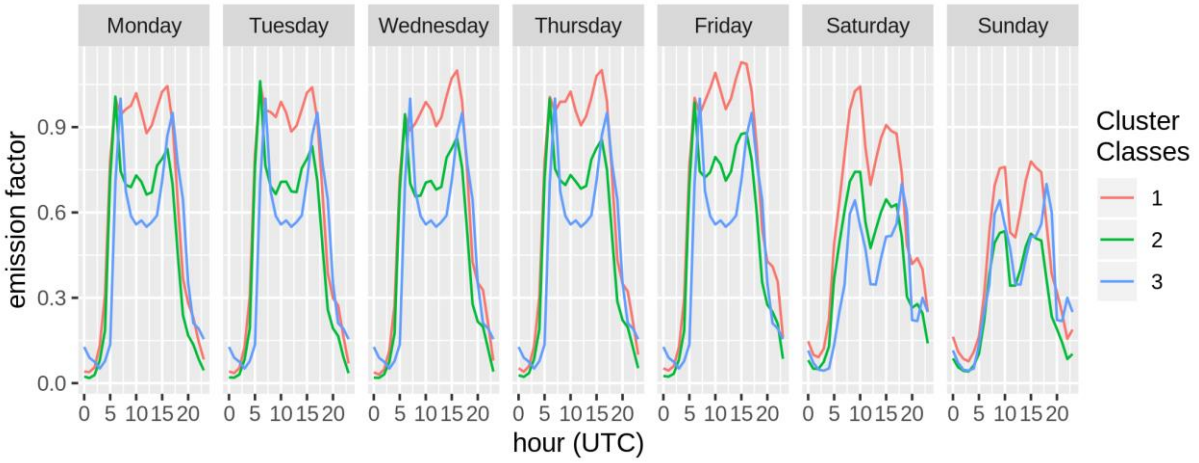

Figure 6.7: Hourly modulation according to the day of the week of the two Clusters computed from the 230 inductive loop spires data (Cluster Classes 1 and 2) and from the traffic modulation campaign (Cluster Class 3).

6.3 Results and discussion

6.3.1 Meteorology

2 m temperature (T2), 10 m wind speed (ws10) and 10 m wind direction (wd10) meteorological fields predicted by WRF-Chem were compared against corresponding surface observations of these variables provided by 20 stations within the d02 domain (see Table 6-5 and Figure 5.6 for the location): 11 stations belong to the RIRER (Rete idro-meteo-pluviometrica integrata) Arpae-Simc network, 5 stations belong to the Archivio dati idro-nivo-meteorologici ARPA Lombardia network, 4 stations belong to the Osservatorio Meteo Idrologico della Regione Liguria (OMIRL) ARPAL network. Other two stations belonging to the Geophysical Observatory of Modena weather network were considered for the micro-scale wind field evaluation. Since observed meteorological data were not available for all the stations considered in the first cases study, Table 6-5 summarize which of them are used to validate models results in chapter 6. Moreover, NO and NO_2 concentrations are measured with chemiluminescence as for NO_x: the measure of NO is performed by reacting the original NO present in an air sample, without the molybdenum converter, with O_3 to form NO_2 and O_2 while emitting light. The concentration of NO is proportional to the emitted light. By contrast, NO_2 is obtained by difference from NO_x and NO concentrations.

Table 6-5: Observation sites. Locations are provided in Geographic coordinates (WGS84). Available parameters are: "T2" for temperature at 2 m height above the ground, "ws10" for wind speed and "wd10" for wind direction at 10 m above the ground, "NO", "NO_2" and "NO_x" respectively for NO, NO_2 and NO_x concentrations.

Station name	Label	Network	Longitude (°)	Latitude (°)	Type	Parameters
Bologna urbana	BOL	Arpae-Simc	11.32879	44.50075	Meteorology	T2, ws10, wd10
Ferrara urbana	FER	Arpae-Simc	11.621138	44.832498	Meteorology	T2, ws10, wd10
Granarolo Faentino	GRA	Arpae-Simc	11.95861	44.36013	Meteorology	T2, ws10, wd10
MBMalborghetto di Boara	MAL	Arpae-Simc	11.66134	44.85799	Meteorology	T2, ws10, wd10
Modena urbana	MOD	Arpae-Simc	10.91699	44.65639	Meteorology	T2, ws10, wd10
Panocchia	PAN	Arpae-Simc	10.29584	44.6837	Meteorology	T2, ws10, wd10
Parma urbana	PAR	Arpae-Simc	10.33049	44.808	Meteorology	T2, ws10, wd10

Reggio Emilia urbana	REG	Arpae-Simc	10.6337	44.69781	Meteorology	T2, ws10, wd10
Rolo	ROL	Arpae-Simc	10.874	44.88481	Meteorology	T2, ws10, wd10
S.Pietro Capofiume	SPC	Arpae-Simc	11.62264	44.65378	Meteorology	T2, ws10, wd10
San Pancrazio	SPA	Arpae-Simc	10.27245	44.80806	Meteorology	T2, ws10, wd10
Cremona	CRE	ARPA Lombardia	10.04414	45.14188	Meteorology	T2
Gonzaga	GON	ARPA Lombardia	10.7678	44.96381	Meteorology	T2, ws10, wd10
Mantova Lunetta	MAL	ARPA Lombardia	10.82421	45.15733	Meteorology	T2, ws10, wd10
Mantova Tridolino	MAT	ARPA Lombardia	10.86007	45.15135	Meteorology	T2, ws10, wd10
Pieve S.Giacomo	PSG	ARPA Lombardia	10.19548	45.12107	Meteorology	T2, ws10, wd10
La Spezia	LAS	ARPAL	9.82819	44.10703	Meteorology	T2, ws10, wd10
Luni	LUN	ARPAL	10.00899	44.07491	Meteorology	T2, ws10, wd10
Monte Rocchetta	MOR	ARPAL	9.93842	44.07129	Meteorology	T2, ws10, wd10
Porto Venere	POV	ARPAL	9.83594	44.052	Meteorology	T2, ws10, wd10
Badia	BAD	Arpae Emilia-Romagna	10.28937	44.65823	Air Quality	NO_2, NO_x
Besenzone	BES	Arpae Emilia-Romagna	10.0192	44.9895	Air Quality	NO_2, NO_x
Febbio	FEB	Arpae Emilia-Romagna	10.43104	44.30071	Air Quality	NO_2, NO_x
Gherardi	GHE	Arpae Emilia-Romagna	11.96125	44.83975	Air Quality	NO_2, NO_x
Ostellato	OST	Arpae Emilia-Romagna	11.94194	44.7409	Air Quality	NO_2, NO_x
Parco Ballirana	PAB	Arpae Emilia-Romagna	11.98236	44.52743	Air Quality	NO_2, NO_x
San Pietro Capofiume	SCA	Arpae Emilia-Romagna	11.62482	44.65423	Air Quality	NO_2, NO_x
San Rocco	SAR	Arpae Emilia-Romagna	10.66478	44.87373	Air Quality	NO_2, NO_x
Schivenoglia	SCH	ARPA Lombardia	11.0761	45.01688	Air Quality	NO_2, NO_x
Spinadesco	SPN	ARPA Lombardia	9.930599	45.15047	Air Quality	NO_2, NO_x
Policlinico	POL	Geophysical Observatory MO	10.94429	44.63580	Meteorology	ws10, wd10
Geophysical	OSS	Geophysical	10.92981	44.64809	Meteorology	ws10, wd10

Observatory		Observatory MO				
"Parco Ferrari"	VGA	Arpae Emilia-Romagna	10.90731	44.65157	Air Quality	NO, NO_2, NO_x
"via Giardini"	PFE	Arpae Emilia-Romagna	10.90572	44.63699	Air Quality	NO, NO_2, NO_x

The performance of WRF-Chem in reproducing hourly 2 m temperatures in the d02 domain (3 km resolution) are consistent with observations at most of the stations since the Pearson correlation coefficient (*r*) is between 0.60 and 0.90, except for two stations, both located on to the Ligurian Sea shore, Monte Rocchetta and Porto Venere, where the correlation is not particularly high and equal to 0.52 at both the sites. By contrast, six stations present *r* equal or greater than 0.85, Rolo (0.85), San Pancrazio (0.86), Cremona (0.87), Gonzaga (0.85), Mantova Lunetta (0.86), Pieve San Giacomo (0.90), confirming the ability of WRF-Chem in reproducing observed meteorological variability quite well also when it is applied in forecast mode. On the other hand, poor *r* values close to the Ligurian Sea shore can be attributed to the difficulties of the model in representing areas characterized by a strong influence of land-sea breeze.

The Mean Bias MB of the model tends to be between -1 °C and +1 °C for most of the stations, the minimum MB is -1.7 °C achieved at the Parma urbana and Reggio Emilia urbana stations and the maximum MB is +1.6 °C achieved at Granarolo Faentino station. These results are in the same range as the MB that Gsella et al., (2014) found using MM5, WRF and TRAMPER meteorology models for the same area. Figure 6.8 shows the statistical performance of WRF-Chem in reproducing 2 m temperature. *r* is plotted as a function of MB for the two different model resolutions: 15 km (d01) and 3 km (d02). The variability of MB tends to increase by increasing the model resolution, conversely, the average *r* including all the stations is 0.72 for the d01 WRF-Chem domain and 0.75 for the d02 domain, showing that there is no clear evidence that increasing the resolution from 15 to 3 km increase the forecasting performance in reproducing 2 m temperature for one day ahead.

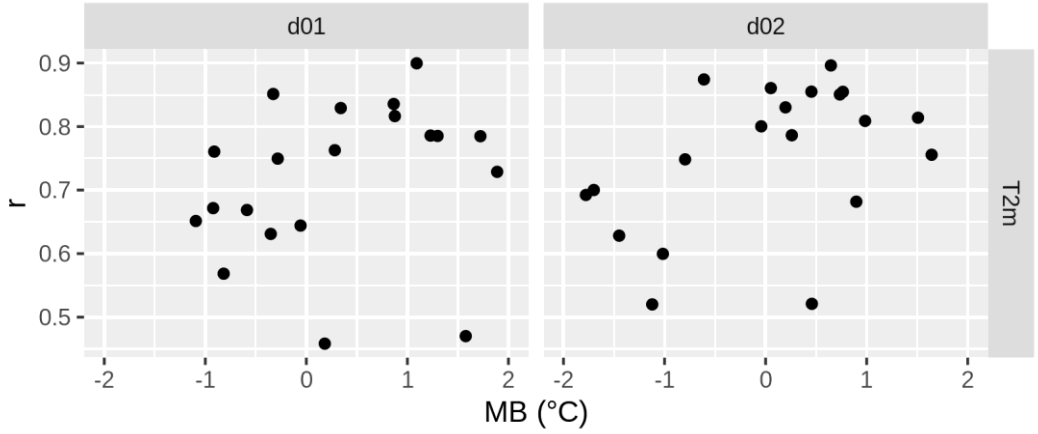

Figure 6.8: Pearson correlation coefficient (r) reported as function of the Mean Bias (MB) between modelled hourly 2 m temperature (T2) and observation at 20 measurements sites for the two WRF-Chem resolutions: 15 km (d01) and 3 km (d02).

The model on average tends to be positively biased in reproducing hourly wind speed at the d02 domain, with a MB smaller than +1 m s^{-1} for most of the stations, where only two of them exceed this value respectively at the La Spezia (+1.12 m s^{-1}) and Porto Venere stations (+1.82 m s^{-1}). On the other hand, the minimum MB is -0.81 m s^{-1}, achieved at the Monte Rocchetta station, confirming the difficulties of the model in reproducing the meteorology on to the Ligurian Sea shore. All the other stations generally express performance in line with range suggested by Malm et al. (2009) and by European Environmental Agency (EEA) guidelines (EEA, 2011), (MB between -0.5 m s^{-1} and +0.5 m s^{-1}).

The second statistical indicator commonly used in wind speed evaluation is the Root Mean Square Error (RMSE), for which the recommended benchmark is less than 2 m s^{-1}. As for the MB, the stations that are generally outside this threshold are the one on to the Ligurian Sea shore, with respectively RSME equal to 3.29 m s^{-1} (Porto Venere), 2.38 m s^{-1} (Monte Rocchetta), 2.26 m s^{-1} (La Spezia) and 2.17 m s^{-1} (Luni). The large bias and the high RMSE values found in this area suggests that the model might have difficulties in forecasting the wind speed in regions close to the sea where complex orography and local breeze characterize the territory, however for the rest of the stations the MB and RMSE values are consistent with the reference benchmarks proposed in literature.

In Figure 6.9 the performance of WRF-Chem in reproducing wind speed for the two different resolutions is shown: RMSE is plotted as a function of the MB. Moving from d01 to d02, the model tends to show MB closer to zero. Similarly, the RMSE generally tends to moderately decrease as well with increasing resolution. It is therefore possible to conclude that in

increasing model resolution from 15 km to 3 km there is a slight improvement of performance in wind speed reconstruction.

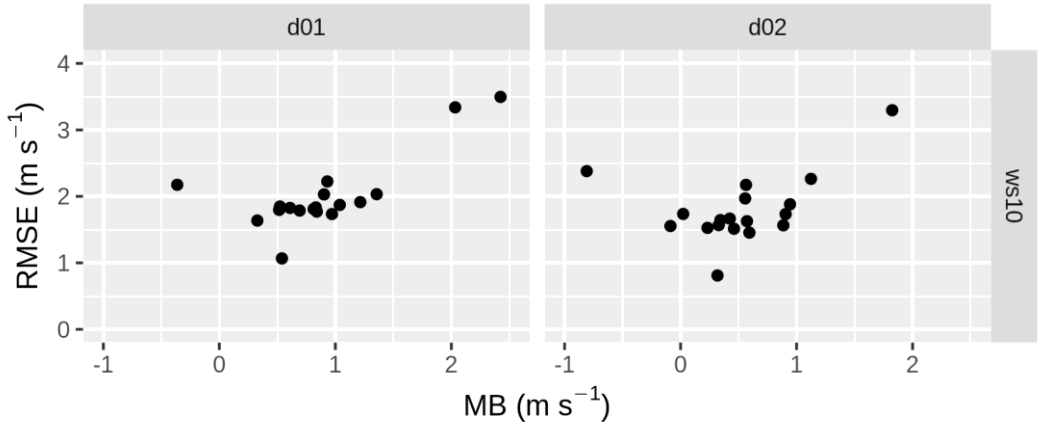

Figure 6.9: Root Mean Square Error (RMSE) reported as function of the Mean Bias (MB) between modelled hourly 10 m wind speed (ws10) and observation at 19 measurements sites for the two WRF-Chem resolutions: 15 km (d01) and 3 km (d02).

The statistical indicator used to investigate the performance of WRF-Chem in reproducing wind direction is the Mean Absolute Error (MAE), modified as indicated in section 5.4 to meet the special requirement for circular data and in Figure 6.10 MAE is plotted in function of RMSE. WRF-Chem captured quite well wind direction at almost all the stations, with MAE between 46° (Bologna urbana) and 83° (Luni). On the other hand, despite the RMSE was not particularly good for four stations (Luni 173°, Porto Venere 163°, Monte Rocchetta 159° and La Spezia 155°) at the other sites is between 102° (Gonzaga) and 131° (Malborghetto di Boara), and thus in line with other case studies within the Po Valley (Gsella et al., 2014, de Meij et al., 2009), confirming the good results obtained with WRF-Chem in reproducing wind speed when it is applied in forecast mode.

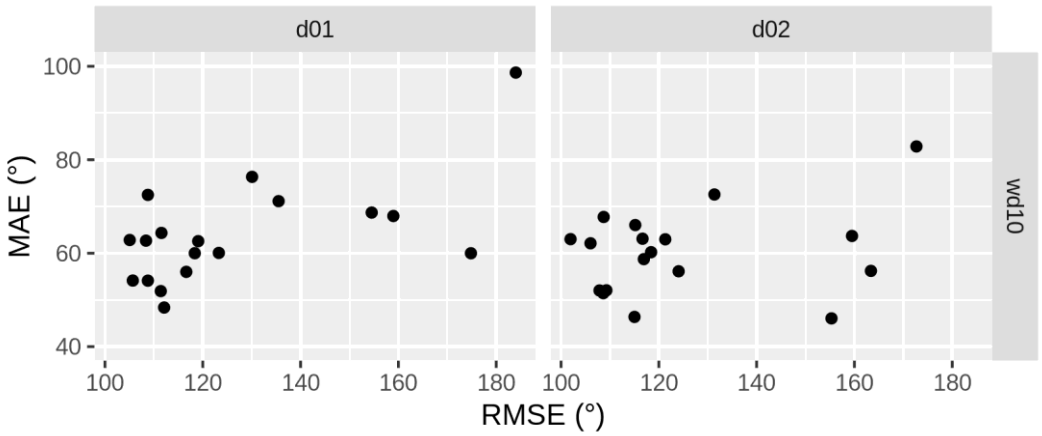

Figure 6.10: Mean Absolute Error (MAE) reported as function of the Root Mean Square Error (RMSE) between modelled hourly 10 m wind direction (wd10) and observation at 19 measurements sites for the two WRF-Chem resolutions: 15 km (d01) and 3 km (d02).

6.3.2 WRF-Chem nitrogen dioxides and nitrogen oxides

Since the role of WRF-Chem in this second section of the study was to provide background concentrations for NO and NO_2 produced outside the urban area of Modena or by emissions sectors different from traffic, hourly concentrations modelled with WRF-Chem were compared with observed concentrations at 10 rural background sites (8 of them from the Arpae Emilia-Romagna network and 2 of them from Arpa Lombardia network, see Table 6-5 and Figure 5.6) within the d02 WRF-Chem domain. It is worth noting that NO is a primary pollutant emitted directly into the atmosphere, by contrast NO_2 can be produced as a primary pollutant as well but it mainly comes from photochemical reactions starting from NO. The evaluation of WRF-Chem carried out in this chapter will focus on rural background sites then it is expected that the relative stations are representative of a background situation i.e. located far from direct sources of pollution. For this reason following evaluation will regard only nitrogen dioxides and nitrogen oxides, which are more representative of those areas.

Modelled NO_x concentrations at 3 km resolution is biased negatively for all the stations, with a minimum MB equal to -64.5 µg m^{-3} (-74% of NMB), followed by -49.7 µg m^{-3} (-63% of NMB) achieved at Schivenoglia and Spinadesco. At these two stations WRF-Chem failed to capture observed trend and an explanation of this behaviour can be given by looking at the observed concentrations, which present very high values at both sites between February 7 and 10, with a peak of 250 µg m^{-3} at Spinadesco and of 330 µg m^{-3} at Schivenoglia, not characteristic for rural background sites and thus very hard to predict by a forecast model. By contrast at all the other stations the NMB is greater than -50% (minimum equal to -46% at Febbio and maximum equal to -29% at Badia). FAC2 is between 48% (Febbio) and 71% (Badia).

As far NO_2 is concerned, forecasted concentrations are generally negatively biased at all the stations except at Parco Ballirana, where MB is equal to +2.1 µg m^{-3} (+12% of NMB). The poorest behaviour of modelled concentrations is still expressed at the stations of Schivenoglia and Spinadesco, with respectively MB equal to -48.1 µg m^{-3} (-70% of NMB) and -32.4 µg m^{-3} (-54% of NMB). Observed NO_2 concentrations exhibit high concentrations as well, with a peak of 150 µg m^{-3} on February 8 at Spinadesco, and a peak of 135 µg m^{-3} at Schivenoglia on the same day.

For all the other stations the NMB is between -30% (Febbio) and 12% (Parco Ballirana), and the FAC2 is between 58% (Parco Ballirana) and 80% (San Rocco).

Finally, in order to test the differences in modelled concentrations at the two WRF-Chem domains, observed NO_x and NO_2 concentrations were compared with modelled concentrations at 15 km (d01) and 3 km (d02) resolutions in terms of FAC2 and NMB (Figure 6.11). The model at 15 km resolution presents on average higher variability for NMB with respect d02 for both NO_2 and NO_x, but at 3 km resolution the model tend to reduce the absolute value of NMB. On the other hand the fraction of predicted values within a factor of two of observations on average tends to remain the same.

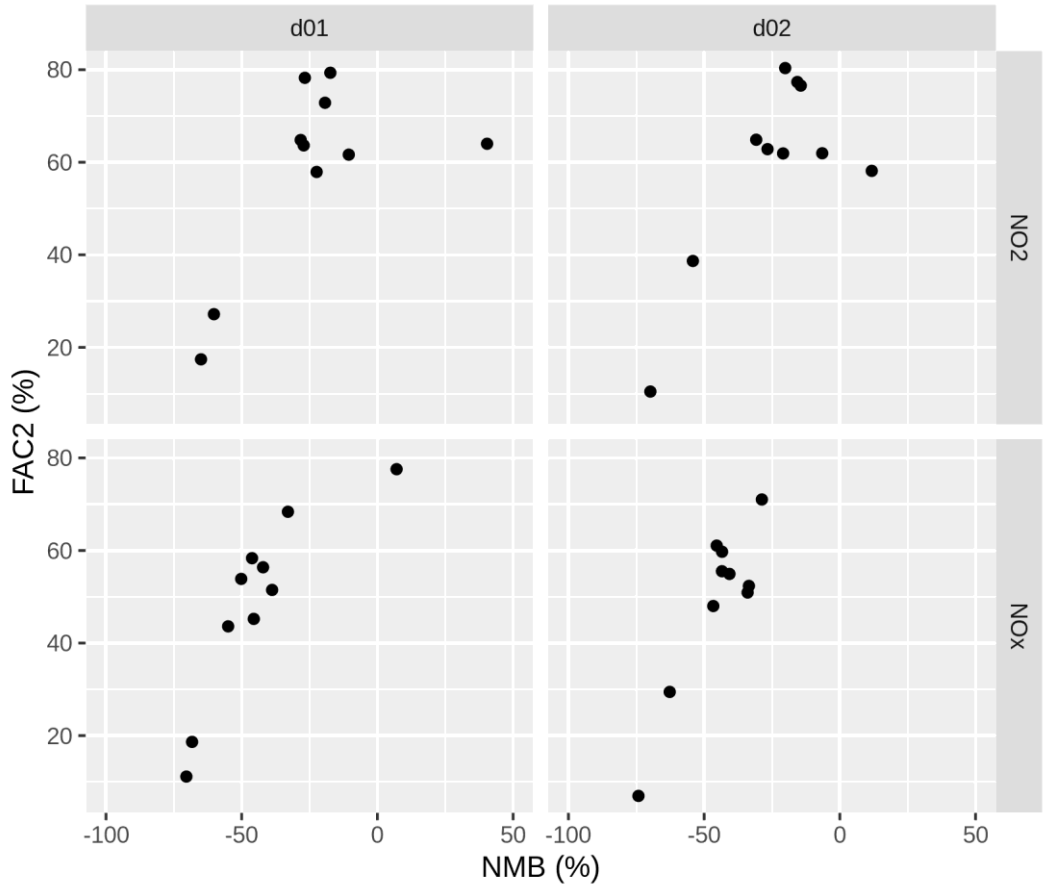

Figure 6.11: Factor of two (FAC2) reported in function of the Normalized Mean Bias (MB) between modelled hourly NO_x and NO_2 concentrations and observation at 10 rural background sites for the two WRF-Chem resolutions: 15 km (d01) and 3 km (d02).

6.3.3 WRF-Chem combined with PMSS

6.3.3.1 Micro-scale wind field

Micro-scale wind fields estimated at hourly time step with the Micro-SWIFT model were compared with observed wind speed and direction at three different meteorological sites located within the urban centre of Modena. These stations, as described in chapter 5.5.3.1, are located on top to the Geophysical Observatory tower at 42 m height above the ground (referred as OSS), above the public hospital to the Est of the historical city centre at about 20 m height (referred as POL), and on top to the municipality building at 40 m height, to the West of the historical city centre (MOD station). In Figure 6.12 is shown the comparison between modelled and measured hourly wind speed for the three urban meteorological sites. Notwithstanding a few remarkable overestimations on February 1, 11, and 27, on which (February 1 and 27) Micro-SWIFT clearly failed to capture measured wind speed at all the three urban stations, modelled wind speed reproduced observed trend quite well for the whole month, also during February 12 and 23 characterized by high wind velocity (between 6 and 8 m s^{-1}). Only at the POL site on February 23 the model tends to overestimate the observed trend.

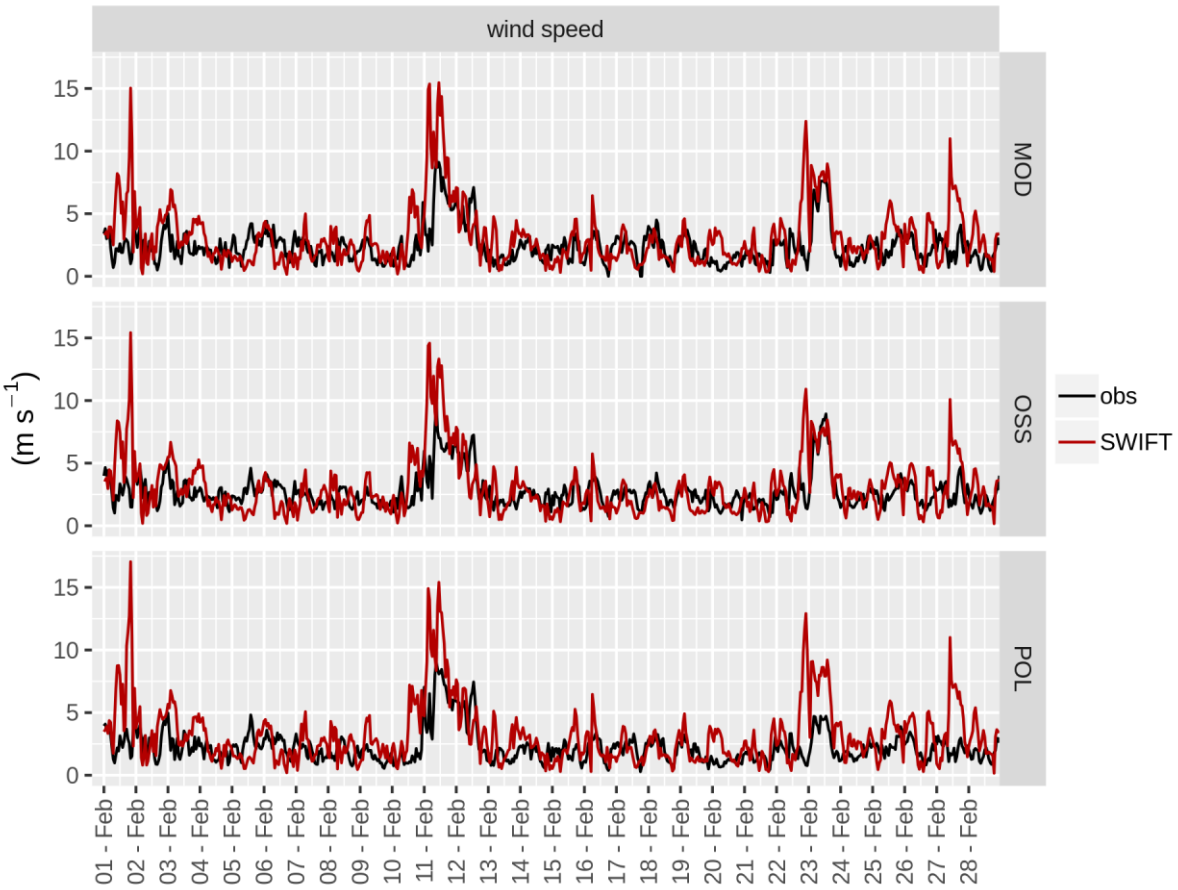

Figure 6.12: Hourly observed wind speed at MOD (on top), at OSS (in the middle) and at POL (on bottom) meteorological site along with hourly simulated wind speed by Micro-SWIFT, from February 1 to February 28, 2019.

The performances of Micro-SWIFT in reproducing observed wind speed were also evaluated in terms of statistical metrics. The model tend to overestimate measured values at all the three stations, in spite of this the NMB is less or equal than +30% for all the three stations (+11% at POL, +12% at OSS and +30% at MOD) and RMSE is between 2.21 and 0.93 m s^{-1}. FAC2 is 0.67 at MOD, 0.72 at OSS and 0.76 at POL, in line with the values found during the validation of the PMSS modelling suite in urban environment (Oldrini and Armand, 2019). Table 6-6 summarizes computed metrics.

Table 6-6: Statistics of hourly wind speed computed for the period between February 1 and February 28 at the three urban meteorological stations. MB and RMSE are expressed in m s^{-1}.

Station	FB	MB	NMB	RMSE	FAC2
MOD	-0.26	0.71	0.3	2.21	0.67
OSS	-0.11	0.33	0.12	2	0.72
POL	-0.36	0.17	0.11	0.93	0.76

In Figure 6.13 hourly simulated wind directions are compared with hourly observed wind for the same three locations. As for wind speed, the observed trend is reproduced quite well by Micro-SWIFT with MAE equal to 56° for both MOD and OSS sites and equal to 60° at POL station, confirming the agreement shown in Figure 6.13. Moreover the performances of Micro-SWIFT are evaluated also in terms of FB and NMSE with results in line with other application of Micro-SWIFT in urban environment (Oldrini and Armand, 2019). FB is equal to 0.16 at MOD and 0.14 at both OSS and POL stations; by contrast NMSE is equal to 0.27 at MOD, 0.34 at OSS and 0.30 at POL.

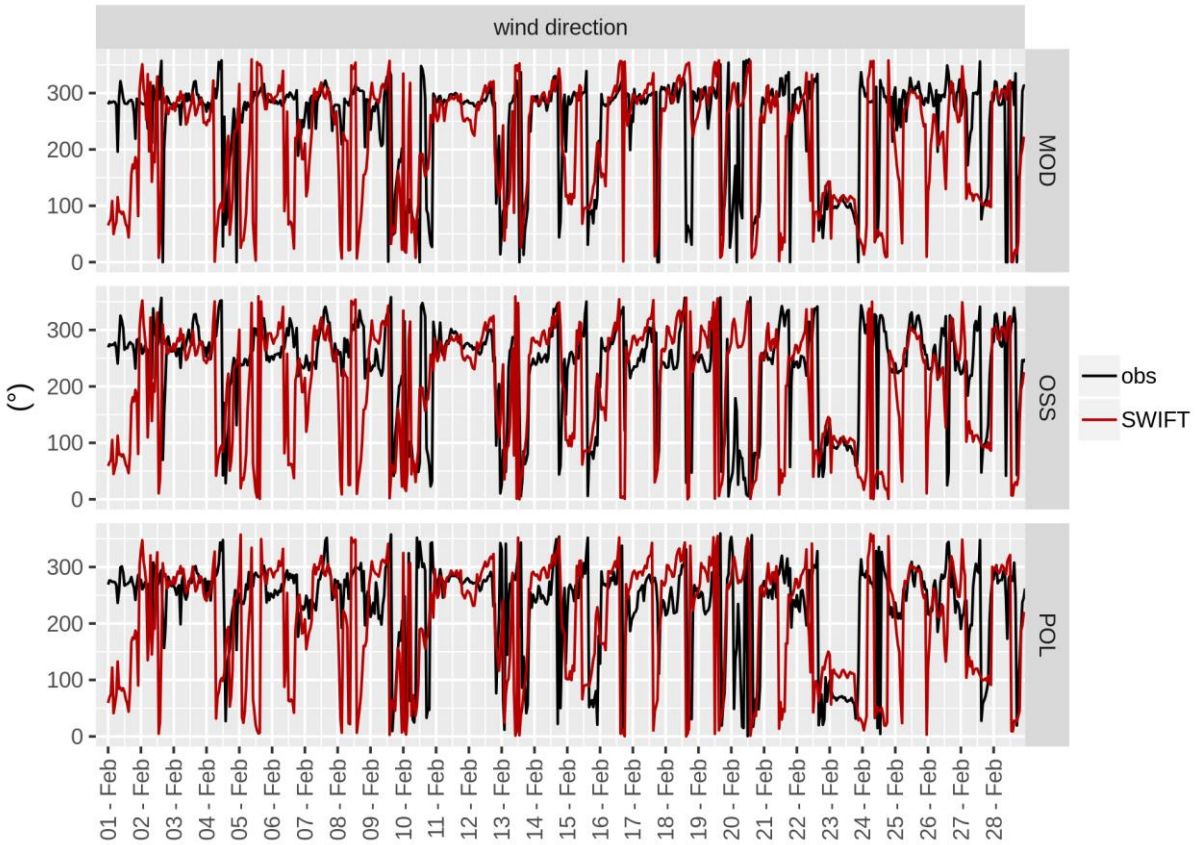

Figure 6.13: Hourly observed wind direction at MOD (on top), at OSS (in the middle) and at POL (on bottom) meteorological sites along with hourly simulated wind direction by Micro-SWIFT, from February 1 to February 28, 2019.

6.3.3.2 Micro-scale concentrations

Following the hybrid approach described in chapter 2.2, PMSS forecasted the hourly field concentrations produced by vehicular traffic in the urban area of Modena in terms of NO and NO_2 (see chapter 6.2 for the traffic emissions estimation). The total NO and NO_2 concentrations (as well as their sum, NO_x) in urban environment were computed adding the background concentrations (NO and NO_2) forecasted by WRF-Chem to the contribution estimated by PMSS.

In order to assess the performance of the modelling system, modelled concentrations were compared with observations at two urban stations: the first one at a traffic site, located in the proximity of a busy street close to the urban ring road, named "via Giardini", and the second one at background site, within a public park to the West of the historical city centre, named "parco Ferrari" (Figure 5.4).

In Figure 6.14, the hourly NO, NO_2 and NO_x concentrations predicted by PMSS in combination with WRF-Chem at 3 km resolution are compared through scatter plots for both urban traffic and background stations. The solid line represents perfect agreement with observations and within the dashed lines modelling results and observations agree with a factor of two.

Most of the modelled data at urban traffic site are within a factor of two of observations for all three pollutants, especially for NO_2 concentrations which very rarely exceed the dashed lines, whereas for the urban background station an under estimation is more noticeable, especially for NO concentrations which observed values above 100 µg m^{-3} are in most of the cases underestimated by the model. NO_x concentrations at urban background site depict similar behaviour of NO but with a less pronounced underestimation. In spite of this, NO_2 concentrations are well reproduced also at background station, confirming the successful combination between PMSS and WRF-Chem in reproducing this pollutant at both sites.

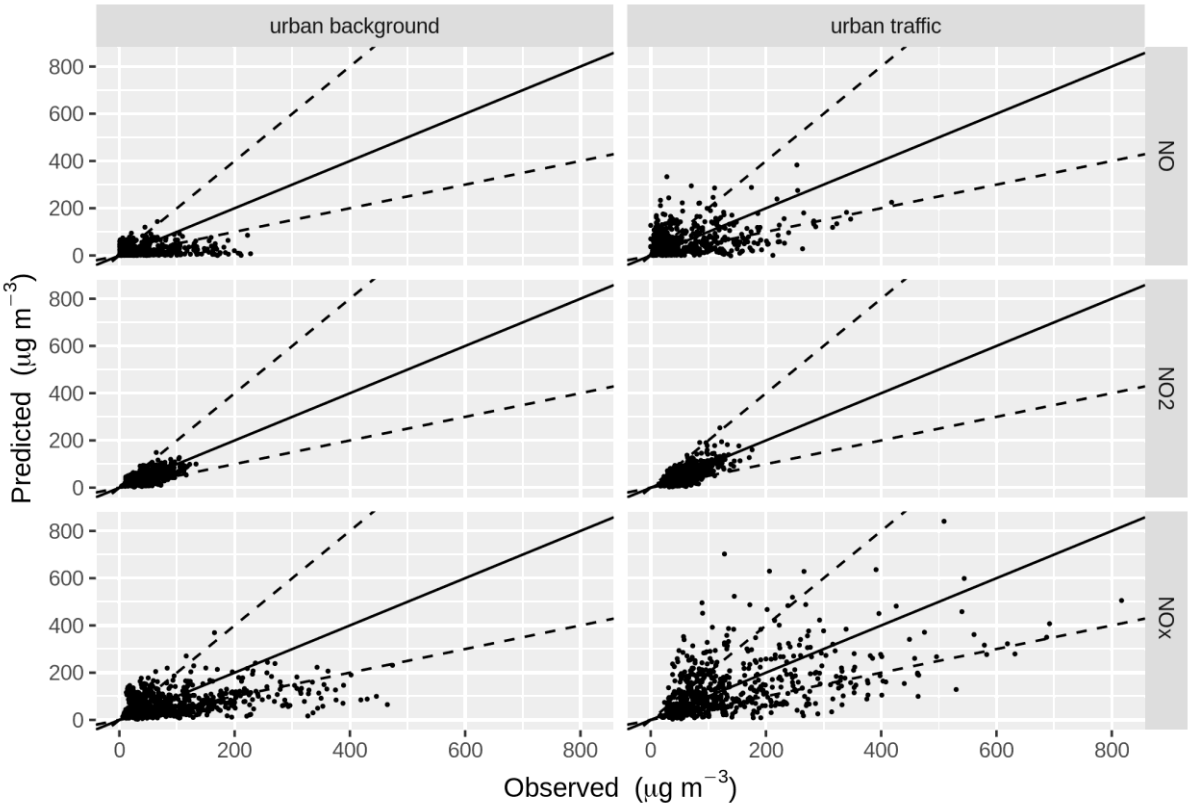

Figure 6.14: Scatter plots of predicted NO, NO_2 and NO_x concentrations by PMSS combined with WRF-Chem at 3 km resolution, at urban traffic ("via Giardini") and urban background ("parco Ferrari") stations.

Modelled hourly concentrations are biased negatively in both urban stations, in particular at the "parco Ferrari" background site the MB is generally larger than at traffic site for NO and NO_x, conversely for NO_2 is the opposite. Simulated NO and NO_x concentrations by PMSS and WRF-Chem present MB respectively equal to -15.6 µg m^{-3} (-44% of NMB) and -28.6 µg m^{-3} (-29% of NMB) at urban background site, and at urban traffic site MB is respectively equal to -0.8 µg m^{-3} (-1% of NMB) and -7.6 µg m^{-3} (-5% of NMB). By contrast MB for NO_2 at "via Giardini" station is -7.5 µg m^{-3} (-13% of NMB) and -4.7 (-11% of NMB) at "parco Ferrari" station.

Despite the Pearson correlation coefficient between forecasted and observed NO concentrations at urban background site is very low (0.15), modelled hourly concentrations correlate reasonably well with observations for NO at traffic site (0.42) and for NO_2 and NO_x at both sites: *r* is respectively equal to 0.61 and 0.40 at "parco Ferrari" station and respectively equal to 0.69 and 0.51 at "via Giardini" station.

A quantitative estimation of the agreement between simulated and observed concentrations was also assessed following the statistical metrics proposed by Hanna and Chang, (2012) for urban dispersion model evaluation. FB, NMSE, FAC2 and NAD were computed for both the urban stations located in Modena and for NO, NO_2 as well as their sum (NO_x). Table 6-7 summarizes all the computed statistics.

Table 6-7: Statistics of hourly NO, NO_2 and NO_x concentrations computed for the period between February 1 and February 28.

Pollutant	Station	FB	NMSE	FAC2	NAD
NO	urban traffic	0.02	1.50	0.42	0.41
	urban background	0.57	3.30	0.23	0.58
NO_2	urban traffic	0.13	0.22	0.78	0.19
	urban background	0.11	0.27	0.78	0.20
NO_x	urban traffic	0.06	0.72	0.61	0.30
	urban background	0.34	1.07	0.46	0.36

The statistical analysis shows that PMSS combined with WRF-Chem fulfill all the acceptance criteria defined by Hanna and Chang (2012) for NO_2 and NO_x at both urban sites. Conversely, for NO all the statistical metrics are fulfilled only at urban traffic site, while observed NO concentrations at "parco Ferrari" station are poorly reproduced by the models and this is especially evident looking at the FAC2 and NMB metrics.

Regarding the FB, the results are always less than the threshold of 0.67, in particular at urban traffic site the outcomes of this metric are particularly good with values equal to 0.02 for NO, 0.06 for NO_x and 0.13 for NO_2. At urban background station the results are larger than the previous one for NO and NO_x with values respectively equal to 0.57 and 0.34, by contrast for NO_2 are more or less the same (0.11). As far as the NMSE is concerned, the models show their best performances with scores lower than the acceptance benchmark (6), with a maximum value of 3.30 at urban background station for NO concentrations, meaning that predicted values very rarely differ strongly from observations.

Regarding the FAC2 and the NAD there is a significant agreement between model results and relative acceptance criteria at both urban stations for NO_2 and NO_x, by contrast as introduced before only modelled NO concentrations at traffic site are in line with the acceptance criteria defined by Hanna and Chang (2012). The maximum FAC2 is achieved for NO_2 with value

equal to 0.78 at both the urban stations, for NO_x is equal to 0.61 at traffic site and 0.46 at urban background site. Conversely, for NO FAC2 is 0.42 at "via Giardini" and 0.23 at "parco Ferrari" stations.

Minimum and maximum NAD are equal to 0.19 at urban traffic site for NO_2 and 0.58 at urban background station for NO, all the other values are less than the benchmark (0.50) suggested by Hanna and Chang for urban dispersion model evaluation.

The statistical analysis confirms the results obtained through scatterplots (Figure 6.14), which show that NO concentrations are well reproduced at "via Giardini" station where traffic emissions are expected to be most source of pollution, confirming the ability of the hybrid approach in reproducing traffic concentrations at high resolution. In contrast with this, at background station where traffic emissions less affect NO level, primary pollution concentrations are poorly reproduced. An explanation of the strong NO underestimation can be given considering the coarser resolution at which the emissions from other sectors are simulated by WRF-Chem (3 km) and thus not able to properly capture the observed trend.

On the other hand, NO_2 concentrations are well reproduced at both urban sites endorsing the ability of WRF-Chem to forecast this secondary pollutant with modelled concentrations very close to the measured pattern. Finally, NO_x concentrations reflect the NO trend at both sites, resulting well captured at "via Giardini" station and, despite a greater bias than at traffic site, also at "parco Ferrari" station all the metrics are in line with the benchmark values suggested by the literature.

In order to study which part of day primarily affected the general underestimation of the models and to investigate the WRF-Chem contribution to the total concentrations during the day, the variation of observed and predicted concentrations by hour of the day was assessed.

Mean observed daily cycles show very similar behaviour between the "via Giardini" and "parco Ferrari" stations (Figure 6.15): two main peaks occur on average during the day for NO, NO_2 and for NO_x, one between 07:00 and 08:00 a.m. UTC, about 100 µg m^{-3} for NO, 75 µg m^{-3} for NO_2 and 250 µg m^{-3} for NO_x at traffic site and about 75 µg m^{-3} for NO, 50 µg m^{-3} for NO_2 and 150 µg m^{-3} for NO_x at background site. The observed second daily peak at "via Giardini" station occurs between 06:00 and 07:00 p.m. UTC, about 150 µg m^{-3} for NO, 100 µg m^{-3} for NO_2 and 340 µg m^{-3} for NO_x, while at urban background site the second daily peak

is delayed of one hour (between 07:00 and 08:00 p.m. UTC) with mean concentrations about 85 µg m^{-3} for NO, 75 µg m^{-3} for NO_2 and 200 µg m^{-3} for NO_x.

Modelled daily concentrations present a good agreement with observed daily cycle for traffic station, in particular for NO_2 which simulated trend overlap with good accuracy the two daily peaks and the central hours of the day. For NO, daily peaks are well captured in magnitude but slightly delayed in the morning and a little anticipated in the afternoon, conversely during daytime modelled concentrations are overestimated on average of 25 µg m^{-3}. This latter behaviour can be explained looking at the contribution of PMSS to NO concentrations, which represent the most relevant part of modelled concentrations at traffic site. Since PMSS is a Lagrangian particle model, is unable to reproduce photo-chemical reactions that occur in atmosphere, therefore the consequence is that the NO emitted and modelled by PMSS cannot transform into NO_2 or other secondary products, with the result that NO concentrations are overestimated especially during the central hours of the day.

The issue of not accounting for chemical reactions in the micro-scale dispersion carried out by PMSS affects also simulated NO_2 concentrations. Indeed, despite the inclusion of chemical reactions between nitrogen oxides, ozone and other organic compounds would improve the results for NO it would make the results for NO_2 worse, especially during the central hours of the day when the solar radiation reaches its maximum.

In contrast with the behaviour of NO, more NO_2 would be produced starting from precursor and an overestimation of the observed concentrations would occur. In fact, when NO_2 is present in sunlight it is dissociated into NO and ground-state oxygen (O), then O combines with O_2 naturally present in the atmosphere to form O_3, which in turn combines again with NO to form NO_2 and O_2. Since the oxygen atom is so reactive that it disappears as fast as it is formed, one can invoke the pseudo-steady-state approximation and thereby assume that the rate of formation is equal to the rate of disappearance, in this way a sort of closed loop on which NO, NO_2 and O_3 coexist, is established. However, NO_2 is also produced through an alternative route that does not involve the removal of O_3: NO is oxidized by peroxide radicals forming additional NO_2 (Seinfeld and Pandis, 2016). The overall result is that not accounting for chemical and photolytic reactions in the micro-scale dispersion of traffic emissions, the final modelled concentrations would overestimate the observed mean trend.

NO_x simulated daily trend at “via Giardini” station is very similar to the simulated NO pattern: daily peaks are well captured in magnitude but slightly delayed in the morning and

anticipated in the afternoon, on the other hand during daytime the overestimation of primary NO affects also the mean NO_x concentrations, resulting overestimated as well.

At urban background site observed daily NO_2 concentrations are very well captured by the models, with the same behaviour shown at traffic site: both the daily peaks and central hours of the day express satisfactory simulated concentrations. It is also worth noting that most of the NO_2 concentrations at "parco Ferrari" station are given by WRF-Chem, thus primary traffic contribution seems to give a minor contribution with respect the total NO_2 concentrations. However, even if the contribution of PMSS at background site is rather small, the production of secondary NO_2 from traffic emissions is neglected as at traffic site, with the consequence that an overestimation of the observed NO_2 trend would be expected. Furthermore, the PBL height reproduced by SURFPRO and reported in Figure 6.15, seems to be consistent with the observed concentrations daily trend at both traffic and background sites, affecting positively modelled concentrations.

In contrast to NO_2, modelled NO concentrations at background site were poorly reproduced by the hybrid approach, indeed the morning peak is almost missed, with a modelled daily pattern rising up to about 25 µg m^{-3} at 08:00 a.m. UTC, followed by a constant trend for the rest of the morning. In the afternoon the concentrations slightly decrease to then rise up again to 45 µg m^{-3} at 06:00 p.m. UTC when the second daily peak is reached, anticipated of about 2 hours with respect mean observed trend. Despite the more accurate modulation employed for traffic emissions compared to the analysis case study (chapter 5), primary NO concentrations seem to be not well reconstructed at urban background station. A possible explanation can be attributed to the coarse representation of other emissions sectors, whose contribution to total concentration may increase of importance at larger distance from busy streets. In particular, since domestic heating contributes up to 15% of total annual NO_x emission in Modena (INEMAR, 2013), can be one of the emission sector whose more accurate representation could provide better results in terms of primary NO and NO_x concentrations. A potential solution to improve the forecast could be to include the domestic heating emissions in the micro-scale dispersion performed by PMSS at high resolution; however the drawback of this inclusion is the increased computing time required to perform a daily simulation, which does not fit with the need to keep the computing cost limited in order to produce a daily forecast.

Finally, simulated NO_x daily trend at background site reflect the performance of modelled NO pattern at the same location, with the two daily peaks underestimated in term of absolute

concentrations and the afternoon peak anticipated of about two hours. On the other hand, during daytime modelled NO_x concentrations are generally overestimated. Notwithstanding these lacks of agreement, the performance of the hybrid modelling system in forecasting NO_x concentrations can be considered acceptable also at "parco Ferrari" station.

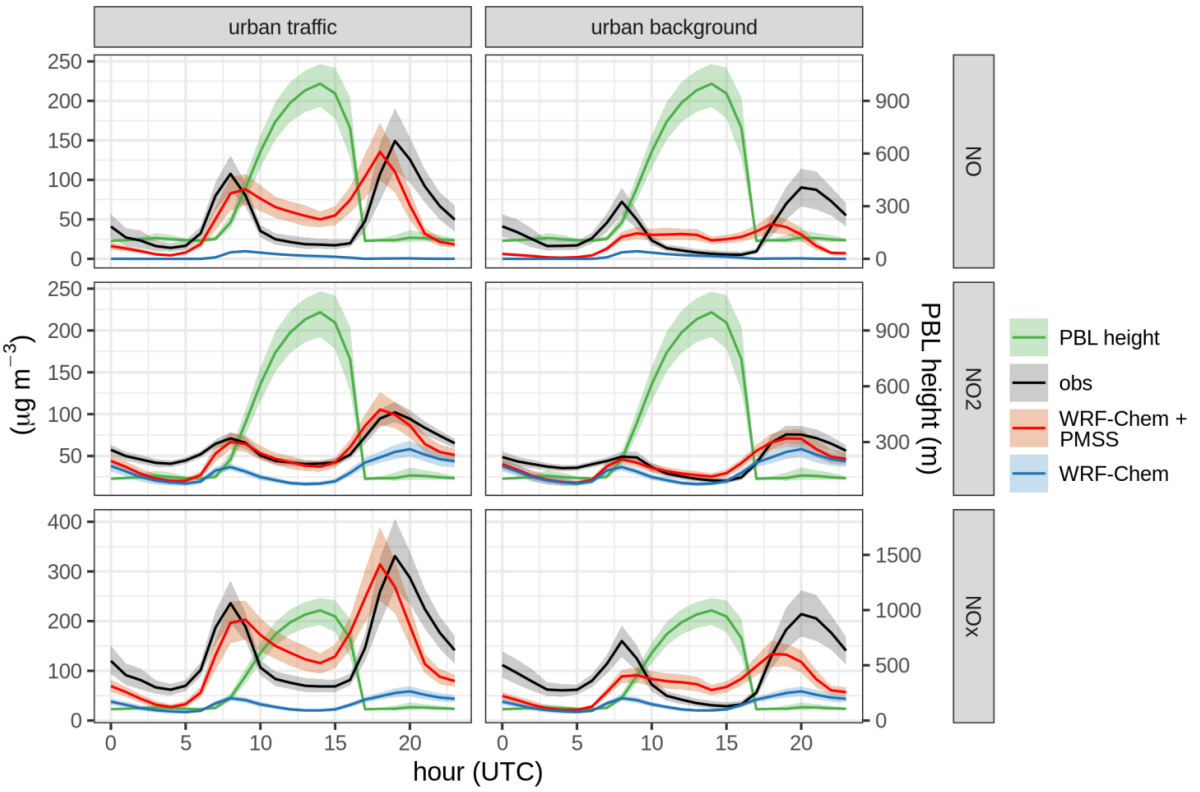

Figure 6.15: Mean daily cycle of observed NO, NO_2 and NO_x concentrations (black), modelled by the combination of WRF-Chem and PMSS model (red) and the only contribution of WRF-Chem (light blue), by station type (traffic or background). Green lines show the mean daily cycle of planetary boundary layer height modelled by SURFPRO and used in the micro-scale dispersion. Solid lines represent the daily mean cycle, meanwhile shaded area show the variability between 25th and 75th percentiles. Please note the different scale for NO_x concentrations.

7. Conclusions

In this thesis a hybrid modelling system consisting of the chemical transport model WRF-Chem and the Parallel Micro SWIFT SPRAY (PMSS) modelling suite has been evaluated for the urban area of Modena with the aim of providing NO, NO_2 as well as their sum (NO_x) concentration maps at building-resolving scale and at hourly temporal resolution, suitable to resolve the variability of emissions and atmospheric state.

Two case studies are presented. In the first one the WRF-Chem model was applied over three nested domains with an increasing resolution from 15 km to 1 km passing by 3 km, in order to simulate the emission, transport and chemical transformations of pollutants at the regional scale by accounting also at the same time for meteorological phenomena at the synoptic scale. Driven by these meteorological fields, the PMSS modelling suite was run over a domain of 6 km x 6 km with 4 m grid step size, to reconstruct micro-scale wind streams inside the urban area of Modena and then to simulate the dispersion of NO_x, coming from traffic emissions, by accounting for the presence of buildings. The simulation was performed for the period between 28 October 2016 and 8 November 2016, the same period whereby a traffic measurement campaign was carried out with 4 Doppler radar counters (one for each road lane) in a four-lane road in the proximity of the intersection with the urban ring road of Modena.

In the second case study, the same modelling system composed by WRF-Chem and PMSS was set-up to produce hourly forecast of NO_2 and NO (and their sum, NO_x) concentrations, up to one day ahead, for the entire month of February 2019 for the urban of Modena. The WRF-Chem model was run for every day of February 2019 in order to provide synoptic meteorological forecast and background concentrations of NO and NO_2. On the other hand PMSS forecast the urban concentrations of NO and NO_2, coming from traffic, at 4 m resolution over the same domain of 6 km x 6 km considered in the first case study. Moreover, additional traffic data recorded by 230 inductive loop spires were used to increase the accuracy of traffic emissions modulation during the day.

Besides these two case studies, a part of the PhD was spent also to develop a tool (VERT) able to estimate primary NO and NO_2 traffic emissions using a bottom-up approach and the Tier 3 methodology suggested by the EMEP/EEA guidelines. This tool, written in R language, is able to estimate cold and hot traffic emissions starting from the number of

vehicle that travel within a road network in a certain period of time and a specific vehicle fleet composition, accounting also for emission degradation due to vehicles age.

The results obtained in the first cases study show that the 2 m temperature and 10 m wind speed were captured well by the WRF-Chem model with statistical metrics in line with benchmark values suggested by the guidelines of the European Environmental Agency for meteorological mesoscale reconstruction, and with similar case studies related to the same area. Only few exceptions were observed at particular locations such as in mountainous area or close to the Ligurian sea, where complex orography and the local sea breeze strongly influenced the model bias in reproducing the meteorology. Despite, 10 m wind direction was poorly reproduced by WRF-Chem, its performance in terms of MAE and RMSE was in line with other cases studies focusing on the Po Valley, suffering both from the models difficulties in reproducing wind field during the situations with very little atmospheric circulation and low wind speed. Moreover, increasing WRF-Chem resolution from 15 km to 1 km resolution generally tended to slightly improve the model performance in reproducing 2 m temperature and 10 m wind speed.

NO_x concentrations reproduced in the Po Valley area by WRF-Chem were on average simulated reasonably well, but generally underestimated in almost all the background monitoring stations. The comparison with observations showed also that with an emissions inventory of 7 km horizontal resolution, the 1 km model resolution does not generally improve the results and the model configuration at 3 km resolution expressed the best performance in modelling NO_x concentrations.

Simulated and observed NO_x hourly concentrations in the urban area of Modena exhibit a large agreement, in particular for urban traffic site ("via Giardini" measurement station), where detailed traffic emissions estimation (real traffic modulation combined with a bottom-up approach) proved to be very successful in reproducing the observed NO_x pattern, confirming that reasonable time modulation for traffic emissions are among the main parameters to trim for urban atmospheric dispersion. Despite the morning rush-hour peak (between 08:00 a.m. and 09:00 a.m.) tending to be generally underestimated, the magnitude of the afternoon peak around 07:00 p.m. was well captured by PMSS with an anticipation of about two hours. At the urban background station, notwithstanding a general underestimation of the observed concentrations (more pronounced than at the urban traffic site), the analysis of

hourly daily modelled concentrations shows that PMSS combined with WRF-Chem provided a daily pattern in line with observations.

These features highlight the strength of this modelling chain in representing urban air quality, in particular at traffic sites, whose concentration levels make them the most critical area of the city; characteristics that chemical transport models alone cannot express, due to the coarser resolution to which they operate and to their inability to reproduce street canyons and urban structures.

Despite the inclusion of external emission sources for computational cells at PMSS boundaries, WRF-Chem at 3 km resolution generally presented slightly better results than the 1 km resolution, demonstrating that the contribution of background sources to urban pollution levels were generally underestimated and a better quantification of the emissions also in the surrounding area of Modena could improve the final result. The background underestimation may depend also on WRF–Chem perfectible effectiveness in reproducing the effects of the air mass homogenization on a regional scale that characterizes the climate conditions in central Po Valley.

The statistical analysis showed finally that PMSS combined with WRF-Chem at both the resolutions (3 km and 1 km) and both the urban measurement stations fulfil the acceptance criteria proposed in the literature for urban dispersion model evaluation.

In the second case study 2 m temperature and 10 m wind speed forecasted by WRF-Chem in the Po Valley are consistent with observations at most of the stations with good accuracy in reproducing 2 m temperature and 10 m wind speed, and statistical metrics in line with similar case studies related to the same area. The only exception that presents results outside these ranges were the stations close to the Ligurian Sea shore, where modelled 10 m wind speed was overestimated and observed and modelled 2 m temperature presented low correlation. These outcomes suggest that the model might have difficulties in forecasting the meteorology in regions close to the sea where local complex phenomena occur. On the other hand 10 m wind direction was well captured by WRF-Chem at most of the stations, with better statistical metrics compared to the first case study.

In order to test the reliability of WRF-Chem in predicting background concentrations, forecast NO_2 and NO_x concentrations were compared with observations at rural background stations located in the Po Valley. Related results show that NO_x concentrations are underestimated for

all the stations, in particular for the two placed in the Lombardy region where the model failed to capture the measured trend. This behaviour might be explained looking at the observed concentrations, which present very high values during the simulated period for rural back ground area and thus very difficult to predict for a Chemical Transport Model. By contrast, observed NO_x concentrations in the other background stations are simulated reasonably well.

NO_2 concentrations predicted by WRF-Chem, despite a general underestimation, presented satisfactory statistical metrics, in line with the benchmark values suggested by the literature. The poorest behaviour of modelled concentrations is still expressed at the two stations located in the Lombardy region where observed concentrations presented high peaks during the simulation period also for NO_2.

The performance of the hybrid approach in reproducing measured concentrations in the urban area of Modena are satisfactory, especially for traffic site where NO, NO_x and in particular NO_2 exhibit large agreement with observations. In contrast with this, at background site where traffic emissions reduce their importance compared to traffic site, measured NO and NO_x concentrations are in general underestimated, while NO_2 concentrations are really well captured, confirming the ability of WRF-Chem in forecasting the formation of secondary NO_2.

Analysing the variation of observed and predicted concentrations by hour of the day at traffic site, simulated NO_2 trend overlap with good accuracy the two daily peaks and the central hours of the day. While for NO, the two daily peaks are well captured in magnitude but slightly delayed in the morning and a little anticipated in the afternoon, conversely during daytime modelled concentrations are generally overestimated. This behaviour can be addressed to the inability of PMSS to reproduce photo-chemical reactions that occur in atmosphere, therefore the consequence is that the primary NO emitted by the traffic, which contribution is simulated by PMSS, cannot be converted into NO_2. The result is that NO concentrations are overestimated, especially during the central hours of the day. The same remarks can be also done for modelled NO_2 concentrations, which levels would overestimate the observed trend if chemical reactions would be taken into account.

On the other hand, modelled NO_x trend at the same station is very similar to the NO simulated pattern, with the two daily peaks well captured but slightly delayed in the morning and anticipated in the afternoon. While a general overestimation during the central hours of the day, due to the contribution of NO to total NO_x concentrations, is noticeable.

Daily NO_2 observations at the background site are very well captured by the models, as well as at the traffic site. By contrast, NO concentrations were poorly reproduced by the hybrid approach, which failed to capture the daily trend. A possible explanation of these misleading results can be attributed to the coarse representation of other emissions sectors, which contribution far from busy streets may increases of importance in terms of total concentrations, leading to an increment of the model bias. Due to low NO simulated concentrations at background site also the two NO_x daily peaks are underestimated, but in spite of this, the statistical analysis shows that the performance of the hybrid system in reproducing NO_x concentrations can be considered acceptable.

The outcomes of the modelling activity carried out during this thesis confirmed and proved how a tool composed by three complex modelling systems (WRF-Chem, PMSS and VERT) can be employed to support environmental policies, epidemiological studies and urban mobility planning.

Despite the ability of models to make predictions or simulate specific emissions scenario, it is also worth saying that the modelling activity cannot disregard from atmospheric observation, which constitute a fundamental part of the pollution mitigation and management. It's thus imperative to keep observations systems up to date and in sufficient number to guarantee the correct representativeness and coverage of the territory. Only a combined action of modeling techniques and observations can tackle the air pollution issue at all the levels, from local to global.

References

"A new operational approach to deal with dispersion around obstacles: The MSS (Micro Swift Spray) software suite (Conference) | ETDEWEB". (n.d.). , available at: https://www.osti.gov/etdeweb/biblio/20538864 (accessed 25 November 2019).

Abrams, J.Y., Klein, M., Henneman, L.R.F., Sarnat, S.E., Chang, H.H., Strickland, M.J., Mulholland, J.A., et al. (2019), "Impact of air pollution control policies on cardiorespiratory emergency department visits, Atlanta, GA, 1999-2013", *Environment International*, Vol. 126, pp. 627–634.

"Air quality in Europe 2019". (n.d.). *European Environment Agency*, Publication, , available at: https://www.eea.europa.eu/publications/air-quality-in-europe-2019 (accessed 18 November 2019).

Annavarapu, R.N. and Kathi, S. (2016), "Cognitive disorders in children associated with urban vehicular emissions", *Environmental Pollution (Barking, Essex: 1987)*, Vol. 208 No. Pt A, pp. 74–78.

Anfossi D., Ferrero E., Tinarelli G., Alessandrini S. (1996). A simplified version of correct boundary conditions for skewed turbulence in Lagrangian Particle Models. Atmospheric Environment, Vol. 31, No. 2, pp. 301-308.

Anfossi D., Ferrero E., Sacchetti D., Trini Castelli S. (1997). Comparison among empirical probability density functions of the vertical velocity in the surface layer based on higher order correlations. Boundary Layer Meteorology, Vol. 82, No. 2, pp. 193-218.

Bellasio, R., Bianconi, R., 2012: The LAPMOD modelling system for simulating atmospheric pollution in complex orography. Ingegneria Ambientale, vol. XLI, n. 6, 492-500.

Berchet, A., Zink, K., Oettl, D., Brunner, J., Emmenegger, L. and Brunner, D. (2017), "Evaluation of high-resolution GRAMM–GRAL (v15.12/v14.8) NO_x simulations over the city of Zürich, Switzerland", *Geoscientific Model Development*, Vol. 10 No. 9, pp. 3441–3459.

Beres, J.H., Garcia, R.R., Boville, B.A. and Sassi, F. (2005), "Implementation of a gravity wave source spectrum parameterization dependent on the properties of convection in the Whole Atmosphere Community Climate Model (WACCM)", *Journal of Geophysical Research: Atmospheres*, Vol. 110 No. D10, available at:https://doi.org/10.1029/2004JD005504.

Bigi, A., Bianchi, F., De Gennaro, G., Di Gilio, A., Fermo, P., Ghermandi, G., Prévôt, A.S.H., et al. (2017), "Hourly composition of gas and particle phase pollutants at a central urban background site in Milan, Italy", *Atmospheric Research*, Vol. 186, pp. 83–94.

Bigi, A. and Ghermandi, G. (2016), "Trends and variability of atmospheric $PM_{2.5}$ and $PM_{10–2.5}$ concentration in the Po Valley, Italy", *Atmospheric Chemistry and Physics*, Vol. 16 No. 24, pp. 15777–15788.

Bigi, A., Ghermandi, G. and Harrison, R.M. (2012), "Analysis of the air pollution climate at a background site in the Po valley", *Journal of Environmental Monitoring*, Vol. 14 No. 2, pp. 552–563.

Bivand, R., Keitt, T., Rowlingson, B., Pebesma, E., Sumner, M., Hijmans, R., Rouault, E., et al. (2019), *Rgdal: Bindings for the "Geospatial" Data Abstraction Library*, available at: https://CRAN.R-project.org/package=rgdal (accessed 3 December 2019).

Bivand, R., Lewin-Koh, N., Pebesma, E., Archer, E., Baddeley, A., Bearman, N., Bibiko, H.-J., et al. (2019), *Maptools: Tools for Handling Spatial Objects*, available at: https://CRAN.R-project.org/package=maptools (accessed 3 December 2019).

Block, M.L. and Calderón-Garcidueñas, L. (2009), "Air pollution: mechanisms of neuroinflammation and CNS disease", *Trends in Neurosciences*, Vol. 32 No. 9, pp. 506–516.

Borrego, C., Tchepel, O., Barros, N. and Miranda, A.I. (2000), "Impact of road traffic emissions on air quality of the Lisbon region", *Atmospheric Environment*, Vol. 34 No. 27, pp. 4683–4690.

Borrego, C., Tchepel, O., Barros, N. and Miranda, A.I. (2000), "Impact of road traffic emissions on air quality of the Lisbon region", *Atmospheric Environment*, Vol. 34 No. 27, pp. 4683–4690.

Bove, M.C., Brotto, P., Cassola, F., Cuccia, E., Massabò, D., Mazzino, A., Piazzalunga, A., et al. (2014), "An integrated PM2.5 source apportionment study: Positive Matrix Factorisation vs. the chemical transport model CAMx", *Atmospheric Environment*, Vol. 94, pp. 274–286.

Bowatte, G., Lodge, C.J., Knibbs, L.D., Erbas, B., Perret, J.L., Jalaludin, B., Morgan, G.G., et al. (2018), "Traffic related air pollution and development and persistence of asthma and low lung function", *Environment International*, Vol. 113, pp. 170–176.

Byun, D.W., Ching, S. (Eds.), 1999. Science algorithms of the EPA Models-3 Community Multiscale Air Quality (CMAQ) modeling system, EPA/600/R-99/030, US EPA, Research Triangle Park, NC.

Carlino, G., Pallavidino, L., Prandi, R., Avidano, A., Matteucci, G., Ricchiuti, F., Bajardi, P., Bolognini, L., 2016: Micro-scale modelling of urban air quality to forecast NO_2 critical levels in traffic hot-spots. 10th International Conference on Air Quality, Milano, Italy.

Carslaw, D.C. (2005), "Evidence of an increasing NO2/NOX emissions ratio from road traffic emissions", *Atmospheric Environment*, Vol. 39 No. 26, pp. 4793–4802.

Caserini, S., Pastorello, C., Gaifami, P. and Ntziachristos, L. (2013), "Impact of the dropping activity with vehicle age on air pollutant emissions", *Atmospheric Pollution Research*, Vol. 4 No. 3, pp. 282–289.

Chang, J.C. and Hanna, S.R. (2004), “Air quality model performance evaluation”, *Meteorology and Atmospheric Physics*, Vol. 87 No. 1, pp. 167–196.

Chen, F. and Dudhia, J. (2001), “Coupling an Advanced Land Surface–Hydrology Model with the Penn State–NCAR MM5 Modeling System. Part I: Model Implementation and Sensitivity”, *Monthly Weather Review*, Vol. 129 No. 4, pp. 569–585.

Cimorelli, A.J., Perry, S.G., Venkatram, A., Weil, J.C., Paine, R.J., Wilson, R.B., Lee, R.F., et al. (2005), “AERMOD: A Dispersion Model for Industrial Source Applications. Part I: General Model Formulation and Boundary Layer Characterization”, *Journal of Applied Meteorology*, Vol. 44 No. 5, pp. 682–693.

Colette, A., Aas, W., Banin, L., Braban, C.F., Ferm, M., Gonzalez Ortiz, A., Ilyin, I., et al. (2016), “Air pollution trends in the EMEP region between 1990 and 2012”, Publication - Report, , May, available at: http://www.unece.org/fileadmin/DAM/env/lrtap/ExecutiveBody/35th_session/cccr1-2016_FINAL.pdf (accessed 18 November 2019).

Costa, L.G., Chang, Y.-C. and Cole, T.B. (2017), “Developmental Neurotoxicity of Traffic-Related Air Pollution: Focus on Autism”, *Current Environmental Health Reports*, Vol. 4 No. 2, pp. 156–165.

Costa, L.G., Cole, T.B., Coburn, J., Chang, Y.-C., Dao, K. and Roqué, P.J. (2017), “Neurotoxicity of traffic-related air pollution”, *Neurotoxicology*, Vol. 59, pp. 133–139.

A. de Meij, A., Gzella, A., Cuvelier, C., Thunis, P., Bessagnet, B., Vinuesa, J.F., Menut, L., Kelder, H.M., (2009), "The impact of MM5 and WRF meteorology over complex terrain on CHIMERE model calculations". *Atmospheric Chemistry and Physics*, Vol 9 No. 17, pp.6611-6632.

Du S. (1997), "Universality of the Lagrangian velocity structure function constant (C_0) across different kinds of turbulence". Boundary Layer Meteorology, Vol. 83, No. 2, pp. 207-219.

Emmons, L.K., Walters, S., Hess, P.G., Lamarque, J.-F., Pfister, G.G., Fillmore, D., Granier, C., et al. (2010), "Description and evaluation of the Model for Ozone and Related chemical Tracers, version 4 (MOZART-4)", *Geoscientific Model Development*, Vol. 3 No. 1, pp. 43–67.

European Environment Agency, 2011: The application of models under the European Union's Air Quality Directive: A technical reference guide, https://doi.org/10.2800/80600 technical report 10/2011.

Ferrero E., D. Anfossi (1998). Comparison of PDFs, closure schemes and turbulence parameterizations in Lagrangian stochastic models. International Journal of Environmental Pollution, Vol. 9, No. 4, pp. 384-410.

Ferrero, L., Riccio, A., Perrone, M.G., Sangiorgi, G., Ferrini, B.S. and Bolzacchini, E. (2011), "Mixing height determination by tethered balloon-based particle soundings and modeling simulations", *Atmospheric Research*, Vol. 102 No. 1, pp. 145–156.

Finzi G., Pirovano G., Volta M. L. (2001). Gestione della qualità dell'aria. Modelli di simulazione e previsione. Mc Graw-Hill, pp. 400.

Fonken, L.K., Xu, X., Weil, Z.M., Chen, G., Sun, Q., Rajagopalan, S. and Nelson, R.J. (2011), "Air pollution impairs cognition, provokes depressive-like behaviors and alters hippocampal cytokine expression and morphology", *Molecular Psychiatry*, Vol. 16 No. 10, pp. 987–995, 973.

Garcia, E., Berhane, K.T., Islam, T., McConnell, R., Urman, R., Chen, Z. and Gilliland, F.D. (2019), "Association of Changes in Air Quality With Incident Asthma in Children in California, 1993-2014", *JAMA*, Vol. 321 No. 19, pp. 1906–1915.

Garcia, R.R., Yue, J. and Russell, J.M. (2019), “Middle Atmosphere Temperature Trends in the Twentieth and Twenty-First Centuries Simulated With the Whole Atmosphere Community Climate Model (WACCM)”, *Journal of Geophysical Research: Space Physics*, Vol. 124 No. 10, pp. 7984–7993.

Gauderman, W.J., Urman, R., Avol, E., Berhane, K., McConnell, R., Rappaport, E., Chang, R., et al. (2015), “Association of Improved Air Quality with Lung Development in Children”, *New England Journal of Medicine*, Vol. 372 No. 10, pp. 905–913.

Ghermandi, G., Fabbi, S., Bigi, A., Veratti, G., Despini, F., Teggi, S., Barbieri, C., et al. (2019), “Impact assessment of vehicular exhaust emissions by microscale simulation using automatic traffic flow measurements”, *Atmospheric Pollution Research*, Vol. 10 No. 5, pp. 1473–1481.

Ghermandi, G., Fabbi, S., Zaccanti, M., Bigi, A. and Teggi, S. (2015), “Micro–scale simulation of atmospheric emissions from power–plant stacks in the Po Valley”, *Atmospheric Pollution Research*, Vol. 6 No. 3, pp. 382–388.

Ghermandi, G., Teggi, S., Fabbi, S., Bigi, A. and Zaccanti, M.M. (2015), “Tri-generation power plant and conventional boilers: pollutant flow rate and atmospheric impact of stack emissions”, *International Journal of Environmental Science and Technology*, Vol. 12 No. 2, pp. 693–704.

Gowardhan, A.A., Pardyjak, E.R., Senocak, I. and Brown, M.J. (2011), “A CFD-based wind solver for an urban fast response transport and dispersion model”, *Environmental Fluid Mechanics*, Vol. 11 No. 5, pp. 439–464.

Grell, G.A. and Freitas, S.R. (2014), “A scale and aerosol aware stochastic convective parameterization for weather and air quality modeling”, *Atmospheric Chemistry and Physics*, Vol. 14 No. 10, pp. 5233–5250.

Grell, G.A., Peckham, S.E., Schmitz, R., McKeen, S.A., Frost, G., Skamarock, W.C. and Eder, B. (2005), "Fully coupled 'online' chemistry within the WRF model", *Atmospheric Environment*, Vol. 39 No. 37, pp. 6957–6975.

Gsella, A., de Meij, A., Kerschbaumer, A., Reimer, E., Thunis, P. and Cuvelier, C. (2014), "Evaluation of MM5, WRF and TRAMPER meteorology over the complex terrain of the Po Valley, Italy", *Atmospheric Environment*, Vol. 89, pp. 797–806.

Guenther, A.B., Jiang, X., Heald, C.L., Sakulyanontvittaya, T., Duhl, T., Emmons, L.K. and Wang, X. (2012), "The Model of Emissions of Gases and Aerosols from Nature version 2.1 (MEGAN2.1): an extended and updated framework for modeling biogenic emissions", *Geoscientific Model Development*, Vol. 5 No. 6, pp. 1471–1492.

Han, J., and Pan H.-L. (2011), "Revision of convection and vertical diffusion schemes in the NCEP Global Forecast System". *Weather Forecasting*, Vol. 26, pp. 520–533, https://doi.org/10.1175/WAF-D-10-05038.1.

Hanna S. R. (1982). Applications in air pollution modelling, Atmospheric turbulence and air pollution modelling, Ed. by Nieuwstadt S.T.M. and van Dop H., Reidel, pp. 275-310.

Hanna S. R.,Han, J. and Pan, H.-L. (2011), "Revision of Convection and Vertical Diffusion Schemes in the NCEP Global Forecast System", *Weather and Forecasting*, Vol. 26 No. 4, pp. 520–533.

Hanna, S. and Chang J. C. (1991). Boundary-layer parameterizations for applied dispersion modelling over urban areas. Boundary-Layer Meteorology, Vol. 58, No. 3, pp. 229-259.

Hanna, S.R., Chang, J.C., 2012: Acceptance criteria for urban dispersion model evaluation. Meteorological Atmospheric Physics 116, 133–146, https://doi.org/10.1007/s00703-011-0177-1.

Hausberger, S., Matzer, C., Lipp, S., Weller, K., Dippold, M., Röck, M., Rexeis, M. and Silberholz, G., 2019: Consistent Emission Factors from PEMS and Chassis Dyno Tests for HBEFA 4.1; TAP Conference, Thessaloniki, Greece.

HBEFA, 2019, https://www.hbefa.net/e/index.html (last access 9 December 2019).

Hodzic, A. and Jimenez, J.L. (2011), "Modeling anthropogenically controlled secondary organic aerosols in a megacity: a simplified framework for global and climate models", *Geoscientific Model Development*, Vol. 4 No. 4, pp. 901–917.

Hoek, G., Beelen, R., de Hoogh, K., Vienneau, D., Gulliver, J., Fischer, P., Briggs, D. (2008), "A review of land-use regression models to assess spatial variation of outdoor air pollution", *Atmospheric Environment*, Vol. 42 Issue 33, pp. 7561-7578.

Hong, S.-Y. (2010), "A new stable boundary-layer mixing scheme and its impact on the simulated East Asian summer monsoon", *Quarterly Journal of the Royal Meteorological Society*, Vol. 136 No. 651, pp. 1481–1496.

Ibarra-Espinosa, S., Ynoue, R., O'Sullivan, S., Pebesma, E., Andrade, M. de F. and Osses, M. (2018), "VEIN v0.2.2: an R package for bottom–up vehicular emissions inventories", *Geoscientific Model Development*, Vol. 11 No. 6, pp. 2209–2229.

Irwin, J. S. (1983). Estimating Plume Dispersion-A Comparison of Several Sigma Schemes. Journal of Climate and Applied Meteorology, Vol. 22, pp. 92-114.

INEMAR, 2013, https://www.arpae.it/dettaglio_generale.asp?id=4094&idlivello=1691(last access 2 September 2019).

Kaplan H., Dinar N. (1996). A Lagrangian dispersion model for calculating concentration distribution within a built-up domain. Atmospheric Environment, Vol. 30, No. 24, pp. 4197-4207.

Khan, K.M., Weigel, M.M., Yonts, S., Rohlman, D. and Armijos, R. (2019), "Residential exposure to urban traffic is associated with the poorer neurobehavioral health of Ecuadorian schoolchildren", *NeuroToxicology*, Vol. 73, pp. 31–39.

Kolmogorov A. N. (1941). The local structure of turbulence in incompressible viscous fluid for very large Reynolds numbers. Proceedings of the USSR Academy of Sciences, Vol. 30, pp. 299-303

Kuenen, J.J.P., Visschedijk, A.J.H., Jozwicka, M. and Denier van der Gon, H. a. C. (2014), "TNO-MACC_II emission inventory; a multi-year (2003–2009) consistent high-resolution European emission inventory for air quality modelling", *Atmospheric Chemistry and Physics*, Vol. 14 No. 20, pp. 10963–10976.

Kuik, F., Kerschbaumer, A., Lauer, A., Lupascu, A., Schneidemesser, E. von and Butler, T.M. (2018), "Top–down quantification of NO_x emissions from traffic in an urban area using a high-resolution regional atmospheric chemistry model", *Atmospheric Chemistry and Physics*, Vol. 18 No. 11, pp. 8203–8225.

Kuik, F., Lauer, A., Churkina, G., Denier van der Gon, H.A.C., Fenner, D., Mar, K.A. and Butler, T.M. (2016), "Air quality modelling in the Berlin–Brandenburg region using WRF-Chem v3.7.1: sensitivity to resolution of model grid and input data", *Geoscientific Model Development*, Vol. 9 No. 12, pp. 4339–4363.

Kwak, K.-H., Baik, J.-J., Ryu, Y.-H. and Lee, S.-H. (2015), "Urban air quality simulation in a high-rise building area using a CFD model coupled with mesoscale meteorological and chemistry-transport models", *Atmospheric Environment*, Vol. 100, pp. 167–177.

Laden, F., Schwartz, J., Speizer, F.E. and Dockery, D.W. (2006), "Reduction in Fine Particulate Air Pollution and Mortality", *American Journal of Respiratory and Critical Care Medicine*, Vol. 173 No. 6, pp. 667–672.

Lenschow, P., Abraham, H.-J., Kutzner, K., Lutz, M., Preuß, J.-D. and Reichenbächer, W. (2001), "Some ideas about the sources of PM10", *Atmospheric Environment*, Vol. 35, pp. S23–S33.

Lertxundi, A., Andiarena, A., Martínez, M.D., Ayerdi, M., Murcia, M., Estarlich, M., Guxens, M., et al. (2019), "Prenatal exposure to $PM_{2.5}$ and NO_2 and sex-dependent infant cognitive and motor development.", *Environmental Research*, Vol. 174, pp. 114–121.

Lin, Y.-L., Farley, R.D. and Orville, H.D. (1983), "Bulk Parameterization of the Snow Field in a Cloud Model", *Journal of Climate and Applied Meteorology*, Vol. 22 No. 6, pp. 1065–1092.

Malm, W.C., Collett Jr., J.L., Barna, M.G., Gebhart, K.A., Schichtel, B.A., Beem, K., Carrico, C.M., Day, D.E., Hand, J.L., Kreidenweis, S.M., Lee, T., Levin, E., McDade, C., McMeeking, G.R., Molenar, J.V., Raja, S., Rodriguez, M.A., Schwandner, F., Sullivan, A.P., Taylor, C., 2009: RoMANS Rocky Mountain Atmospheric Nitrogen and Sulfur Study Report Appendix 2. MM5 Performance Evaluation and Quality Assurance Review for the White River Field Office Ozone Assessment, URS Corporation, Denver.

Mar, K.A., Ojha, N., Pozzer, A. and Butler, T.M. (2016), "Ozone air quality simulations with WRF-Chem (v3.5.1) over Europe: model evaluation and chemical mechanism comparison", *Geoscientific Model Development*, Vol. 9 No. 10, pp. 3699–3728.

Masiol, M., Benetello, F., Harrison, R.M., Formenton, G., De Gaspari, F. and Pavoni, B. (2015), "Spatial, seasonal trends and transboundary transport of PM2.5 inorganic ions in the Veneto region (Northeastern Italy)", *Atmospheric Environment*, Vol. 117, pp. 19–31.

Mlawer, E.J., Taubman, S.J., Brown, P.D., Iacono, M.J. and Clough, S.A. (1997), "Radiative transfer for inhomogeneous atmospheres: RRTM, a validated correlated-k model for the longwave", *Journal of Geophysical Research: Atmospheres*, Vol. 102 No. D14, pp. 16663–16682.

Monin A. S., Yaglom A. M. (1971). Statistical fluid mechanics: mechanics of turbulence, Vol. 2, MIT Press, Cambridge, UK, pp. 874.

Moussafir, J., Oldrini, O., Tinarelli, G., Sontowski, J., Dougherty, C., 2004: A new operational approach to deal with dispersion around obstacles: the MSS (Micro-Swift-Spray) software suite. 9th International Conference on Harmonisation within Atmospheric Dispersion Modelling for Regulatory Purposes Garmisch 1-4 June 2004.

Moussafir, J., Olry, C., Nibart, M., Albergel, A., Armand, P., Duchenne, C., Mahe, F., Thobois, L., Le Loaëc, S., Oldrini, O., 2013: Aircity: a very high-resolution 3d atmospheric dispersion modeling system for Paris. Proc. 15th International Conference on Harmonisation within Atmospheric Dispersion Modelling for Regulatory Purpose, Madrid, Spain, May 6-9, 2013.

Moussiopoulos, N., Sahm, P. and Kessler, Ch. (1995), "Numerical simulation of photochemical smog formation in Athens, Greece—A case study", *Atmospheric Environment*, Vol. 29 No. 24, pp. 3619–3632.

Ntziachristos, L., Samaras, Z., 2016: EMEP/Eea Emission Inventory Guidebook; Road Transport: Passenger Cars, Light Commercial Trucks, Heavy-Duty Vehicles Including Buses and Motorcycles. European Environment Agency, Copenhagen.

Oettl, D. (2015), "Evaluation of the Revised Lagrangian Particle Model GRAL Against Wind-Tunnel and Field Observations in the Presence of Obstacles", *Boundary-Layer Meteorology*, Vol. 155 No. 2, pp. 271–287.

Oldrini, O., Olry, C., Moussafir, J., Armand, P., Duchenne, C., 2011: Development of PMSS, the Parallel Version of Micro SWIFT SPRAY. Proc. 14th Int. Conf. on Harmonisation within Atmospheric Dispersion Modelling for Regulatory Purposes, 443-447.

Oldrini, O., Nibart, M., Armand, P., Olry, C., Moussafir, J., Albergel, A., 2014. Introduction of momentum equation in Micro-SWIFT. In: Proc. of the 16 th Int. Conf. on Harmonisation

within Atmospheric Dispersion Modelling for Regulatory Purposes, Varna (Bulgaria), September 8-11, 2014, pp. 412–417.

Oldrini, O., Nibart, M., Duchenne, C., Armand, P., Moussafir, J., 2016. Development of the parallel version of a CFD – RANS flow model adapted to the fast response in built-up environments. In: Proc. of the 17 th Int. Conf. on Harmonisation within Atmospheric Dispersion Modelling for Regulatory Purposes, May 9-12, 2016, Budapest (Hungary).

Oldrini, O., Armand, P., Duchenne, C., Olry, C., Tinarelli, G., 2017. Description and preliminary validation of the PMSS fast response parallel atmospheric flow and dispersion solver in complex built-up areas. J. Environ. Fluid Mech. 17 (3), 1–18, https://doi.org/10.1007/s10652-017-9532-1.

Oldrini, O. and Armand, P. (2019), "Validation and Sensitivity Study of the PMSS Modelling System for Puff Releases in the Joint Urban 2003 Field Experiment", *Boundary-Layer Meteorology*, Vol. 171 No. 3, pp. 513–535.

Oldrini, O., Armand, P., Duchenne, C., Olry, C., Moussafir, J. and Tinarelli, G. (2017), "Description and preliminary validation of the PMSS fast response parallel atmospheric flow and dispersion solver in complex built-up areas", *Environmental Fluid Mechanics*, Vol. 17 No. 5, pp. 997–1014.

Pebesma, E., Bivand, R., Rowlingson, B., Gomez-Rubio, V., Hijmans, R., Sumner, M., MacQueen, D., et al. (2019), *Sp: Classes and Methods for Spatial Data*, available at: https://CRAN.R-project.org/package=sp (accessed 3 December 2019).

Pepe, N., Pirovano, G., Lonati, G., Balzarini, A., Toppetti, A., Riva, G.M. and Bedogni, M. (2016), "Development and application of a high resolution hybrid modelling system for the evaluation of urban air quality", *Atmospheric Environment*, Vol. 141, pp. 297–311.

Peters, A., Veronesi, B., Calderón-Garcidueñas, L., Gehr, P., Chen, L.C., Geiser, M., Reed, W., et al. (2006), "Translocation and potential neurological effects of fine and ultrafine particles a critical update", *Particle and Fibre Toxicology*, Vol. 3, p. 13.

Pirovano, G., Colombi, C., Balzarini, A., Riva, G.M., Gianelle, V. and Lonati, G. (2015), "PM2.5 source apportionment in Lombardy (Italy): Comparison of receptor and chemistry-transport modelling results", *Atmospheric Environment*, Vol. 106, pp. 56–70.

Quinn, A.K., Ae-Ngibise, K.A., Jack, D.W., Boamah, E.A., Enuameh, Y., Mujtaba, M.N., Chillrud, S.N., et al. (2016), "Association of Carbon Monoxide exposure with blood pressure among pregnant women in rural Ghana: Evidence from GRAPHS", *International Journal of Hygiene and Environmental Health*, Vol. 219 No. 2, pp. 176–183.

Quinn, A.K., Ae-Ngibise, K.A., Kinney, P.L., Kaali, S., Wylie, B.J., Boamah, E., Shimbo, D., et al. (2017), "Ambulatory monitoring demonstrates an acute association between cookstove-related carbon monoxide and blood pressure in a Ghanaian cohort", *Environmental Health*, Vol. 16 No. 1, p. 76.

Rani, B., Singh, U., Chuhan, A.K., Sharma, D. and Maheshwari, R. (2011), "Photochemical Smog Pollution and Its Mitigation Measures", *Journal of Advanced Scientific Research*, Vol. 2 No. 4, pp. 28–33.

Rayan P.H. and LeMasters G.K. (2007), "A review of land-use regression models for characterizing intraurban air pollution exposure", *Inhalation Toxicology*, Vol 19 No. 1, pp. 127-133.

R: A language and environment for statistical computing. R Foundation for Statistical Computing, Vienna, Austria. URL https://www.R-project.org/.

Reynolds O. (1895). On the dynamical theory of incompressible viscous fluids and the determination of the criterion. Philosophical Transaction of the Royal Society of London, Vol. 186, pp. 123-164.

Rockle R. (1990). Bestimmung der Stomungsverhaltnisse im Bereich komplexer Bebauungsstrukturen. Ph. D. thesis, Vom Fachbereich Mechanik, der Technischen Hochschule, Darmstadt, Germany.

Rodean H. C. (1996). Stochastic Lagrangian Models of Turbulent Diffusion. Monographs of American Meteorological Society (AMS), Vol. 26, pp. 84.

Sahsuvaroglu, T., Arain, A., Kanaroglou, P., Finkelstein, N., Newbold, B., Jerrett, M., Beckerman, B., et al. (2006), "A Land Use Regression Model for Predicting Ambient Concentrations of Nitrogen Dioxide in Hamilton, Ontario, Canada", *Journal of the Air & Waste Management Association*, Vol. 56 No. 8, pp. 1059–1069.

Seinfeld J. H., Pandis S. N. (2016), "Atmospheric Chemistry and Physics - From air pollution to climate change" *Third edition*.

Sjödin, A, Borken-Kleefeld, J., Carslaw, D., Tate, J., Alt, G.-M., De la Fuente, J., Bernard, Y., Tietge, U., McClintock, P., Gentala, R., Vescio, N., Hausberger, S., 2018: Real-driving emissions from diesel pas-senger cars measured by remote sensing and as compared with PEMS and chassis dynamometer measurements -CONOX Task 2 report; Commissioned by the Federal Office for the Environment (FOEN), Switzerland; ISBN: 978-91-88319-70-8.

Skamarock, W. C., J. B. Klemp, J. Dudhia, D. O. Gill, D. M. Barker, M. G. Duda, X.-Y. Huang, and W. W. et al., 2008: A description of the advanced research WRF version 3. Tech. rep., NCAR Technical Note TN-475+STR, 125.

Smit, R., Ntziachristos, L. and Boulter, P. (2010), "Validation of road vehicle and traffic emission models – A review and meta-analysis", *Atmospheric Environment*, Vol. 44 No. 25, pp. 2943–2953.

Stein, A.F., Isakov, V., Godowitch, J. and Draxler, R.R. (2007), “A hybrid modeling approach to resolve pollutant concentrations in an urban area”, *Atmospheric Environment*, Vol. 41 No. 40, pp. 9410–9426.

Sozzi R. (2003). La micrometeorologia e la dispersione degli inquinanti in aria. Centro tematico Nazionale Atmosfera Clima Emissioni.

Stull R. B. (1989). An introduction to Boundary layer meteorology. Springer Science & Business Media, pp. 666.

Taylor G. I. (1921). Diffusion by Continuous Movements. Proc. London Mathematical Society, Vol. 20, pp. 196-211.

Tennekes H. (1979). The exponential Lagrangian correlation function and turbulent diffusion in the inertial subrange. Atmospheric Environment, Vol. 13, No. 11, pp. 1565-1567.

Thomson D. J. (1987). Criteria for the selection of stochastic–models of particle trajectories in turbulent flows, Journal of Fluid Mechanics, Vol. 180, pp. 529-556.

Thunis, P., Triacchini, G., White, L., Maffeis, G., Volta, M., 2009: Air pollution and emission reductions over the Po-Valley: Air quality modelling and integrated assessment. 18th World IMACS / MODSIM Congress, Cairns, Australia 13-17 July, p. 2009 2335-2341.

Thunis, P. (2018), “On the validity of the incremental approach to estimate the impact of cities on air quality”, *Atmospheric Environment*, Vol. 173, pp. 210–222.

Tiao, G.C., Box, G.E.P. and Hamming, W.J. (1975), “Analysis of Los Angeles Photochemical Smog Data: A Statistical Overview”, *Journal of the Air Pollution Control Association*, Vol. 25 No. 3, pp. 260–268.

Tinarelli, G., Giostra, U., Ferrero, E., Tampieri, F., Anfossi, D., Brusasca, G., Trombetti, F., 1992: SPRAY, a 3-D particle model for complex terrain dispersion", Proc. of 10th

Symposium on Turbulence and Diffusion, American Meteorological Society, Portland, Oregon (USA), 29-Sept. 2-Oct, P2.9, 147-150.

Tinarelli, G., Brusasca, G., Oldrini, O., Anfossi, D., Castelli, S.T. and Moussafir, J. (2007), "Micro-Swift-Spray (MSS): A New Modelling System for the Simulation of Dispersion at Microscale. General Description and Validation", in Borrego, C. and Norman, A.-L. (Eds.), *Air Pollution Modeling and Its Application XVII*, Springer US, Boston, MA, pp. 449–458.

Tinarelli, G., Mortarini, L., Castelli, S.T., Carlino, G., Moussafir, J., Olry, C., Armand, P., et al. (2013), "Review and Validation of MicroSpray, a Lagrangian Particle Model of Turbulent Dispersion", *Lagrangian Modeling of the Atmosphere*, American Geophysical Union (AGU), pp. 311–328.

Tositti, L., Brattich, E., Masiol, M., Baldacci, D., Ceccato, D., Parmeggiani, S., Stracquadanio, M., et al. (2014), "Source apportionment of particulate matter in a large city of southeastern Po Valley (Bologna, Italy)", *Environmental Science and Pollution Research*, Vol. 21 No. 2, pp. 872–890.

Trini Castelli, S., Armand, P., Tinarelli, G., Duchenne, C. and Nibart, M. (2018), "Validation of a Lagrangian particle dispersion model with wind tunnel and field experiments in urban environment", *Atmospheric Environment*, Vol. 193, pp. 273–289.

Trini Castelli, S., Tinarelli, G. and Reisin, T.G. (2017), "Comparison of atmospheric modelling systems simulating the flow, turbulence and dispersion at the microscale within obstacles", *Environmental Fluid Mechanics*, Vol. 17 No. 5, pp. 879–901.

Veratti, G., Fabbi, S., Bigi, A., Lupascu, A.. Tinarelli, G., Teggi, S., Brusasca, G., Butler, T., Ghermandi, G.: Towards the coupling of a chemical transport model with a micro-scale Lagrangian modelling system for evaluation of urban NO_x levels in a European hotspot. Under review to the Atmospheric Environment journal.

Weil J. C. (1990). A diagnosis of the asymmetry in top-down and bottom-up diffusion using a Lagrangian stochastic model. Journal of Atmospheric Science, Vol. 47, No. 4, pp. 501-515.

White Alexandra J. and Sandler Dale P. (n.d.). "Indoor Wood-Burning Stove and Fireplace Use and Breast Cancer in a Prospective Cohort Study", *Environmental Health Perspectives*, Vol. 125 No. 7, p. 077011.

"WHO | Ambient air pollution: A global assessment of exposure and burden of disease". (n.d.). *WHO*, available at: http://www.who.int/phe/publications/air-pollution-global-assessment/en/ (accessed 17 November 2019).

Whiteman, C. D. (2000): Mountain Meteorology: Fundamentals and Applications. Oxford University Press, 2000, 355 pp.

Win-Shwe, T.-T., Yamamoto, S., Fujitani, Y., Hirano, S. and Fujimaki, H. (2008), "Spatial learning and memory function-related gene expression in the hippocampus of mouse exposed to nanoparticle-rich diesel exhaust", *Neurotoxicology*, Vol. 29 No. 6, pp. 940–947.

Win-Shwe, T.-T., Yamamoto, S., Fujitani, Y., Hirano, S. and Fujimaki, H. (2012), "Nanoparticle-rich diesel exhaust affects hippocampal-dependent spatial learning and NMDA receptor subunit expression in female mice", *Nanotoxicology*, Vol. 6 No. 5, pp. 543–553.

Yolton, K., Khoury, J.C., Burkle, J., LeMasters, G., Cecil, K. and Ryan, P. (2019), "lifetime exposure to traffic-related air pollution and symptoms of depression and anxiety at age 12 years", *Environmental Research*, Vol. 173, pp. 199–206.

Zaveri, R.A., Easter, R.C., Fast, J.D. and Peters, L.K. (2008), "Model for Simulating Aerosol Interactions and Chemistry (MOSAIC)", *Journal of Geophysical Research: Atmospheres*, Vol. 113 No. D13, available at:https://doi.org/10.1029/2007JD008782.

Acknowledgments

I would like to pay my special regards to my supervisor Prof. Grazia Ghermandi and my co-supervisor Prof. Alessandro Bigi for their support and great help they gave me along these years and also for leaving me the freedom to act following my ideas.

Thanks to Prof. Tim Butler and Dr. Aurelia Lupascu, who helped and followed me in the application of the WRF-Chem model during my stay at the Insitute for Advanced Sustainability Studies of Potsdam (Germany).

Thanks to Dr. Gianni Tinarelli and Dr. Giuseppe Brusasca from Arianet S.r.l. for their assistance for the usage of the PMSS model and for helping in the first design of the project.

Thanks to Dr Dietmar Oettl and Prof. Giovanni Lonati for their comments and advices in reviewing this PhD thesis.

And finally a special thanks for all the guys of the LARMA group, who helped me during hard time with a joke or a word of comfort, thanks for making these years unforgettable!